Encoding and control of motor prediction and feedback in the cerebellar cortex

A DISSERTATION

SUBMITTED TO THE FACULTY OF

UNIVERSITY OF MINNESOTA

BY

Martha Laura Streng

IN PARTIAL FULFILLMENT OF THE REQUIREMENTS

FOR THE DEGREE OF

DOCTOR OF PHILOSOPHY

Timothy J. Ebner, adviser

August, 2017

Acknowledgements

First and foremost, I would like to express my deepest gratitude to my advisor, Tim Ebner. I cannot say enough about how much I have valued his mentorship. Over the past four years, I could always depend on Tim for encouragement, support, and constructive feedback whenever needed. I know that whatever progress I may experience as a scientist will be the result in part of the training he has given me. It has been a privilege to be a member of the Ebner lab.

I would like to acknowledge all the other members of the Ebner lab for their contributions. Laurentiu Popa helped with the analysis and interpretation of the research presented in this thesis. He also patiently taught me everything I know about MATLAB, and could always provide big ideas and a sympathetic ear. Russ Carter was always available for helpful advice on lab procedures, experiments and analysis. Lijuan Zhuo trained me on animal handling procedures and provided technical assistance. Gang Chen and Claudia Hendrix helped with and performed surgical procedures. I would also like to acknowledge Tersea Kim and Samatha Gibson for their help with data processing. Kris Bettin, Orbe Walther, and Kathleen Beterams assisted with manuscript preparation, grant submissions, and generally keeping the lab running.

It is not possible to acknowledge every member of the Graduate Program in Neuroscience who have supported me during my time as a graduate student, but I am grateful to you all. In particular, thank you to my classmates for their support and friendship along the way. Geoff Ghose, Matthew Chafee, Hubert Lim also provided helpful feedback and troubleshooting advice. John Paton could always be relied on for answers to logistical questions and help with whatever I needed.

I would like to acknowledge my parents, Rick and Kay, and my sister Elaine for their support. Finally, my partner Zoé, for her calming presence and constant reassurance. It is

difficult to lose sight of the context for my thesis research when I get to see it every time she dances on stage.

Dedication

I would like to dedicate my thesis to my parents, Rick and Kay Streng. They have provided me endless encouragement, afforded me infinite patience, and given me every opportunity I have needed to succeed. They are a daily reminder of the value of hard work, perseverance, and pursuit of what you love.

And to the memory of my grandmother, Elaine Kroeff (1921-2017). Her love and enthusiasm were limitless. Even until the very end, she never failed to ask me how the monkeys were doing.

Abstract

Extensive research implicates the cerebellum as a forward internal model that predicts the sensory consequences of motor commands and compares them to their actual feedback, generating prediction errors that guide motor learning. However, lacking is a characterization of how information relevant to motor control and sensory prediction error is processed by cerebellar neurons. Of major interest is the contribution of Purkinje cells, the primary output neurons of the cerebellar cortex, and their two activity modalities: simple and complex spike discharges. The dominant hypothesis is that complex spikes serve as the sole error signal in the cerebellar cortex. However, no current hypotheses fully explain or are completely consistent with the spectrum of previous experimental observations.

To address these major issues, Purkinje cell activity was recorded during a pseudo-random manual tracking task requiring the continuous monitoring and correction for errors. The first hypothesis tested by this thesis was whether climbing fiber discharge controls the information present in the simple spike firing. During tracking, complex spikes trigger robust and rapid changes in the simple spike modulation with limb kinematics and performance errors. Moreover, control of performance error information by climbing fiber discharge is followed by improved tracking performance, suggesting that it is highly important for optimizing behavior.

A second hypothesis tested was whether climbing fiber discharge is evoked by errors in movement. Instead, complex spikes are modulated predictively with behavior. Additionally, complex spikes are not evoked as a result of a specific 'event' as has been previously suggested. Together, this suggests a novel function of complex spikes, in which climbing fibers continuously optimize the information in the simple spike firing in advance of changes in behavior.

A third hypothesis tested is whether the simple spike discharge is responsible for encoding the sensory prediction errors crucial for online motor control. To address this, two novel manipulations of visual feedback during pseudo-random tracking were implemented to assess whether disrupting sensory information pertinent to motor error prediction and feedback modulates simple spike activity. During these manipulations, the simple spike modulation with behavior is consistent with the predictive and feedback components of sensory prediction error. Together, this thesis addresses a major outstanding question in the field of cerebellar physiology and develops a novel hypothesis about the interaction between the two activity modalities of Purkinje cells.

Table of contents

Table of Figures

CHAPTER 2

CHAPTER 3

CHAPTER 4

CHAPTER 5

CHAPTER 1: CEREBELLAR CONTRIBUTION TO ONLINE MOTOR CONTROL

Introduction

"The cerebellum is important for the production of smooth, continuous movements." This statement, in some form or another, can be found in just about any neuroscience or anatomy textbook. Such straightforward language can leave the impression that the contribution of the cerebellum to behavior is minimal and clearly defined, relegated purely to abstract tasks such as tracing a line. However, generating a movement that is both 'smooth' and 'continuous' is not as trivial as it seems. For a motor action to be both 'smooth' and 'continuous,' its performer must be able to anticipate and correct for any potential errors, either externally or internally generated, without altering the trajectory of the movement itself. Additionally, the movement must be effective and accurate in often ever changing environments. Consider the ballet dancer who produces graceful and effortless movements no matter the venue, costume, or state of her pointe shoes (all of which will vary considerably from rehearsal to the stage). During a performance, she will be required to make numerous corrective movements in order to maintain her balance and control, but a well-trained ballerina will implement those corrections so well that they are imperceptible to the average audience member. The complexity of neural control of smooth, continuous movement is evident in the fact that despite major progress in computer science and engineering, even the most advanced robotics fail to replicate the coordinated movements that most humans accomplish with relative ease. Thus, while the

role of the cerebellum in behavior is often reduced to a simple, one sentence description, the functions to which the cerebellum contributes are critical for everyday life.

While understanding the mechanisms by which the cerebellum controls movement is of course essential for the treatment of cerebellar disease, its role in optimizing behavior is also of relevance to fields such as robotics, neural prosthetics, and other brain computer interfaces. However, lacking is a characterization of how information relevant to motor control is processed by cerebellar neurons. Of major interest is the contribution of Purkinje cells, the primary output neurons of the cerebellar cortex. These cells are unique in that they exhibit two functionally different activity modalities: the complex spike (CS), resulting from a powerful depolarization by climbing fiber activation, and the high frequency simple spikes (SSs), which are modulated by input from over 100,000 parallel fibers. A major outstanding question in cerebellar physiology is the role of and interaction between SS and CS discharges, but no current hypotheses fully explain or are completely consistent with the spectrum of previous experimental observations. Thus, a crucial issue in understanding cerebellar function is the characterization of CS and SS activity during motor control.

Excerpts from this chapter have been published in *The Neuronal Codes of the Cerebellum* (Popa LS*, Streng ML*, Ebner TJ. "Signaling of predictive and feedback information in Purkinje cell simple spike activity." In The Neuronal Codes of the Cerebellum. Heck, D., Editor, Elsevier, New York, NY. 2015.)

Online control of movement

Effective motor control requires the continuous monitoring and correcting of errors in an ever-changing environment (Todorov and Jordan, 2002;Berniker and Kording, 2008;Shadmehr et al., 2010;Wolpert and Ghahramani, 2000). For example, taking a drink from a glass will require different motor commands depending on how full the glass is, but the central nervous system accomplishes this task with relative ease. Early views suggested that error correction is accomplished by closed-loop control, in which motor commands are updated by sensory feedback (Miall and Wolpert, 1996;Wolpert and Ghahramani, 2000;Shadmehr et al., 2010;Kawato, 1999). However, the inherent delays present in sensory feedback loops render such control subject to discontinuous, over-corrective movements. One highly relatable example of this sensation is the experience of trying to reach the desired water temperature in the shower (Shadmehr et al., 2010). The delay between a given turn of the temperature controller and the perceived change in temperature can often result in alternating between undesirably hot and cold water.

Additionally, error correction occurs more rapidly than (Flanagan and Wing, 1997) and even in the absence of sensory feedback (Shadmehr et al., 2010;Xu-Wilson et al., 2009;Golla et al., 2008;Wagner and Smith, 2008). This is particularly evident in the fine control of brief, ballistic eye movements known as saccades, which are too short in duration for visual feedback to be processed while the eyes are in flight (Keller and Robinson, 1971;Guthrie et al., 1983). In humans, repeated saccades to a visual target will

result in a decrease in the velocity of the eye movement over time. In these conditions, however, the motor command is altered in flight resulting in a prolonged movement of the eyes, allowing for an overall accurate movement towards the visual target (Xu-Wilson et al., 2009). Somehow, the central nervous system is able to anticipate a potential error caused by the decreased eye velocity and implement a corrective movement during the ongoing motor command, despite the fact that no visual feedback about eye position relative to the visual target is available. Similarly, in the context of the shower example described above, the desired temperature can only be reached effectively when one is able to predict a change in water temperature that will result from a given turn of the controller. Thus, these observations necessitate alternative mechanisms for error detection and correction.

One solution is that the central nervous system accomplishes this rapid correction for potential errors by predicting the consequences of motor commands using a forward internal model (Flanagan et al., 2003;Morton and Bastian, 2006;Robinson, 1975;Xu-Wilson et al., 2009;Maschke et al., 2004;Shadmehr et al., 2010;Imamizu et al., 2000;Diedrichsen et al., 2005). The forward internal model receives information about the current state as well as an efference copy of a motor command, using the two to estimate a prediction as to the outcome of that motor command. If the predicted sensory consequences are incongruent with the behavioral goal, a corrective movement is implemented prior to the sensory feedback of the actual movement itself. The ability of the central nervous system to compute and integrate predictions into behavior is crucial

for effective interaction with the world. For example, consider the common procedure of making a right-hand turn at a red light when driving. If there are cars approaching from the left on the intersecting street, it is necessary for the driver to make a prediction as to whether the time it takes the approaching car to enter the intersection exceeds that which is required to complete the necessary motor commands (e.g., rotating the steering wheel to the right, pressing the gas pedal, etc) for a right hand turn. If not, it would be safest to wait until the oncoming car passes through to make the turn. If so, then the driver can successfully make the right turn on red. In this example, relying on the delayed sensory feedback alone would be woefully insufficient when considering the potential consequences of a poorly executed turn into traffic.

While the feedforward predictions generated by a forward internal model are helpful for familiar behaviors, a crucial aspect is the ability to adapt to changing conditions and novel environments and alter predictions accordingly. One mechanism by which this adaptation can be achieved is by comparing the feedforward predictions to the actual sensory consequences of the movement. This integration of prediction and feedback, known as a sensory prediction error, serves as a measure of accuracy used both to improve subsequent predictions and guide future actions. Extensive evidence suggests that humans use sensory prediction errors, particularly during learning and adaptation (Wallman and Fuchs, 1998;Noto and Robinson, 2001;Mazzoni and Krakauer, 2006;Shadmehr et al., 2010). Although other error-related signals such as the actual corrective movements (Kawato, 1996;Miles and Lisberger, 1981), or sensory feedback at

the end of a movement contribute (Magescas and Prablanc, 2006;Cameron et al., 2010), sensory prediction errors appear to have a dominant role in controlling movement and motor learning (Held and Freedman, 1963;Wolpert and Ghahramani, 2000;Izawa and Shadmehr, 2011;Mazzoni and Krakauer, 2006;Gaveau et al., 2014;Taylor and Ivry, 2012;Shadmehr et al., 2010).

Cerebellum as a candidate for the forward internal model

While extensive evidence suggests that the central nervous system acquires and implements forward internal models in order to achieve effective motor control, the mechanisms by which this is accomplished remain unknown. The cerebellum has long been implicated in control of movement, beginning in part with Dr. Gordon Holmes' studies on World War I soliders with damage to the cerebellum, which was somewhat common due to insufficient helmet coverage of the skull overlying the cerebellum and visual cortex. Dr. Holmes observed that patients with cerebellar damage exhibited hypotonia and disorders of voluntary movement (Holmes, 1939). More recent studies have demonstrated that patients with cerebellar damage often have difficulties adapting to repeated disruptions of movement, suggesting a failure to compensate for predictable errors (Maschke et al., 2004;Smith and Shadmehr, 2005). These findings raise the possibility that the cerebellum plays a role in implementing forward internal models. In support of this, disruption of cerebellar activity by transcranial magnetic stimulation results in inaccurate reaches towards a target (Miall et al., 2007). During this task, subjects were instructed to make a reach towards and intercept a moving target on a

screen. Intriguingly, in trials in which the stimulation was applied, the subjects' reaches would have been accurate if made at earlier time points (e.g. arm position prior to stimulation onset). These results suggest that disrupting cerebellar activity impaired the generation of internal predictions, requiring the motor commands be planned and initiated using delayed sensory feedback information about arm position.

In addition to its role in generating feedforward predictions about movements, substantial clinical evidence implicates the cerebellum in processing sensory prediction errors during adaptation. For example, one task in which accuracy is highly dependent on sensory prediction error-driven adaptation is throwing an object towards a visual target. Once we take aim and throw an object, like a dart towards a dart board, the trajectory can't be altered in flight. Accuracy can only be improved by comparing the outcome of the throw to where we originally intended the dart to land, and then adjust subsequent throws accordingly. Flexibility is crucial in tasks such as this, as motor commands will differ based on how far away the target is or the weight of the object being thrown. Sensory prediction error can also be artificially induced by subjecting a participant to prism goggles that shift the visual field to the left or right. Initially, the subject will exhibit errors in the same direction of the visual transformation. After repeated throws, and thus exposure to sensory prediction error, however, the subject will learn to correct for this visual field shift (Tseng et al., 2007). That the resulting adaptation is sensory prediction error dependent is evident immediately after the prism goggles are removed. Instead of producing accurate throws, subjects will make errors in the opposite direction of the

visual transformation. This suggests that participants are not merely making a cognitive strategy adjustment, but rather updating their motor commands based on previous experience. Importantly, patients with damage to the cerebellum do not exhibit the same adaptation and after-effects. Even after repeated throws, they fail to adapt to the visual transformation induced by prism goggles (Tseng et al., 2007). However, after removal of the goggles, the patients return to baseline performance, indicating the sensory prediction error induced by the prism goggles has not been integrated into their subsequent motor commands (Tseng et al., 2007).

Numerous other studies also support the hypothesis that the cerebellum serves as a forward internal model and processes sensory prediction errors (Wolpert et al., 1998;Shadmehr et al., 2010;Pasalar et al., 2006;Shadmehr and Krakauer, 2008;Kawato and Wolpert, 1998). As described above, saccades are too brief in duration to allow for sensory input in flight (Keller and Robinson, 1971;Guthrie et al., 1983), and thus must be controlled by internal, sensory prediction error-mediated mechanisms (Shadmehr et al., 2010;Chen-Harris et al., 2008;Robinson, 1975). Patients with cerebellar damage, including those with spinocerebellar ataxia type 6 that primarily results in Purkinje cell degeneration, are unable to adapt to variability in saccade motor commands (Xu-Wilson et al., 2009;Golla et al., 2008). In healthy subjects, increases in cerebellar activation are observed during errors (Diedrichsen et al., 2005;Ide and Li, 2011;Imamizu et al., 2000), such as the divergence between movement goal and the actual consequences induced by an unexpected force field (Schlerf et al., 2012). In a reaching experiment, healthy

subjects given an explicit instruction on how to compensate for a visuomotor rotation showed a gradual decay in performance consistent with an implicit motor adaptation process driven by sensory prediction errors (Mazzoni and Krakauer, 2006). In a similar experiment, patients suffering from spinocerebellar ataxia exhibited an attenuated reduction in performance compared to the controls (Taylor et al., 2010), suggesting the cerebellum is required for processing of the sensory prediction errors. Together, these results strongly implicate the cerebellum in the generation and use of sensory prediction errors in motor adaption.

Evidence for cerebellar processing of sensory prediction errors also extends to the sensory domain. Increased cerebellar activation occurs with omission of an expected somatosensory stimulus (Tesche and Karhu, 2000). On a single cell level, neurons in the cerebellar nuclei, the targets of Purkinje cells, encode temporal aspects of stimulus omission (Ohmae et al., 2013). Clearly, there is a need to understand how sensory prediction errors are represented in the firing of cerebellar neurons, but the mechanisms by which sensory prediction error is encoded on the cellular level remain unknown.

Anatomy and physiology of the cerebellar cortex

The cerebellar cortex exhibits relatively homogeneous cytoarchitecture. In particular, the cortex is characterized by primary output neurons known as Purkinje cells. Purkinje cells of the cerebellar cortex receive two main inputs, climbing fibers and parallel fibers (Eccles et al., 1967;Ito, 1984). The dendritic tree of a mature Purkinje cell receives

extensive glutamatergic synaptic input from a single climbing fiber originating from the inferior olive. Climbing fiber activation of a Purkinje cell produces a powerful post-synaptic depolarization, which generates Ca^{2+} spikes throughout the entire dendritic tree and a CS, which consists of a large Na^{+} somatic spike and a burst of smaller spikelets (Llinas and Sugimori, 1980;Davie et al., 2008). Parallel fibers provide the second main input with over 100,000 individual glutamatergic synapses on each Purkinje cell. Parallel fibers produce small, post-synaptic excitatory responses in Purkinje cells and modulate the intrinsic SS discharge (Raman and Bean, 1997). CS discharge occurs at a low frequency (~0.5-2.0/sec) compared to the high frequency SS discharge (~50-150/sec).

Climbing fiber discharge in the cerebellar cortex

The primary hypothesis has been that climbing fiber input provides motor error signals. (Gilbert and Thach, 1977;Kitazawa et al., 1998;Ito, 2000;Ito, 2013;Stone and Lisberger, 1986;Kawato and Gomi, 1992). This view is a central tenet of the Marr-Albus-Ito hypothesis in which long-term depression (LTD) of parallel fiber-Purkinje cell synapse results from co-activation of parallel fiber and climbing fiber inputs (Marr, 1969;Albus, 1971;Ito and Kano, 1982). This framework for understanding the role of the climbing fiber input and CSs is supported by numerous studies. CS discharge is coupled with errors during saccades, smooth pursuit and ocular following (Barmack and Simpson, 1980;Graf et al., 1988;Kobayashi et al., 1998;Medina and Lisberger, 2008;Soetedjo and Fuchs, 2006). Undoubtedly, CS discharge in response to retinal slip provides one of the strongest demonstrations of error encoding (Graf et al., 1988;Kobayashi et al.,

1998;Barmack and Shojaku, 1995). For example, CS modulation during a phenomenon known as the ocular following response, or the reflexive eye tracking movement evoked by the motion of a visual stimulus, has been extensively characterized. During the ocular following response, accurate tracking of the visual stimulus requires generating motor commands to smoothly move the eyes at the same velocity as the stimulus in order to stabilize the image on the retina. Inaccurate motor commands will result in the movement of the stimulus across the retina, an eye movement error referred to as retinal slip. In the vermis, CS firing rates are correlated linearly with retinal slip error during the ocular following response, such that increases in retinal slip velocity are associated with increases in CS discharge (Kobayashi et al., 1998). During reaching, CSs are modulated by unexpected loads (Gilbert and Thach, 1977), movement redirection (Kim et al., 1987), and end point errors (Kitazawa et al., 1998). Additionally, CS discharge is also associated with perturbations applied during locomotion (Kim et al., 1987;Lou and Bloedel, 1986;Andersson and Armstrong, 1987).

However, other studies found limited support for the classical view, suggesting that error processing in the cerebellum is more multi-faceted than originally proposed. For example, as described above, CS discharge is associated with end point errors during saccades. One method by which saccade end point errors can be experimentally induced is by changing the location of a target to which the subject has been instructed to make a saccade while the eyes are in flight (Catz et al., 2005). Over time, the subject will learn to predict the change in target location, prolonging the motor command such that the eyes

are able to successfully reach the target end point. During this type of saccadic adaptation, the classical error encoding hypothesis predicts that CSs would be highly modulated early during adaptation, when errors are maximal. As the animal learns to predict the change in target position and errors are reduced, the CS modulation should decrease. However, the opposite relationship is observed: CS discharge in the oculomotor vermis increases late in adaptation when errors have decreased greatly (Catz et al., 2005;Dash et al., 2010;Prsa and Thier, 2011).

Similarly, perturbations and performance errors during reaching in cats do not evoke responses in inferior olive neurons, the origin of the climbing fiber projection (Horn et al., 1996). CS modulation could not be related to direction or speed errors during reaching (Fu et al., 1997b;Ebner et al., 2002). Even when climbing fiber input is associated with errors during reaching movements, the CSs occur only in a small percentage of trials (Ojakangas and Ebner, 1994;Kitazawa et al., 1998). A similar dissociation between CS modulation and error amplitude occurs during reach adaptation to a visuo-motor perturbation (Ojakangas and Ebner, 1992). In the oculomotor vermis, CS error modulation with saccades appears limited to direction errors, and whether they encode error magnitude is unclear (Soetedjo and Fuchs, 2006;Soetedjo et al., 2008a). Therefore, the precision, specificity and extent to which CSs encode error information remains unknown.

Moreover, the motor learning/error hypothesis does not account for spontaneous CS firing and the observation that removal of climbing fiber input results in a dramatic change in the SS firing pattern and a cerebellar-like motor disorder (Llinas et al., 1975;Horn et al., 2013;Colin et al., 1980;Montarolo et al., 1982;Cerminara and Rawson, 2004). Therefore, climbing fiber input must play a role in on-line cerebellar function and motor control. Several hypotheses on CS contribution to real time motor control emphasize short-term changes in Purkinje cell excitability. The "gain change" and "bi-stability" hypotheses suggest CSs control the responses of a Purkinje cell to parallel fiber inputs (Ebner et al., 1983) and switch between 'up' and 'down' SS firing states (Loewenstein et al., 2005;Yartsev et al., 2009;McKay et al., 2007), respectively. Also, during behavior CSs and SSs exhibit a reciprocal firing pattern that is mediated by climbing fiber input (Graf et al., 1988;Simpson et al., 1995;Yakhnitsa and Barmack, 2006;Badura et al., 2013). The rhythmicity and synchronicity of climbing fibers suggests a role in movement timing independent of their action on SS firing (Welsh et al., 1995;Lang et al., 1999;Llinas, 2013). However, in the awake, behaving animal the evidence for strong CS rhythmicity or that CSs act to control gain or bi-stability is controversial (Simpson et al., 1995;Engbers et al., 2013;Schonewille et al., 2006;Keating and Thach, 1995). Therefore, lacking is a comprehensive understanding of climbing fiber function and its role in cerebellar information processing.

One potentially unifying hypothesis is that the continuous climbing fiber input to the cerebellar cortex acts to control the sensitivity of Purkinje cells to particular aspects of

the movement. Similar to the gain change hypothesis, climbing fiber discharge may increase or decrease the SS sensitivity, but manifest as a change in the information present in the SS discharge rather than the overall firing rates This would also provide a framework for both spontaneous and evoked climbing fiber discharge, with the spontaneous CSs acting to maintain Purkinje cell sensitivity, and the evoked CS firing tuning Purkinje cell sensitivity with respect to external changes during movement.

However, it is still unclear which aspects of movement best modulate CS activity. As described above, CSs are not invariably activated by errors in movement. In a recent study in which monkeys adapted to a transient mechanical perturbation during reach, the rather weak CS modulation evoked could not account for either the learning or the changes in SS firing (Hewitt et al., 2015). Intriguingly, the majority of CS modulation occurred at movement onset rather than the timing of the limb perturbation (and thus error), suggesting a role for climbing fiber activity in motor control beyond error processing. One potential hypothesis is that rather than serving as a pure error 'event' signal, CS firing is modulated linearly with behavior, with the probability of CS firing increasing as the magnitude of the behavioral change increases. In this view, CS firing could be evoked by both movement kinematics and performance errors. Finally, the observation of increased CS firing at the timing of movement onset also suggests a role for CS modulation as a predictive rather than feedback signal.

Purkinje cell simple spike discharge

The SS discharge of Purkinje cells modulates with a host of movement-related parameters. Kinematic signaling in the SS discharge has been reported across a wide range of motor behaviors involving different effectors. During arm movements, the SS firing of Purkinje cells in the intermediate zone of lobules IV-VI of awake monkeys is correlated with limb position, direction, speed, and movement distance (Harvey et al., 1977;Thach, 1970;Fortier et al., 1989;Fu et al., 1997a;Coltz et al., 1999;Roitman et al., 2005;Pasalar et al., 2006;Marple-Horvat and Stein, 1987;Mano and Yamamoto, 1980;Hewitt et al., 2011). The importance of kinematic signaling in the cerebellar cortex is evident in that limb position and velocity are found in the SS discharge during passive limb movements in anesthetized or decerebrate cats and rats (Valle et al., 2000;Kolb et al., 1987;Giaquinta et al., 2000;Rubia and Kolb, 1978). During the vestibulo-ocular reflex (VOR), smooth pursuit, ocular following or saccades, eye movement kinematics have been documented in the SS activity of Purkinje cells in the floccular complex and oculomotor vermis (Stone and Lisberger, 1990a;Shidara et al., 1993;Medina and Lisberger, 2009;Gomi et al., 1998;Dash et al., 2012;Laurens et al., 2013;Miles et al., 1980a;Miles et al., 1980b;Lisberger et al., 1994).

Purkinje cell SS discharge has also been associated with parameters related to task performance. For example, induced dissociation between cursor and hand movement by coordinate transformation shows that in some Purkinje cells, SSs encode cursor position independent of hand kinematics (Liu et al., 2003). SS discharge modulates with target motion during both reaching and tracking tasks (Miles et al., 2006;Cerminara et al.,

2009;Ebner and Fu, 1997). These observations suggest that, in addition to a robust encoding of movement parameters, SS discharge also contains representations of task-specific parameters relevant to the behavioral goal.

The broad range of signals observed in the discharge of Purkinje cells makes constructing a unified theory of the cerebellar cortical function elusive. One theoretical framework that can account for the different signals is that Purkinje cells serve as the output of the forward internal model (Miall and Wolpert, 1996;Pasalar et al., 2006;Shadmehr et al., 2010;Kawato and Wolpert, 1998). If Purkinje cells are the output of a forward model, multiple types of behavioral signals are integrated to predict the consequences of movement commands. In this view, information about movement kinematics, kinetics, timing, and errors are all relevant to generating predictions about the upcoming motor behavior. Consistent with a forward internal model, SS discharge tends to lead effector kinematics during movements (Roitman et al., 2005;Marple-Horvat and Stein, 1987;Gomi et al., 1998;Shidara et al., 1993;Stone and Lisberger, 1990a;Fu et al., 1997a;Dash et al., 2013;Hewitt et al., 2011). The SS modulation leading kinematics of limb movements is independent of the muscle forces necessary to complete a movement. This was demonstrated during a circular tracking task, in which rhesus macaques were trained to track a circularly moving target with a manipulandum under normal conditions and with both viscous and elastic forces applied to the manipulandum (Pasalar et al., 2006). This resulted in limb movements that were identical in kinematics but differed significantly in their dynamics. Importantly, the SS modulation did not significantly

differ in any of the conditions, indicating that the output of Purkinje cells faithfully encodes the predicted kinematics of a movement, consistent with the output of a forward internal model.

Encoding of predictive and feedback information in the cerebellar cortex

There is growing evidence to suggest that Purkinje cell SS discharge also encodes error feedback information. For example, the changes in SS output following smooth pursuit adaptation appear sufficient to drive learning (Kahlon and Lisberger, 2000). In the posterior vermis, SS firing provides a neural correlate of retinal slip (Kase et al., 1979). Cerebellar-dependent VOR adaptation can be driven by instructive signals in the SS firing in the absence of climbing fiber input (Ke et al., 2009). Increasing VOR gain appears dependent on CS-driven LTD while gain decrease depends on non-CS-driven long-term potentiation (LTP) mechanisms (Boyden et al., 2004;Boyden and Raymond, 2003). Moreover, while optogenetic activation of climbing fibers can induce VOR adaptation (Kimpo et al., 2014), similar findings result from optogenetically driven increases in SS discharge (Nguyen-Vu et al., 2013). SS discharge modulates with trial success or failure in a reaching task (Greger and Norris, 2005), and with direction and speed errors during manual circular tracking (Roitman et al., 2009). Together, these observations suggest a need for reevaluating the classical hypothesis that CS discharge is the only or primary channel carrying motor error information in the cerebellum. If Purkinje cell firing represents the output of a forward internal model, a major outstanding

question is whether the SS firing contains the predictive and feedback information necessary for the computation of sensory prediction error.

Most previous studies relied on highly predictable tasks, confounding predictions of motor commands with trial planning, and generating stereotypical and time-locked movements that result in highly correlated kinematic parameters (Paninski et al., 2004;Ebner et al., 2011). Also, task performance and errors are typically highly correlated with kinematics. These constraints limit a thorough understanding of the kinematic and error signals in cerebellar neurons. Pseudo-random tracking allows for the examination of the interactions among CS discharge, SS firing, and behavior in which the correlations between parameters or learning are reduced. Accurate performance on this task requires continuously monitoring the salient behavioral parameters and adjusting for mismatches in hand movement relative to target movement (Hewitt et al., 2011;Popa et al., 2012). This task subverts overly learned, stereotypic behaviors, such as reaching and saccades, in which movement parameters are correlated (Paninski et al., 2004;Soetedjo et al., 2008b). Additionally, tracking a pseudo-randomly moving target is challenging and requires continuous evaluation of motor performance and implementation of corrective movements.

During pseudo-random tracking, both kinematic and performance error signaling were evaluated in the SS firing of Purkinje cells (Hewitt et al., 2011;Popa et al., 2012). The kinematic parameters included position (X and Y), velocity (V_x and V_y) of the arm/hand.

Performance errors were defined as the divergence between the current movement goal, approximated by the target center, and the consequences of the motor commands, indicated by cursor movement. Performance errors evaluated included cursor position relative to the target center (XE and YE). The error parameters provide a continuous measure of the difference between cursor movement relative to the target center rather than discrete errors, such as when cursor strays outside the target boundary. Not only are these "natural" measures of motor performance for this tracking task, the behavior shows that the monkeys strive to minimize these errors and maintain the cursor in the target center (Hewitt et al., 2011;Popa et al., 2012).

Temporal linear regressions were used to fit the SS firing to the behavioral parameters to determine the lead/lag (τ-value) between Purkinje cell activity and each parameter (Hewitt et al., 2011;Popa et al., 2012). Although this type of regression analysis has been used previously (Ashe and Georgopoulos, 1994;Roitman et al., 2009;Medina and Lisberger, 2009;Gomi et al., 1998), a novel refinement was incorporated such that for each parameter the SS variability associated with the other kinematic and error parameters was removed. This was done for each parameter by first determining the firing residuals from a multi-linear model of SS firing that included the kinematic and error parameters not being evaluated. The firing residuals were then regressed against the parameter of interest, determining the coefficient of determination (R^2) and regression coefficient (βs) as functions of time independent of other parameters. In a majority of Purkinje cells recorded, SS discharge encodes a dual representation of errors at both lead

and lag timing. The representations have opposing effects on the SS firing, consistent with the predictive and feedback signals necessary to compute sensory prediction errors (Popa et al., 2012;Popa et al., 2014). Across the population, the SS firing can be used to reconstruct the behavior by inverting the linear regression equation, indicating that the SS firing contains a highly accurate representation of task performance. However, these correlations between SS firing and behavior were observed during optimal conditions in highly trained animals. Thus, it is necessary to evaluate whether disruptions of either predictive or feedback information about performance errors and kinematics also has appropriate effects on the SS firing.

Hypotheses and rationale

As described above, the cerebellum is essential for online control of movement and extensive evidence suggests that it serves as a forward internal model. The SS discharge of Purkinje cells and their sole climbing fiber afferents modulate with a host of movement related parameters, but a full characterization of their interactions and roles in motor control remains elusive. While previous research has suggested a role of SS firing in encoding predictive and feedback information about performance errors during online motor control (Popa et al., 2012;Popa et al., 2014), the influence of climbing fiber discharge remains unclear. Therefore, we first evaluated the roles of both spontaneous and evoked climbing fiber discharge during our online motor control task, pseudo-random tracking. Pseudo-random tracking also provided the opportunity to investigate CS modulation in a task in which both the kinematic and error workspaces are more

extensively explored. We also tested whether the SS modulation with kinematics and performance errors is consistent with the predictive and feedback information from a forward internal model by introducing novel manipulations of visual feedback and characterizing the effects on SS and CS firing. The experiments and results are described in Chapters 2-4.

Hypothesis 1: CS discharge tunes the sensitivity of SS firing to behavior by altering the SS encoding of performance errors and kinematics during pseudo-random tracking

Hypothesis 2: CS firing is also modulated by kinematics and performance errors, but rather than being evoked by error 'events' as has been described previously, it is linearly modulated with behavior.

Hypothesis 3: SS modulation during online motor control encodes the predictive and feedback components of sensory prediction error.

CHAPTER 2: CLIMBING FIBERS CONTROL PURKINJE CELL REPRESENTATIONS OF BEHAVIOR

Introduction

The distinctive morphological and physiological properties of the climbing fiber-Purkinje cell synapse suggest a unique functional role in the cerebellum (Eccles et al., 1967;Ito, 1984). Climbing fiber afferents originate solely from the inferior olive and provide one of two main inputs to the cerebellar cortex. Firing at low rates (~0.5-2.0/sec), a climbing fiber produces a powerful depolarization of a single Purkinje cell through hundreds of glutamatergic synapses along the proximal dendritic tree. This results in a complex spike (CS) consisting of a large Na^+ somatic spike accompanied by a burst of smaller spikelets as well as Ca^{2+} spikes throughout the entire dendritic tree (Llinas and Sugimori, 1980;Davie et al., 2008). In contrast, a Purkinje cell receives input from over 100,000 parallel fibers that modulate the high frequency simple spike (SS) discharge.

Requisite for elucidating the principles of cerebellar function is an understanding of the interaction between CS discharge and SS firing. Much attention has focused on the long-term effect of CS discharge on SS firing. In the Marr-Albus-Ito hypothesis, long-term depression (LTD) of parallel fiber-Purkinje cell synapses resulting from co-activation of parallel and climbing fiber inputs underlies motor learning (for reviews see(Marr, 1969;Albus, 1971;Ito and Kano, 1982)). In this context, CSs are evoked by errors and provide a teaching signal that modifies subsequent SS activity to correct the behavior

(Gilbert and Thach, 1977;Kitazawa et al., 1998;Yang and Lisberger, 2014;Medina and Lisberger, 2008). While substantial evidence supports a role for climbing fibers in error signaling and motor learning, CSs are not invariably activated by errors (for review see(Popa et al., 2015)). Also, CSs are not essential for cerebellar motor learning (Nguyen-Vu et al., 2013;Ke et al., 2009;Hewitt et al., 2015), SS discharge carries robust error signals (Popa et al., 2012), and there are significant challenges to the role of cerebellar LTD in motor learning (Schonewille et al., 2011).

Moreover, the motor learning/error hypothesis does not account for spontaneous CS firing and the observation that removal of climbing fiber input results in an immediate and dramatic change in the SS firing pattern and a cerebellar-like motor disorder (Llinas et al., 1975;Horn et al., 2013;Colin et al., 1980;Montarolo et al., 1982;Cerminara and Rawson, 2004). Also, spontaneous CSs have been proposed to perturb movements as a probe for initiating plasticity (Bouvier et al., 2016). Therefore, climbing fiber input must play a role in on-line cerebellar function and motor control. Several hypotheses on CS contribution to real time motor control emphasize short-term changes in Purkinje cell excitability. The “gain change” and “bi-stability” hypotheses suggest CSs control the responses of a Purkinje cell to parallel fiber inputs (Ebner et al., 1983) and switch between ‘up’ and ‘down’ SS firing states (Loewenstein et al., 2005;Yartsev et al., 2009;McKay et al., 2007), respectively. Also, during behavior CSs and SSs exhibit a reciprocal firing pattern that is mediated by climbing fiber input (Graf et al., 1988;Simpson et al., 1995;Yakhnitsa and Barmack, 2006;Badura et al., 2013). The

rhythmicity and synchronicity of climbing fibers suggests a role in movement timing independent of their action on SS firing (Welsh et al., 1995;Lang et al., 1999;Llinas, 2013). However, in the awake, behaving animal the evidence for strong CS rhythmicity or that CSs act to control gain or bi-stability is controversial (Simpson et al., 1995;Engbers et al., 2013;Schonewille et al., 2006;Keating and Thach, 1995). Therefore, lacking is a comprehensive understanding of climbing fiber function and its role in cerebellar information processing.

This study evaluates the modulation of SS representations by climbing fiber input. To obtain a comprehensive characterization of the interactions among CS discharge, SS firing and behavior, we tested this question in a pseudo-random tracking task. The key observation is that CSs are followed rapidly by large increases and decreases in the signals encoded by the SS discharge. These novel findings suggest the global depolarization of a Purkinje cell by climbing fiber input allows for a change in the information conveyed by the SS firing.

The content of this chapter has been published in the *Journal of Neuroscience* (Streng ML, Popa LS, Ebner TJ (2017) Climbing fibers control Purkinje cell representations of behavior. J Neurosci 37:1997-2009)

Materials and Methods

Behavioral and electrophysiological data were obtained from two rhesus monkeys (*Macaca mulatta*; female 6.3 kg age 15; male 6.8 kg age 8) during normal daytime hours. Animals were housed in single cages and kept on a 12hr light/dark cycle. All animal experimentation was approved by the Institutional Animal Care and Use Committee of the University of Minnesota and conducted in accordance with the guidelines of the National Institutes of Health.

Random tracking

This study utilized a previously described pseudo-random tracking task (Hewitt et al., 2011;Popa et al., 2012;Paninski et al., 2004) and, therefore, the paradigm is only briefly detailed here. Two rhesus monkeys were trained to use a robotic manipulandum (InMotion²) that controls a cross-shaped cursor to track a circular shaped target (2.5 cm diameter) on a computer screen (Fig. 1A). The paradigm started with an initial hold inside a stationary target for a random period of time (1000 – 2000 msec). The initial target position on the screen was also random. Next, the target moved for 6-10 s along a trajectory selected randomly from 100 trajectories defined *a priori*. Pseudo-random target paths were generated from a sum of sine waves. Target speed was randomly varied so that the average speed was approximately 4 cm/s and conformed to the two-thirds power law (Viviani and Terzuolo, 1982;Lacquaniti et al., 1983). The trajectories were low-pass filtered and selected to avoid sharp turns and large changes in speed, and ended with a final hold period of at least 1000 msec. The paradigm required that the monkey maintain the cursor within the target, and allowed only brief excursions outside the target (<500

msec). Pseudo-random tracking has several advantages compared to other tasks including providing more comprehensive and uniform coverage of parameter workspaces and dissociating kinematic from error parameters (Paninski et al., 2004;Hewitt et al., 2011). Hand (X and Y, based on cursor position) and target (X_{tg}, Y_{tg}) position were sampled at 200 Hz. Cursor velocity (VX, VY) was derived by numerical differentiation and position error (XE, YE) was defined as the difference between cursor and target positions (see Fig. 1B).

Surgical procedures, electrophysiological recordings and data collection

Head restraint hardware and a recording chamber targeting lobules IV-VI of the intermediate and lateral cerebellar zones were chronically implanted over the ipsilateral parietal cortex in each animal using aseptic techniques and full surgical anesthesia. The positions of the electrodes were confirmed by radiographic imaging techniques that combined a CT scan of the skull with an MRI of the cerebellum (Hewitt et al., 2011). After full recovery from chamber implantation surgery, extracellular recordings were obtained during normal daytime hours using Pt-Ir electrodes with parylene C insulation (0.8-1.5 MΩ impedance, Alpha Omega Engineering, Nazareth, Israel). Purkinje cells in lobules IV-VI of the intermediate and lateral cerebellar zones were targeted following previously established methods.(Hewitt et al., 2015) After conventional amplification and filtering (30 Hz-3 kHz band pass, 60 Hz notch), SSs were discriminated online using the Multiple Spike Detector System (Alpha Omega Engineering, Nazareth, Israel). Resulting spike trains were digitized and stored at 1 kHz. The raw electrophysiological data was

also digitized and stored at 32 kHz. CSs were sorted offline using a combination of software and manual confirmation (Hewitt et al., 2015). Using the fractional interval method, the SS trains were transformed to a continuous firing rate in 5 msec bins. Importantly, the SS firing rates were not filtered in order to minimize autocorrelation artifacts. For display and analyses, the mean firing rate for each trial was subtracted from the instantaneous firing rate. The behavioral parameters were filtered (low pass (4^{th} order Butterworth with a 5 Hz cut-off). The analyses evaluating the relation among the SS firing and the behavioral variables were restricted to the tracking period.

Linear modeling of simple spike firing irrespective of complex spike occurrence

The first analysis determined for each Purkinje cell the presence and timing of kinematic and error signals in the SS firing during tracking irrespective of the time of CS discharge. This involved fitting the SS firing to each kinematic and error parameters using the temporal linear regressions on firing residuals, as described previously (Popa et al., 2012;Hewitt et al., 2015). For each Purkinje cell this analysis was performed for the tracking periods across all trials and is referred to as the non-CS aligned linear regression. For a given parameter (e.g. VX), SS variability associated with the rest of the parameters was first removed by determining the firing residuals from a multi-linear model that fitted the SS firing to the other kinematic and error parameters (e.g., X,Y,VY, XE and YE)(see (Popa et al., 2012)). The resulting SS firing residuals were regressed against the individual parameters at 20 msec intervals from -500 to 500 msec, determining the R^2 and regression coefficient (β) temporal profiles as functions of the lead/lag (τ-value). The

significance of the R^2 at each τ-value was determined against a noise distribution defined as the mean ± 3SD of the R^2 values obtained from 100 repeats of the same regression analysis performed on firing and behavioral data uncoupled through random trial shuffling. For each parameter, significant correlations were defined if a local maximum of the R^2 profile at either predictive or feedback timings exceeded the trial shuffled noise level, and the timing (τ-value) of the peak lead and/or lag was determined (Fig. 1C).

Complex spike-aligned analysis of simple spike encoding

CS-coupled changes in encoding were determined for each significant SS representation identified by the non-CS aligned linear regression described above. Next the SS firing and the behavioral data were aligned to the times of CS firing for the entire recording session (i.e., all trials) as diagramed in Fig. 1D1. Then the behavioral parameter was shifted relative to the SS firing by the peak lead or lag (τ) determined in the non-CS aligned regression analysis (Fig. 1D2). To visualize and quantify the CS-coupled changes, the data was partitioned into 64 (8 x 8) equal bins of 0.5 cm ranging from -2 to 2 cm for XE and YE, 3.0 cm/sec ranging from -12 to 12 cm/s for VX and VY, and 6 cm from -6 to 6 cm for X and Y, and averaged using a sliding window of 200 msec in 20 msec intervals. The CS-aligned SS firing was averaged in these bins. This partitioning allowed construction of SS firing maps aligned on all CS occurrences at each time interval for position, velocity and position error, respectively (see Fig. 2A), and was also used for the CS-aligned regression analysis described below.

Using this shifted and partitioned behavior, the SS firing was regressed against the behavioral parameter using the same sliding window of 200 msec in ten 20 msec intervals to quantify the SS encoding strength relative to CS occurrence (Fig. 1D3). To account for the sliding window, the first interval for -200 msec in the pre-CS period was obtained by regressing the firing with behavior data from aligned -400 to -200 msec, and the final pre-CS interval at -20 msec using the data aligned from -220 to -20 msec. The same procedure was used for the post-CS data, with the first post-CS step based on 20 to 220 msec to avoid the brief inactivation period after CS discharge and prevent any overlap between pre- and post-CS periods. The sliding window continued in 20 msec intervals, with the final post-CS interval using the data aligned from 200 to 400 msec. Because the first 20 msec interval following the CS was omitted, we elected to omit the 20 msec interval before the CS to balance the subsequent statistical testing of differences between the pre- and post-CS periods. Therefore, the pre- and post-CS regression analyses were each determined using > 10 sliding regression windows of 200 msec duration at 20 msec intervals. The CS-aligned regression analysis resulted in R^2 and β temporal profiles ranging from -200 to 200 msec before and after CSs for each significantly encoded behavioral parameter (bottom R^2 plots in Fig. 1D3). We also assessed whether changes in encoding occurred for parameters that were not significantly modulated based on the results of the non-CS aligned linear regression analysis. For these data, we preformed the same analysis except that the behavioral data was not shifted relative to the SS firing (i.e., τ of 0 msec).

The significance of the CS-coupled changes in encoding was determined by comparing the difference between mean R^2 pre- vs mean R^2 post-CS to a distribution of pre versus post R^2 changes obtained from 1000 CS shuffled R^2 profiles. The data for this CS-shuffled analysis were restricted to time periods that did not overlap with the window used for the CS-coupled regression analysis. The latter ensured that any random changes in encoding were not being driven by overlap with actual CSs. The analysis focused on identifying changes in the R^2 profile relative to the timing of CSs. While sharp transitions in SS encoding strength were tightly coupled to CS discharge, the time course to reach the peak change in R^2 ranged from 100 to 200 msec (for examples, see Fig. 2B and Fig. 4B). Thus, the mean differences in encoding were computed by collapsing the data across two different time windows: 100 msec pre-100 msec post (pre-CS window = -100:-20 msec, post-CS window =20:100 msec) CS and 200 msec pre-200 msec post CS (pre-CS window = -200:-20 msec, post-CS window = 20:200 msec). A CS-coupled change in encoding was determined to be significant if it was above mean ± 2SD of the CS-shuffled distribution for either the ± 100 msec or ± 200 msec windows. Importantly, the majority of significant encoding changes (>70%) met the criteria for significance at both the ± 100 msec and ± 200 msec windows.

For the representations with significant CS-coupled changes in encoding, we also quantified the changes in sensitivity by computing the difference between the absolute value of the mean post-CS β-values and the absolute value of the mean pre-CS β-values ($|\beta_{post}| - |\beta_{pre}|$). Positive changes indicate increases in sensitivity while negative changes

indicate decreases in sensitivity. Changes in sensitivity were determined using the time window that produced the significant change in encoding strength.

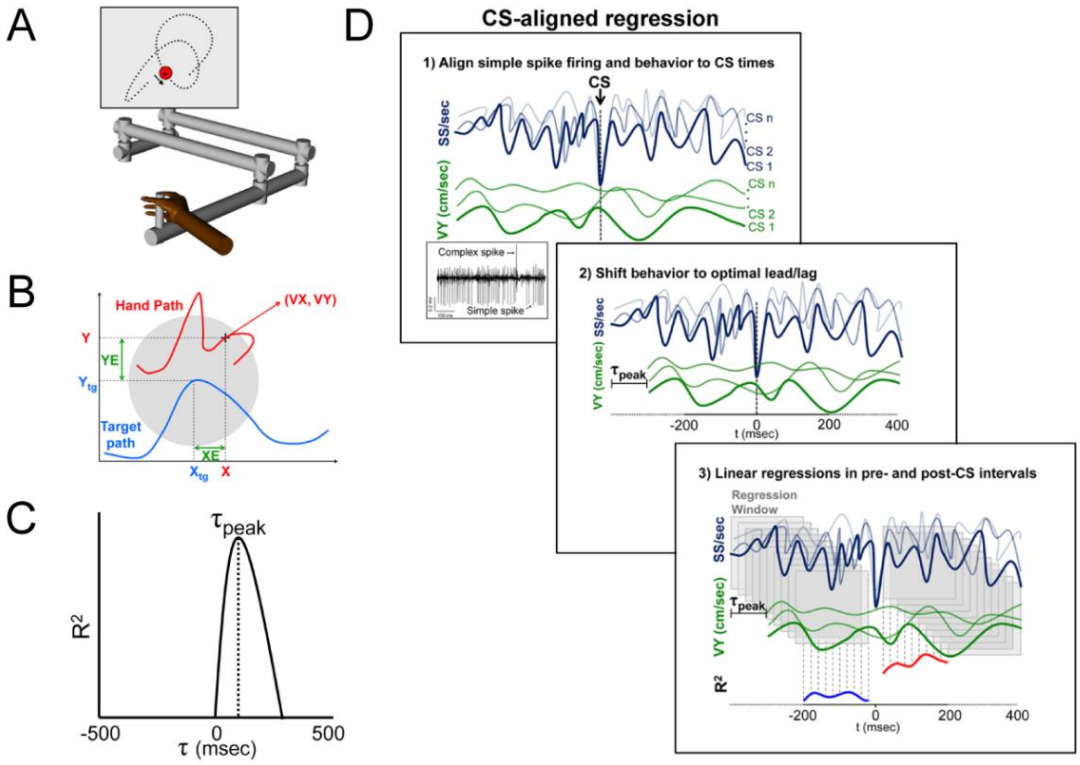

Figure 1: Experimental paradigm and regression analysis. A) Rhesus macaques use a robotic manipulandum to control a cross-shaped cursor to track a circular target (2.5 cm diameter) on a computer screen (Hewitt et al., 2011;Paninski et al., 2004;Popa et al., 2012). B) Kinematic parameters (X, Y, VX, VY) are based on cursor motion (red trace). Position error (XE and YE) is the difference between cursor (X, Y) and target center position (X_{tg}, Y_{tg}). C) Timing of SS signals encoding a parameter was based on the local maxima of the coefficient of determination (R^2) profile determined using the temporal linear regression analysis described previously(Popa et al., 2012). D1) Effects of CS discharge on the SS encoding was assessed by aligning the SS firing (dark blue) and the parameter (green) to CS occurrences. D2) Behavior was then shifted by the peak lead or lag (τ-peak) obtained from the non-CS aligned linear regression (C). D3) Linear regressions were performed 400 msec before and after CS discharge using a 20 msec step sliding window of 200 msec, generating pre (blue) and post (red) R^2 profiles that quantify encoding strength.

It needs to be emphasized that the temporal linear regression analysis used is highly sensitive to the coverage of the parameter workspace, which is minimal on the single CS level or over the small number of CSs that occur in a single trial compared to the non-CS aligned regression analysis. Therefore, a meaningful regression analysis on how the SS encoding changes for a single CS or trial was not possible. Instead, the regression analysis over all trials shows the average effect of the CS discharge on the signals in the SS firing.

Relationship between complex spikes and behavior

The relationship between CS firing and each behavioral parameter was assessed using CS spike triggered averaging. The average behavioral trace of each parameter was computed from 500 msec before to 500 msec after each CS occurrence in 20 msec intervals. We elected to use a ±500 msec time window to make certain we captured all significant changes in behavior both before and after CS discharge. The noise level was determined by randomly shuffling the inter-spike interval of CS times within a trial (ISI-shuffled, 50 repeats) and computing the mean and standard deviation of the ISI-shuffled CS-triggered average behavioral trace. For this analysis, we tested for peak changes in behavior relative to the time of CS firing instead of averaging across pre- and post-CS intervals. As such, we utilized a more stringent criterion for significance. CS-triggered average behavioral parameters with local minima or maxima exceeding a threshold of mean ± 3SD of the CS shuffled noise distribution were considered significant. The magnitude of the behavioral change and timing of the change relative to CS discharge were determined,

with negative times indicating behavioral changes occurring prior to and positive times indicating behavioral changes occurring after CS discharge.

Relationship between complex spikes and simple spike firing properties

The relationship between CS discharge and SS firing was assessed using three methods. For all three analyses described here, we evaluated changes in SS firing properties using both ±200 and ±500 msec windows relative to CS firing, with the post-CS window beginning after the mean + 1SD of the CS-induced inactivation period. Again, the rationale for using two time periods was to fully assess whether the SS firing changes in relation to the CS occurrence. One Purkinje cell was excluded from these analyses due to variability in the inactivation period that exceeded 1000 msec. However, removal of this Purkinje cell did not affect the analysis and conclusions, as this neuron did not exhibit any significant CS-coupled changes in SS encoding. First, we compared the mean SS firing pre- and post-CS to evaluate whether CS firing produced significant changes in SS firing rate across the population. Significant changes in SS firing across the population were assessed using Student's paired t-test ($p < 0.05$). Second, we assessed CS-coupled changes in SS firing rate for each Purkinje cell by comparing each 20 msec interval of CS-aligned SS firing in the post-CS interval to the mean ± 3SD of the CS-aligned SS firing in the pre-CS interval. Finally, to test for changes in SS firing variability, the Fano factor (Fano, 1947), defined as the ratio of variance over the mean, was calculated. Significant changes in the Fano factor before and after CS occurrence were evaluated for each Purkinje cell also using a paired t-test ($p < 0.05$).

Properties of complex spike discharge and the encoding changes

Additional analyses assessed the properties of the CS discharge in relation to the changes in SS encoding. The first of these analyses assessed whether the time course of the encoding changes can be attributed to CS discharge at t = 0 msec, rather than a combination of subsequent CSs. We addressed this by quantifying the number and probability of CS discharges in each bin for the ± 200 msec CS-aligned windows. Rhythmicity in CS discharge has been proposed as essential feature of CS function (Welsh et al., 1995;Lang et al., 1999;Llinas, 2013). To test for rhythmicity, the autocorrelation of the CS discharge was computed over a long time scale (-2000 to 2000 msec) to account for the low CS firing rates in a majority of Purkinje cells. Significance was determined by a change in correlation outside the mean ± 3SD of the autocorrelation computed from randomized CS timing (50 repeats). Additionally, the peak amplitudes of the autocorrelation in the 8-12 Hz range, the frequency of the intrinsic rhythmicity in CS firing, were compared to that of randomized CSs.

Results

Complex spikes modulate simple spike representations of kinematics and errors

Forty Purkinje cells were recorded from two rhesus macaques performing a visually guided, manual pseudo-random tracking task (Fig. 1A, B)(Hewitt et al., 2011;Popa et al., 2012). The overall goal of the analyses is to characterize the effect of CS discharge on the

motor signals present in SS firing, specifically on the encoding of position (X and Y), velocity (VX and VY) and position error (XE and YE). The first step in the analyses determined the significant SS representations and their optimal τ-values as identified by the non-CS aligned regression analysis (see Fig. 1C and Materials and Methods). Next, the SS firing and the behavioral data were aligned to the times of CS firing for the entire recording session (i.e., all trials) as diagramed in Fig. 1D1. For each significant parameter identified, the parameter was shifted relative to the SS firing by the peak lead or lag (τ-values) determined in the non-CS aligned regression analysis (Fig. 1D2). The alignment on CSs involved a large number of occurrences, as the long duration of the random tracking trials (6-10 sec) had an average of 8.06 ± 2.87 CSs per trial. These analyses allowed for visualization of the SS modulation in relation to climbing fiber input by generating firing maps from -200 before to 200 msec after CS occurrence for parameters determined to have significant encoding based on the non-CS aligned regression analysis. Figure 2A presents an example of CS-coupled increase in SS sensitivity to VY. The firing maps reveal weak SS modulation with VY prior to CS occurrence (t = 0). Following CS discharge, the SS modulation with velocity greatly increases (Fig. 2A).

The CS-aligned SS firing and shifted behavior were also used to perform the CS-aligned linear regressions that quantified the changes in the SS representations before and after the CSs (Fig. 1D3). The strength and timing of SS modulation are reflected in the R^2 temporal profile (Fig. 2B), and the changes in SS sensitivity reflected in the β profile (Fig. 2C). The R^2 and β profiles (Fig. 2B and C) mirror the strong increase in VY

encoding visualized in the SS firing maps. The significance of CS-coupled changes in encoding was assessed by comparing the difference between the mean R^2 for pre- and post-CS encoding (Fig. 2D, cyan bar) to a distribution obtained from 1000 profiles aligned to randomized CS times selected outside the real CS time windows, which provides a measure of the encoding changes occurring independent of the climbing fiber input (Fig. 2D, grey bars). Moreover, the skew of this random distribution can characterize the overall encoding stability of an individual cell. For this example, the change in encoding ($R^2_{post} - R^2_{pre} = 0.38$) shows the increase in modulation with VY falls far to the right of the noise distribution, exceeding the significance criterion of the mean ± 2SD ($p < 0.05$). Intriguingly, the distribution of encoding changes occurring outside the CS window skews negatively (-0.12 ± 0.12) in contrast to the CS-coupled increase. The CS-coupled increase in the SS encoding is followed by a significant change in VY (Fig. 2E). However, the significant change in VY occurs after the onset of encoding increase, demonstrating that the change in VY representation cannot be attributed to differences in kinematics prior to CS occurrence.

The SS firing rates are similar before and after CS discharge with the exception of the inactivation period (Fig. 2F). Therefore, the change in SS encoding is not due to an alteration in firing rate, instead reflects an increase in sensitivity to VY as demonstrated by the β profile in which the modulation with VY increases markedly following the CS. Finally, the change in encoding is not influenced by other CSs or CS rhythmicity in the ±200 msec window. The probability of another CS within this period is extremely low,

with only a very few CSs occurring on the boundaries of the window, reaching a maximum probability of only 1%. Furthermore, there is little evidence of CS rhythmicity (Fig. 2G).

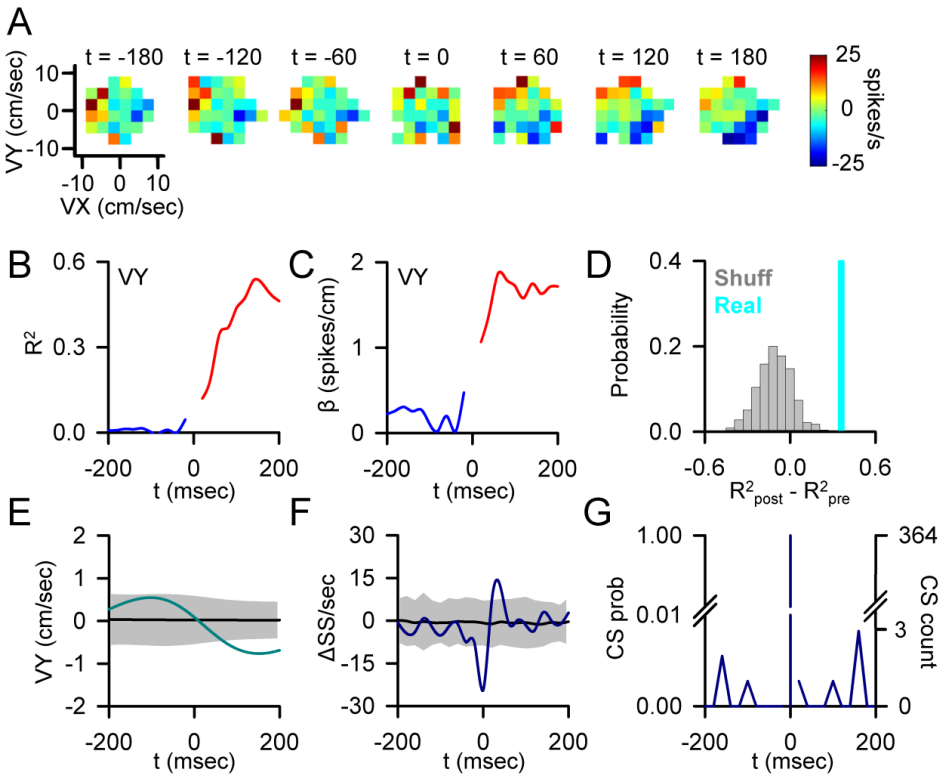

Figure 2: CS-coupled increase in SS encoding. A) Firing maps illustrating an example of Purkinje cell SS modulation with velocity (VY) relative to CS discharge (t = 0). B) Encoding strength (R^2) of VY both pre- (blue trace) and post-CS (red trace). C) Sensitivity (β) of the same Purkinje cell to VY both pre- (blue trace) and post-CS (red trace). D) Magnitude of the CS-coupled change in SS encoding strength as quantified by the difference between $R^2_{post} - R^2_{pre}$ in the +/- 200 msec window (marked by the light blue line) relative to the distribution of changes in encoding strength aligned to randomized CS times selected outside the actual CS window (grey bars). Note that the light blue light in this and subsequent figures only denotes the magnitude of the change in encoding (position along the x-axis) and not a probability (y-axis). E) CS-triggered average of VY (light blue trace) relative to the VY variability from CS-shuffled ISIs (mean ± 3SD, grey region). F) CS-triggered average of SS firing (blue trace) relative to the SS variability from CS-shuffled ISIs (mean ± 3SD, grey region). Note the brief firing rate reduction (t = 0) due to CS inactivation of the SS discharge. G) Distribution of additional CSs in the -200 to 200 msec intervals centered on CS occurrence (CS probability on left axis, CS count on right axis).

Both increases and decreases in SS encoding were observed for all the parameters evaluated. Figure 3 illustrates an example of a CS-coupled decrease in SS encoding for a Purkinje cell modulated with YE (Fig. 3A-D). Over the 200 msec prior to a CS, the firing maps show strong SS modulation with YE. After CS discharge, both the strength of the encoding and the sensitivity are significantly attenuated (Fig. 3B-D, $R^2_{post} - R^2_{pre} = -0.26$). As for the velocity example described above, encoding changes at randomized time points tend to oppose the CS-coupled changes in SS encoding, with a mean change of 0.07 ± 0.16. For this example, the change in encoding is not explained by any significant variations in behavior (Fig. 3E) or SS firing relative to CS (Fig. 3F). As in the previous example, the time course of the encoding change cannot be explained by other CSs in the ±200 msec window or CS rhythmicity (Fig. 3G).

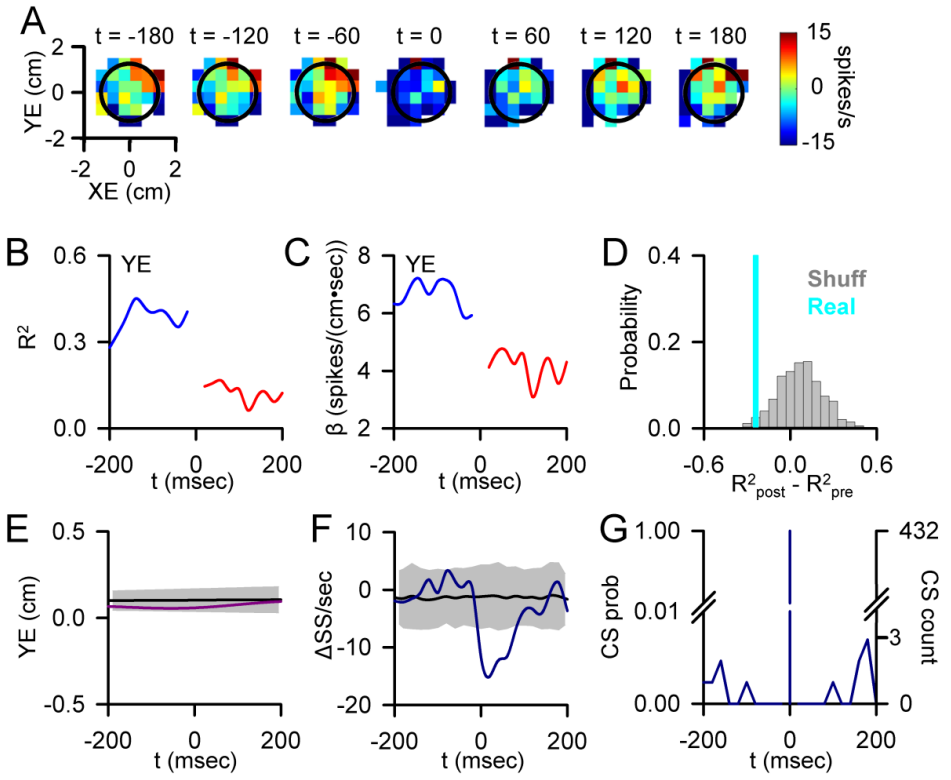

Figure 3: CS-coupled decrease in SS encoding. a) Firing maps of another Purkinje cell with a change in SS modulation with position errors (YE) relative to CS occurrence (t = 0). Black circle denotes target edge. B) Encoding strength (R^2) of YE before (blue trace) and after (red trace) CS discharge. C) Sensitivity (β) of the cell to YE, before (blue trace) and after (red trace) CS discharge. D) Magnitude of the CS-coupled change in SS encoding strength in the +/- 200 msec window (marked by the light blue line) relative to the distribution of profiles aligned to randomized CS times selected outside the actual CS window (grey bars). E) CS-triggered average of YE (purple trace) relative to the YE variability from CS shuffled ISIs (mean ± 3SD, grey region). F) CS-triggered average SS firing (blue trace) relative to the SS variability from CS shuffled ISIs (mean ± 3SD, grey region) showing SS inactivation following CSs. G) Distribution of additional CSs in the -200 to 200 msec intervals centered on CS occurrence (CS probability on left axis, CS count on right axis).

In some Purkinje cells, the CS-coupled changes in SS encoding are characterized as a shift in the preferred area of the parameter workspace represented. For example, Fig. 4A illustrates a Purkinje cell in which the SS firing is strongly modulated by X position in

the pre-CS window. After CS occurrence, the SS modulation shifts with Y position strongly encoded. This change in SS modulation is due to a sharp decrease in X encoding ($R^2_{post} - R^2_{pre} = -0.23$, Fig. 4B, C) and sensitivity (Fig. 4E) and simultaneous increase in Y encoding ($R^2_{post} - R^2_{pre} = 0.25$) and sensitivity. As with the previous two examples, this shift in encoding cannot be explained by significant changes in either parameter (Fig. 4F), SS firing rates (Fig. 4D) or CS rhythmicity (Fig. 4G).

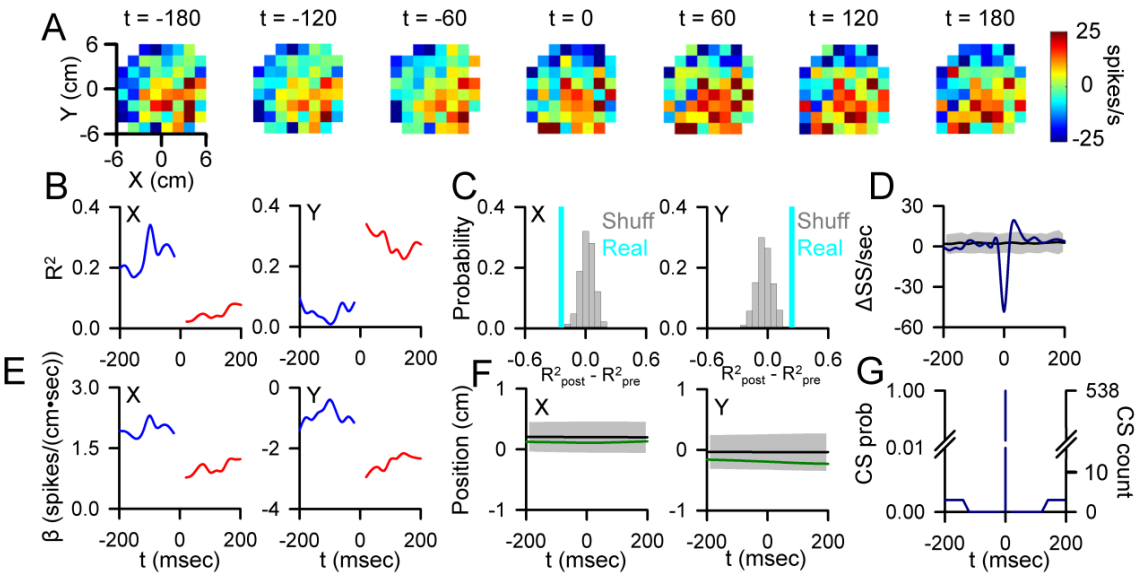

Figure 4: CS-coupled switch in SS encoding. A) Firing maps illustrating an example cell SS modulation with position relative to CS occurrence (t = 0). B). Pre-and post-CS encoding strength of X and Y (conventions as in Figures 2 and 3). C) Magnitude of the CS-coupled change in SS encoding of X (left) and Y (right) in the +/- 100 msec window (marked by the light blue lines) relative to the distribution of profiles aligned to randomized CS times selected outside the actual CS window (grey bars). D) CS-triggered average of SS firing (blue trace) relative to the SS variability CS shuffled ISIs (mean ± 3SD, grey region). E) Pre-and post-CS SS firing sensitivity for this cell to X (left, green trace) and Y (right) (conventions as in Figures 2 and 3). F) CS-triggered average of X (left) and Y (right) relative to the variability from CS-shuffled ISIs (mean ± 3SD, grey region). G) Occurrence of additional CSs in the ± 200 msec window centered on CS discharge (CS probability on left axis, CS count on right axis).

CS-coupled changes in Purkinje cell sensitivity to errors and kinematics

Changes in predictive and feedback SS kinematic and error encoding following a CS are relatively common, occurring in 22/40 Purkinje cells. The changes in the strength of encoding across the population were assessed by separately averaging the significantly increased and decreased R^2 profiles for error, position, and velocity (Fig. 5A-F). The population of R^2 profiles demonstrate that the transitions in SS encoding, both decreases and increases, are tightly timed to CS occurrence. Changes in SS sensitivity were quantified by calculating the difference between the mean absolute values of the regression coefficients both post- and pre-CS (Fig. 5G). All significant increases in encoding were associated with an increase in sensitivity (Fig. 5G, red bars), and all but one of the significant decreases in encoding were associated with a decrease in sensitivity (Fig. 5G, blue bars). The population summary indicates that most of the SS representations exhibit a positive or negative skew in the distribution of encoding changes not associated with CS discharge. As shown for the examples in Figures 2 and 3, the direction of CS-coupled encoding tends to oppose these average changes. Across the population, these encoding changes not associated with CS discharge show a significant negative correlation with the CS-coupled encoding changes ($\rho = -0.51$, $p = 0.003$) (Fig. 5H).

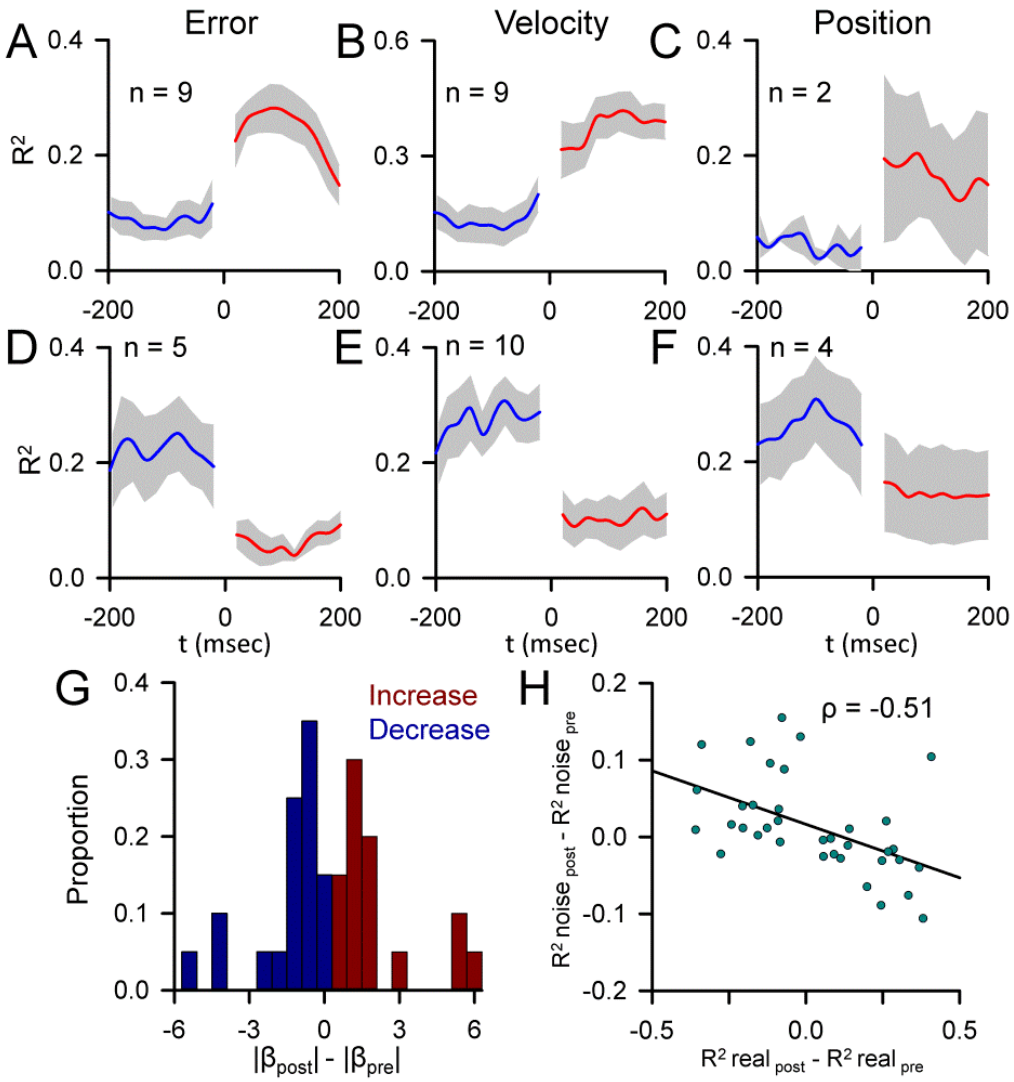

Figure 5: Population summary of CS-coupled changes in encoding and sensitivity. A-F) Mean of the pre- and post- CS R^2 profiles for each parameter with a significant CS-coupled encoding change (blue: pre-CS, red: post-CS) ± S.E.M (grey areas). Increases and decreases in encoding are grouped separately. The "n" refers to the number of profiles. G) Population distribution of changes in SS sensitivity with significant CS-coupled changes in encoding (blue bars: encoding decreases, red bars: encoding increases). H) Distribution of the magnitude of CS-coupled encoding changes vs. mean magnitude of encoding changes not associated with CS firing for all significant CS-coupled encoding changes across the population (n = 40). Proportions for increases and decreases were calculated separately. The Pearson correlation coefficient is included and the line depicts the significant trend of the distribution (p = 0.003).

The CS-coupled changes in SS encoding described above (Figs. 2-5) are based on kinematic or position error signals encoded throughout the entire tracking period as determined by the non-CS aligned linear regression analysis. We also examined CS-coupled encoding changes in the SS firing that did not meet the significance criteria for encoding in the non-CS aligned regression analysis. In 32% of Purkinje cells (n=13), climbing fiber discharge significantly alters the encoding of at least one parameter (Fig. 6), finding both increases (5 parameters) and decreases (9 parameters). Changes in signaling are not due to changes in pre- or post-CS discharge SS firing or CS rhythmicity (Fig. 6D-F), and increases and decreases in encoding are associated with increases and decreases in sensitivity, respectively (Fig. 6I). CS-coupled changes in encoding also tend to oppose encoding changes not associated with CS discharge. When combined with the CS-coupled changes in encoding described in Figures 2-5, this inverse relationship is significant ($\rho = -0.498$, $p = 0.002$).

Overall, CS discharge was followed by a significant alteration in 53 SS representations in 67% of Purkinje cells (n = 27), an average of approximately 2 representations per neuron. The CS-coupled changes include 19 increases (18 Purkinje cells), and 18 decreases (16 Purkinje cells). In the remaining 16 profiles (8 Purkinje cells), the CS-coupled changes involved a paired increase and decrease, manifested as a shift in the preferred area of the parameter workspace represented (e.g. Fig. 4). Together, these results illustrate that CS-coupled changes in SS encoding are common during pseudo-random tracking.

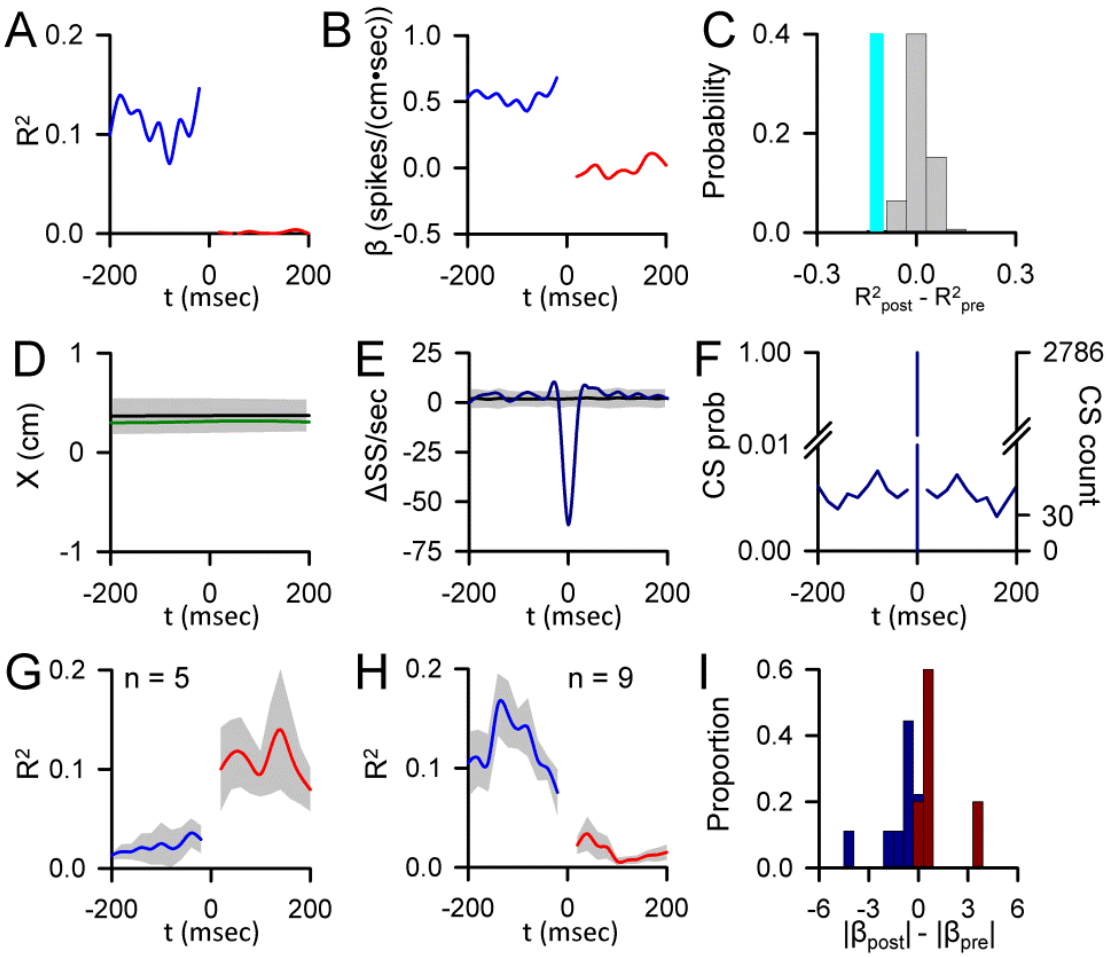

Figure 6: CS-coupled changes in encoding of parameters not initially determined to be significant. A) Encoding strength (R^2) of X positon before (blue trace) and after (red trace) CS occurrence for an example Purkinje cell. B) Sensitivity (β) of same cell to X, before (blue trace) and after (red trace) CS discharge. C) Magnitude of the CS-coupled change in SS encoding strength in the +/- 200 msec window (marked by the light blue bar) relative to the distribution of profiles aligned to randomized CS times selected outside the real CS (grey bars. D) CS-triggered average of X (green trace) relative to the X variability from CS shuffled ISIs (mean ± 3SD, grey region). E) CS-triggered average SS firing (blue trace) relative to the SS variability from CS shuffled ISIs (mean ± 3SD, grey region). F) Distribution of additional CSs in the -200 to 200 msec intervals centered on CS occurrences (CS probability on left axis, CS count on right axis). G-H) Mean of R^2 profiles showing significant CS-coupled increases (G) and decreases (H) in encoding (mean ± SEM) with the number of profiles denoted by "n". I) Population distribution of changes in SS sensitivity to for these parameters with significant CS-coupled changes in encoding (blue bars: encoding decreases, red bars: encoding increases).

Complex spike modulation relative to behavior

Given previous observations of task-evoked CS discharge (Gilbert and Thach, 1977;Kitazawa et al., 1998;Medina and Lisberger, 2008;Yang and Lisberger, 2014), we assessed the relationship between changes in kinematics and position errors and CS firing using spike triggered averaging. A peak change in the CS-triggered average of behavior was considered statistically significant if it exceeded mean ± 3SD noise level as determined by shuffling the CS interspike intervals (ISIs) within a trial. Both the magnitude and timing of significant changes were determined (Fig. 7 B, C, E and F). In 55% of Purkinje cells (n=22), there is a significant change in behavior in relation to CS occurrence (4 cells with a change in only kinematics, 2 with only errors and 16 with both kinematics and errors). Intriguingly, the CS discharge is not driven by behavior, as the behavioral changes occur predominantly after CS discharge with a mean lag of 172.5 ± 98.65 msec for velocity and 100.9 ± 147.2 msec for errors (Fig. 7 C, F). In only 9% of cases (n = 4 parameters) does the behavioral change occur prior to CS occurrence. Additionally, the magnitudes of CS-coupled changes are small compared to the overall behavioral variability, ranging from ± 1.88 cm/sec for velocity and ± 0.64 cm for position error (Fig. 7B,E). These small changes in behavior, while significant, are not likely to explain the large changes in sensitivity observed in the SS encoding. Moreover, the transitions in encoding are tightly coupled to CS occurrence whereas the behavioral changes occur predominantly after CS discharge. Together, these results suggest that neither the CSs nor the SS encoding changes are driven by position errors or changes in

kinematics. Instead, climbing fiber discharge is predictive of changes in behavior that may reflect corrective adjustments made during tracking.

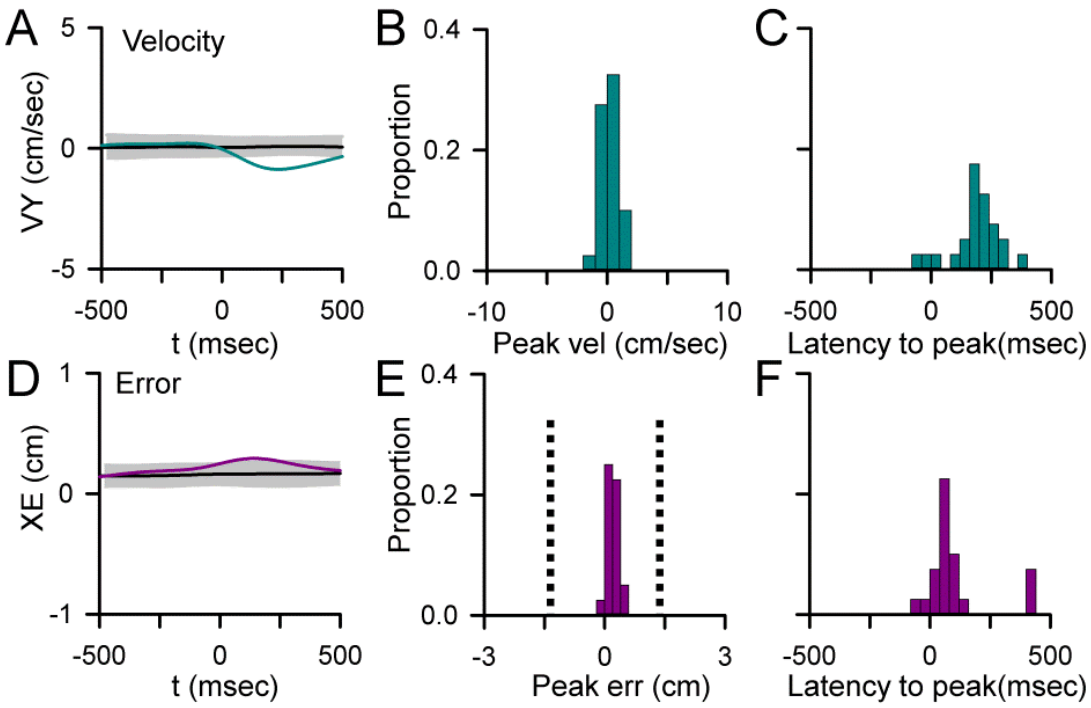

Figure 7: Relationships between CS firing and behavior. A, D) Examples of significant CS-coupled changes in VY (A, blue trace) and XE (D, purple trace) as determined by comparison to mean CS-shuffled control (black trace) ± 3 SD (grey region). B, E) Distributions of peak changes in velocity (B) and error (E) in the 22 Purkinje cells with significant CS-coupled changes in behavior. In E, vertical dashed line marks the target edge. C, F) Timing of peak changes in velocity (C) and error (F) illustrating that behavioral changes lag CSs.

Relationship between CS-coupled changes in SS encoding and behavior

An essential question is the potential influence of the observed CS-coupled changes in SS encoding on the behavior. Therefore, several analyses evaluated the relationship between CS-coupled modulation of SS encoding and changes in behavior. The first observation is

that a CS-coupled change in SS encoding of behavior (e.g., velocity) is associated with a CS-coupled change in that behavior (e.g. velocity) in 38% of profiles (41% of cells). As described, 91% of these changes in behavior occur after the CSs. Therefore, in a large fraction of the neurons SS encoding and changes in behavior are coupled.

The next analysis was undertaken at the population level and assessed whether behavior changed in a consistent pattern following a CS-coupled change in SS encoding. For example, one possibility is that an increase in SS encoding of a kinematic parameter (e.g., VY) following CSs would be followed by a larger change in that parameter (e.g., VY) than for a decrease in the encoding of the same kinematic parameter. To test this possibility, we evaluated if a significant CS-coupled change (i.e. increase or decrease) in SS encoding for a behavioral parameter was related to a change in behavior defined as the magnitude of the mean difference in behavior pre versus post-CS (pre-CS time window: -500 to 0 msec, post-CS time window: 20 to 500 msec). The changes in magnitude were normalized to the maximum change for each parameter. For this analysis, we grouped the four kinematic parameters together because of the relatively small number of SS-encoding changes for any single parameter. The results show that changes in kinematics following CSs correlate with the SS encoding of kinematics with CS-coupled increases in SS encoding of a kinematic parameter (e.g. VY) associated with a significantly larger change in that parameter (e.g. VY) than for CS-coupled decreases (Fig. 8A, unpaired Student's t-test, $t = 2.61$, $p = 0.014$).

We also observed a significant relationship between SS encoding changes and position errors using the same analysis described above. Even a stronger relation was uncovered, as CS-coupled changes in position error encoding are inversely correlated with position errors, such that the magnitude of performance error decreases as the SS encoding of error increases (Fig. 8B, Pearson correlation, $\rho = -0.57$, $p < 0.05$). Together, these results suggest that CS-coupled encoding changes are important for upcoming changes in both kinematics and error performance.

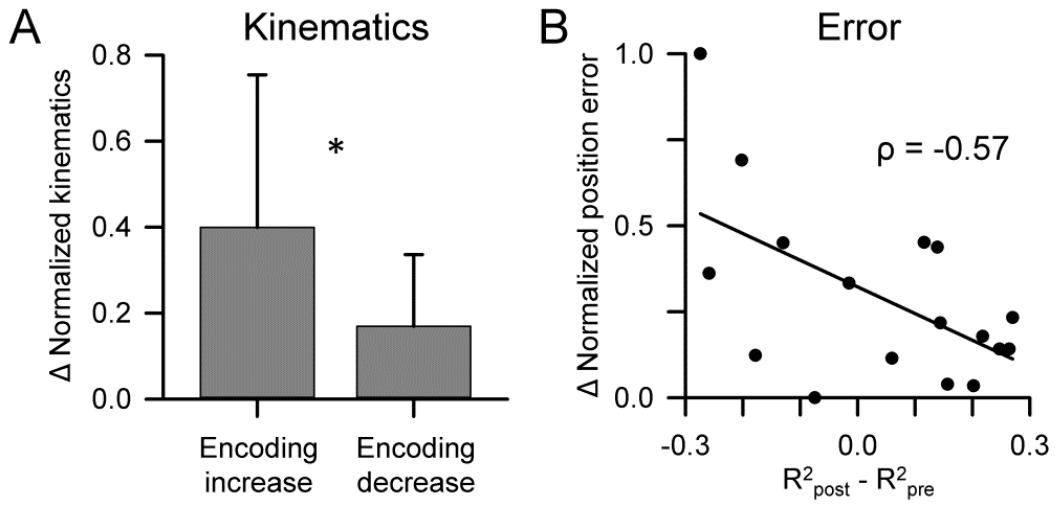

Figure 8: CS-coupled changes in SS encoding are associated with modulation of behavior. A) Mean + SD normalized changes in the kinematic parameters ($mean_{post}$-$mean_{pre}$) for significant CS-coupled increases and decreases in SS encoding. Asterisk (*) indicates $p < 0.05$, unpaired Student t-test. B) Distribution of all normalized changes in the position error parameters ($mean_{post}$-$mean_{pre}$) with the magnitude of significant CS-coupled changes in SS encoding. The Pearson correlation coefficient is included and the line depicts the significant trend of the distribution ($p = 0.017$).

Simple spike firing rates, variability and complex spike rhythmicity do not contribute to encoding changes

Because both short and long-term changes in SS firing have been observed following CSs(Ebner et al., 1983;Loewenstein et al., 2005;Yartsev et al., 2009), we evaluated whether alterations in SS firing rates can account for the CS-coupled changes in encoding. The effect of climbing fiber input on the SS firing rates was evaluated over both ±200 and ±500 msec windows (with the post CS window beginning after the mean + standard deviation of the inactivation period), determining whether at any time (20 msec bins) after a CS the SS firing differed from the pre-CS rates (mean ± 3 SD). A change in SS firing was only observed in 5 Purkinje cells. However, the changes in SS firing were single 20 msec bin transient fluctuations in all but one of the Purkinje cells. Additionally, there was not a significant relationship between pre- and post-CS SS firing rate across the population (Fig. 9A). Also assessed was whether the CS discharge altered the SS variability based on the Fano factor, defined as the ratio of the variance of firing over mean firing. The Fano factor both pre and post CS were determined using the two different time windows defined above. Significant differences in the Fano factor pre versus post-CS occurrence were observed in only two Purkinje cells ($p < 0.05$, paired t-test) in either window, suggesting that climbing fiber discharge has little effect on the variability of SS firing during pseudo-random tracking (Fig. 9B). Furthermore, both the increases and decreases in SS encoding persist well beyond the inactivation period (mean = 48.6 ± 85.7 msec, Fig. 9C), further demonstrating that CS-coupled changes in SS firing rates cannot underlie the changes in encoding.

A major hypothesis is that CS firing is intrinsically rhythmic (8-12 Hz) and used to organize movement timing (Welsh et al., 1995;Lang et al., 1999;Llinas, 2013), raising the possibility that CS rhythmicity plays a role in the changes in SS encoding. To address whether CS rhythmicity is involved, we determined the autocorrelation of CS discharge for each Purkinje cell over a window of $\pm$ 2000 msec, which encompasses the vast majority of CS firing with a mean rate of 0.85 ± 0.33 spikes/sec (Fig. 9D). There are no significant secondary peaks at any lag or lead for any Purkinje cell, including in the 8-12 Hz range, as determined by comparison to the autocorrelation of randomized CS times. There is no CS rhythmicity in the population average (Fig. 9E). Additionally, the lack of CS rhythmicity in the 8-12 Hz range is evident by the low correlation coefficient ($\rho <$ 0.005) and similarity to the shuffled results (Fig. 9F). As found for spontaneous activity in the awake monkey (Keating and Thach, 1995), there is no evidence for CS rhythmicity during pseudo-random tracking. Therefore, CS rhythmicity does not appear to play a role in the SS encoding changes.

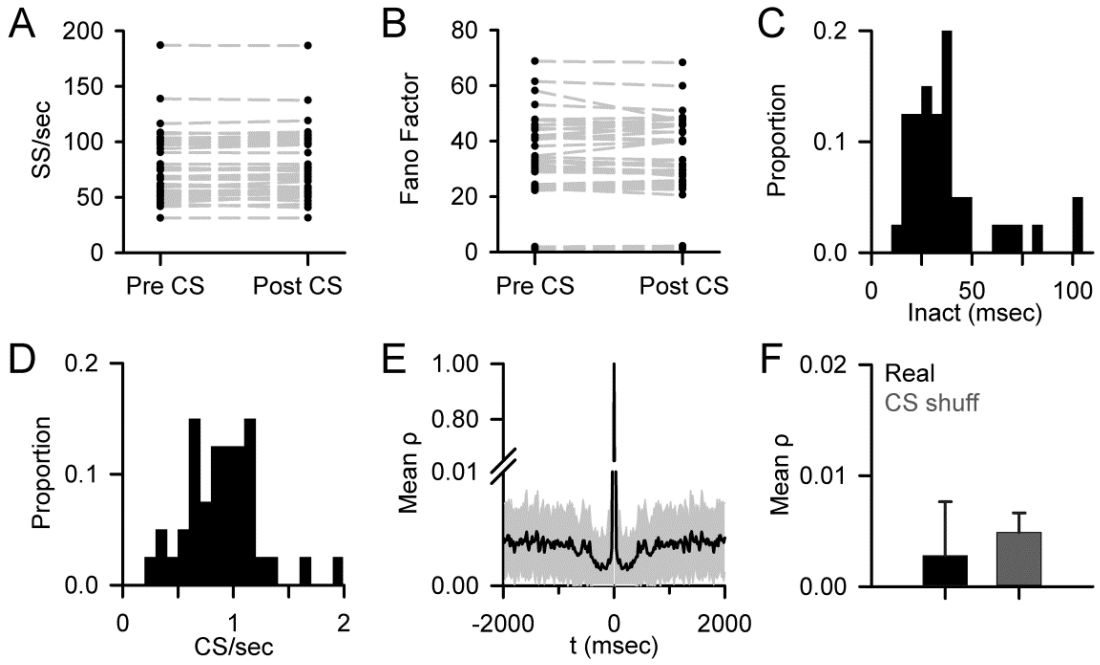

Figure 9: No evidence for CS-associated changes in SS firing properties or CS rhythmicity. A) Mean SS firing before and after CS discharge based on the 200 msec pre-CS and 200 msec post-CS windows (mean + SD of the inactivation period) for 39/40 recorded Purkinje cells. As described in the Materials and Methods one cell was excluded due to high SS variability following the CS; however, this cell did not have significant SS encoding changes. B) Mean Fano factor pre- and post-CS using the same window in A for 39/40 recorded Purkinje cells. C) Distribution of mean SS inactivation periods after CS discharge (Inact) for all 40 Purkinje cells. D) Histogram of mean CS firing rate for all 40 Purkinje cells. E) Population average of CS discharge autocorrelation (mean ± SD). Note the discontinuous Y-axis. F) Average maximum autocorrelation in the 8-12 Hz range for CS firing (Real) and randomly shuffled control data (CS shuff). Error bars indicate SD.

Discussion

This study describes a novel function of climbing fiber input during on-line motor control. Following CS discharge, rapid increases or decreases occur in SS kinematic and error encoding. The CS-coupled changes in SS encoding are common and occur in all the parameters studied. Importantly, the encoding changes are not related to pre- or post-CS firing rates or variability, CS rhythmicity and firing rates, or the inactivation period.

Instead, the powerful synaptic action of a climbing fiber on a Purkinje cell alters the encoding of subsequent parallel fiber inputs, changing the sensitivity to behaviorally relevant measures.

Pseudo-random tracking, complex spikes and changes in simple spike encoding

Pseudo-random tracking allows for the examination of the interactions among CS discharge, SS firing, and behavior in which the correlations between parameters or learning are reduced. Accurate performance on this task requires continuously monitoring the salient behavioral parameters and adjusting for mismatches in hand movement relative to target movement (Hewitt et al., 2011;Popa et al., 2012). This task subverts overly learned, stereotypic behaviors, such as reaching and saccades, in which movement parameters are correlated (Paninski et al., 2004;Soetedjo et al., 2008b). It is possible that during more stereotypic movements, particular aspects of the behavior dominate the CS and SS modulation with little need to adjust the information in the SS firing. In contrast, pseudo-random tracking requires the monitoring of and altering the weights placed on multiple streams of continuously varying kinematic and error information. Therefore, the action of climbing fiber input on SS firing may be markedly different during low dimensional as opposed to high dimensional behaviors.

Intriguingly, in this task CSs are not strongly driven by position errors or movement kinematics. Instead, the CSs consistently lead changes in behavior (Fig. 7A and D), a finding that is similar to an emerging view that CSs can provide predictive information

(Ohmae and Medina, 2015;Ten Brinke et al., 2015). In approximately 41% of the cells in which the CSs preceded a change in kinematics or position error, the encoding of the parameter changed. This finding offers a link to behavior in which CSs are evoked in anticipation of a change in behavior and there is a corresponding change in the encoding of the same parameter. In this manner, the change in SS sensitivity that follows CSs provides a way for Purkinje cells to dynamically focus on the most salient aspects to the behavior.

Changes in simple spike encoding are manifest as a change in sensitivity and not firing rate

Several studies demonstrate that climbing fiber input exerts long-term control over the SS firing rate of Purkinje cells (Colin et al., 1980;Montarolo et al., 1982;Cerminara and Rawson, 2004) and the reciprocal pattern of SS modulation to mossy fiber input (Graf et al., 1988;Simpson et al., 1995;Yakhnitsa and Barmack, 2006;Badura et al., 2013). However, the observations described here emphasize a short term change in the SS encoding not related to SS firing rate. These encoding changes imply that a Purkinje cell responds differently to the same input following a CS. Similar to the gain-change and bi-stability hypotheses, the effects of a climbing fiber on a Purkinje cell's excitability alters its response to subsequent parallel fiber inputs (Loewenstein et al., 2005;Yartsev et al., 2009;Ebner et al., 1983;McKay et al., 2007). Also, similar to these previous hypotheses, the present findings show that a Purkinje cell changes its state and therefore, the information present in the SS firing. However, in contrast the large changes in the SS

encoding are not associated with marked changes in the SS firing rate. Only a small number of Purkinje neurons exhibited altered firing rates following CS discharge and in those cells the duration of the change was brief (~20 msec). Several mechanisms likely explain the lack of CS-coupled changes in SS firing rate. First, as noted in the Introduction, CS-coupled changes in SS firing rates are prominent in reduced or anesthetized preparations but not in the awake animal (Schonewille et al., 2006;Engbers et al., 2013). Second, a large fraction of SS discharge is intrinsic, with parallel fiber input modulating this intrinsic discharge (Raman and Bean, 1997). Third, both increases and decreases in SS encoding occur in single cells. Therefore, in the awake animal, the net effect of climbing fiber input on the SS firing rate is limited. One interpretation of the constant SS firing rate is that climbing fiber activation reallocates the overall bandwidth of a Purkinje cell, with encoding decreases in some parameters to allow increases in others. This reallocation of the bandwidth is consistent with the nearly equal number and magnitude of the increases and decreases (Fig. 5) and the paired increases and decreases in encoding observed in many cells (Fig. 4).

Bi-directional changes in SS encoding

Several mechanisms could explain why both increases and decreases in SS encoding occur. Recent studies show that climbing fiber activation of a Purkinje cell is not all-or-none, but instead varies with the properties of the pre-synaptic climbing fiber burst, the excitability state of the Purkinje cell and the local inhibitory circuitry. The number of spikes in the incoming climbing fiber modulates the CS burst pattern, dendritic Ca^{2+}

spiking and parallel fiber-Purkinje cell synaptic plasticity (Bazzigaluppi et al., 2012;Mathy et al., 2009). Post-synaptically, the Ca^{2+} response to climbing fiber input varies with stimulus properties and is enhanced when triggered by an unexpected sensory event, suggesting that the level of parallel fiber input modulates the Ca^{2+} response (Najafi et al., 2014b;Najafi et al., 2014a). The amplitude of the Ca^{2+} transients depends on the location in the dendritic tree, local membrane potential and concurrent parallel fiber input (Kitamura and Hausser, 2011). GABAergic inhibition generated by cerebellar interneurons locally modifies the conductance changes and Ca^{2+} fluxes evoked by climbing fiber input (Callaway et al., 1995;Kitamura and Hausser, 2011). Decreases in gain occur following a CS when high Ca^{2+} levels reduce parallel fiber input by activation of BK channels and/or endocannabinoid release (Brenowitz and Regehr, 2003;Rancz and Hausser, 2010) and modelling suggests gain increases occur with local increases in Ca^{2+} (Forrest, 2014). These same sources of variability in the response to climbing fiber input determine whether long-term facilitation or depression results at parallel fiber–Purkinje cell synapses (Coesmans et al., 2004;Rasmussen et al., 2013;Medina and Lisberger, 2008). Also, the timing of climbing fiber discharge may differentially modulate parallel fiber input and thereby, determine the direction of synaptic potentiation (Piochon et al., 2012;Suvrathan et al., 2016). Therefore, multiple factors regulate a Purkinje cell's response to climbing fiber input that potentially underlie the bidirectional SS encoding changes.

Do the complex spikes cause the change in simple spike encoding?

The present study does not prove unequivocally that the CSs produce the change in SS sensitivity. However, two findings support this view. First, the changes in SS encoding are tightly coupled to and follow the occurrence of a CS, both in individual Purkinje cells (Figs. 2-4) and in the population (Fig. 5). Second, the CSs are rarely preceded by behavioral changes, also arguing against the notion that an unknown factor is driving the sensitivity recalibration (Fig. 7). However, these observations do not imply that the encoding changes are not related to the prior status of the SS representation in Purkinje cells. The direction of CS-coupled encoding changes tends to be in the opposite direction to the state of SS encoding not associated with CS discharge, with CS-coupled increases in encoding associated with net decreases in the shuffled data, and vice versa (Fig. 5H). Taken together, these observations suggest a role in online motor control in which the CS actively controls the sensitivity of a Purkinje cell, either in anticipation of a change in behavior or in response to an encoding state that is suboptimal.

Complex spike-coupled changes in simple spike encoding reflect the need to adjust to constantly changing conditions

The motor system produces highly accurate movements under constantly changing conditions and goals. To achieve this level of task performance, the motor system processes and uses different information including kinematics and errors. For example, the motor system as needed can include or exclude an internal gravitation model from estimations of target motion (Zago et al., 2004). That the cerebellum engages in switching among and utilizing multiple representations can be inferred from the temporal

and spatial overlap of activation patterns when subjects use different tools to perform similar tasks (Imamizu et al., 2004). Pseudo-random tracking requires a dynamic representation of behavior with constantly varying target kinematics and a continual effort to minimize performance errors. Consistent with the CSs playing a role, CS-coupled increases in SS encoding of kinematics coincide with larger changes in kinematics than decreases in SS encoding. Furthermore, CS-coupled increases in error encoding correlate with decreases in performance errors. These observations suggest that climbing fiber input adjusts SS encoding in a manner consistent with upcoming changes in behavior. The changes in SS encoding show that the motor information at the level of a single Purkinje cell is highly dynamic and suggest that climbing fiber input is continually updating the encoding state of Purkinje cells.

CHAPTER 3: CLIMBING FIBERS PREDICT MOVEMENT KINEMATICS AND PERFORMANCE ERRORS

Introduction

Purkinje cells of the cerebellar cortex receive two main inputs, climbing fibers and parallel fibers (Eccles et al., 1967;Ito, 1984). The dendritic tree of a mature Purkinje cell receives extensive glutamatergic synaptic input from a single climbing fiber originating from the inferior olive. Climbing fiber activation of a Purkinje cell produces a powerful post-synaptic depolarization, which generates Ca^{2+} spikes throughout the entire dendritic tree and a complex spike (CS), which consists of a large Na^{+} somatic spike and a burst of smaller spikelets (Llinas and Sugimori, 1980;Davie et al., 2008). Parallel fibers provide the second main input with over 100,000 individual glutamatergic synapses on each Purkinje cell. Parallel fibers produce small, post-synaptic excitatory responses in Purkinje cells and modulate the intrinsic simple spike (SS) discharge (Raman and Bean, 1997). CS discharge occurs at a low frequency (~0.5-2.0/sec) compared to the high frequency SS discharge (~50-150/sec). To understand the function of CSs, we need to understand the signals carried by climbing fibers.

The primary hypothesis has been that climbing fiber input provides motor error signals. Supporting this view is the CS modulation with retinal slip during smooth pursuit adaptation and induced saccade errors (Graf et al., 1988;Soetedjo et al., 2008b;Medina and Lisberger, 2008;Yang and Lisberger, 2014;Kobayashi et al., 1998;Barmack and

Shojaku, 1995;Stone and Lisberger, 1990b). In addition to sensory derived errors, CSs modulate in response to inferred errors related to eye performance (Frens et al., 2001;Winkelman et al., 2014;Winkelman and Frens, 2006) and prediction errors during eye blink conditioning (Ohmae and Medina, 2015). During reaching movements, CSs modulate with unexpected loads (Gilbert and Thach, 1977), reach redirection (Wang et al., 1987), end point errors (Kitazawa et al., 1998), and adaptation to visuomotor transformations (Ojakangas and Ebner, 1994). The error signals conveyed by climbing fibers are hypothesized to play a teaching role in cerebellar motor learning, specifically in long-term depression at parallel fiber-Purkinje cell synapses (for reviews see (Boyden et al., 2004;Hansel et al., 2001;Gao et al., 2012;Ito, 2001;Marr, 1969;Albus, 1971;Jorntell and Hansel, 2006)).

However, climbing fiber activation cannot always be placed in an error framework. Inferior olivary neurons respond poorly to limb movement perturbations in the cat (Horn et al., 1996) as do CSs in response to error-inducing force pulses during reaching in the monkey (Hewitt et al., 2015). Complex spikes do not appear to unambiguously encode the magnitude of saccadic error (Soetedjo and Fuchs, 2006;Soetedjo et al., 2008b). It has even been suggested that climbing fibers are activated only by unexpected sensory input and do not respond during motor behavior (Gibson et al., 2004). One of the strongest demonstrations that climbing fiber input does not simply report errors is that in the oculomotor vermis, changes in CS discharge during saccade and smooth pursuit adaptation are most prominent after the vast majority of adaptation has occurred, when

retinal slip errors are minimal (Catz et al., 2005;Dash et al., 2010;Prsa and Thier, 2011). Furthermore, CSs encode non-error information about motor behavior, including reach and eye kinematics (Fu et al., 1997b;Ebner et al., 2002;Kitazawa et al., 1998;Kobayashi et al., 1998). These observations demonstrate that CSs do not only or always signal errors. In addition, climbing fibers are not the only source of error information in the cerebellar cortex, as SS firing provides robust performance error signals (Popa et al., 2012;Ke et al., 2009).

One common feature of CS modulation, whether with errors, unexpected sensory inputs or kinematics, is that the responses are primarily feedback related. During limb movements and saccades, increases in CSs occur predominantly after movement onset (Fu et al., 1997b;Ebner et al., 2002;Meyer-Lohmann et al., 1977;Mano et al., 1986;Catz et al., 2005;Soetedjo and Fuchs, 2006;Noda and Suzuki, 1979). Recently, however, feedforward CS responses have been described during eye blink conditioning, with CS increases prior to and predicting the conditioned response (Ohmae and Medina, 2015;Ten Brinke et al., 2015). In our study of Purkinje cell firing during pseudo-random tracking, CSs occur primarily in advance of a change in hand kinematics and performance errors (Streng et al., 2017). However, that initial study focused on how CSs trigger a change in the information encoded in the SS firing and did not fully assess the spatio-temporal aspects of CS modulation during pseudo-random tracking. These observations of CSs leading behavior further the view that climbing fiber input provides signals that are not limited to error processing.

To fully understand the information signaled by the CSs, it is necessary to expand the behaviors studied. This is particularly true for previous arm movement studies that primarily used single joint movements or reaching tasks (Gilbert and Thach, 1977;Wang et al., 1987;Kitazawa et al., 1998;Ojakangas and Ebner, 1994;Fu et al., 1997b;Mano et al., 1986). Further, most investigations of CS modulation evaluated stereotypic behaviors, including vestibular and oculomotor reflexes, reaching or saccades, in which movement parameters are strongly correlated (Reimer and Hatsopoulos, 2009;Hewitt et al., 2011). Also, there is a need to examine CS activity during tasks that require the continuous monitoring of behavior and correction for errors, as previous studies have emphasized the importance of spontaneous climbing fiber input in ongoing movements (Llinas et al., 1975;Horn et al., 2013;Colin et al., 1980;Montarolo et al., 1982;Cerminara and Rawson, 2004;White and Sillitoe, 2017). Therefore, this study evaluates CS modulation during pseudo-random tracking that demands constant monitoring and adjusting for mismatches in hand movement relative to target movement and allows for the examination of the interactions between CS discharge and behavior in which the correlations between parameters are minimized (Hewitt et al., 2011;Popa et al., 2012). During this task, CS firing is strongly and linearly modulated with hand kinematics including position, velocity and acceleration, and position error, a measure of tracking performance. Intriguingly, the most frequent CS modulation occurs with acceleration. Contrary to the error feedback encoding hypothesis, the vast majority of the CS modulation leads the changes in behavior. Also, CS firing does not respond to ‘events,’ either for position error

or kinematics. These results provide novel observations about the diversity and properties of the signals carried by climbing fiber input.

The content of this chapter is in press in the *Journal of Neurophysiology* (Streng ML, Popa LS, Ebner TJ (2017). Climbing fibers predict movement kinematics and performance errors.)

Materials and Methods

Behavioral and electrophysiological data were obtained from two rhesus monkeys (*Macaca mulatta*; female 6.3 kg, age 15; male 6.8 kg, age 8) during normal daytime hours. All animal experimentation was approved by the Institutional Animal Care and Use Committee of the University of Minnesota and conducted in accordance with the guidelines of the National Institutes of Health.

Random tracking

This study utilized a previously described pseudo-random tracking task (Hewitt et al., 2011;Popa et al., 2012;Paninski et al., 2004;Streng et al., 2017) and, therefore, the paradigm is only briefly detailed here. Two monkeys were trained to use a robotic manipulandum (InMotion^2, Watertown, MA) that controls a cross-shaped cursor to track a circular shaped target (2.5 cm diameter) on a computer screen (Fig. 10A). The paradigm started with an initial hold period in which the animals placed and maintained the cursor inside a stationary target for a random period of time (1000-3000 msec). The

initial target position on the screen was also randomized. Next, during the track period, the target moved for 6-10 s along a trajectory selected randomly from 100 trajectories defined *a priori*. Pseudo-random target paths were generated from a sum of sine waves. Target speed was randomly varied so that the average speed was approximately 4 cm/s and conformed to the two-thirds power law (Viviani and Terzuolo, 1982;Lacquaniti et al., 1983). The trajectories were low-pass filtered and selected to avoid sharp turns and large changes in speed, and ended with a final hold period of 1000-3000 msec. The paradigm required that the monkey maintain the cursor within the target, and allowed only brief excursions outside the target (<500 msec). Pseudo-random tracking has several advantages, including providing more comprehensive and uniform coverage of parameter workspaces and dissociating kinematic from error parameters (Paninski et al., 2004;Hewitt et al., 2011). Random tracking also results in extensive combinations of the different kinematic parameters and position error, providing a rich data set to assess what information the CSs encode. Hand (X and Y) and target (X_{tg}, Y_{tg}) position were sampled at 200 Hz. The velocity (VX, VY) and acceleration (AX, AY) of the hand movements were derived by numerical differentiation (Hewitt et al., 2011). Position error (XE, YE) was defined as the difference between cursor and target positions (Fig. 10B).

Surgical procedures, electrophysiological recordings and data collection

Head restraint hardware and a recording chamber targeting lobules IV-VI of the intermediate and lateral cerebellar zones were chronically implanted over the parietal cortex ipsilateral to the arm used to track in each animal using aseptic techniques and full

surgical anesthesia. The positions of the electrodes were confirmed by radiographic imaging techniques that combined a CT scan of the skull with an MRI of the cerebellum (Hewitt et al., 2011). After full recovery from chamber implantation surgery, extracellular recordings were obtained during normal daytime hours using Pt-Ir electrodes with parylene C insulation (0.8-1.5 MΩ impedance, Alpha Omega Engineering, Nazareth, Israel). Purkinje cells in lobules IV-VI of the intermediate and neighboring lateral cerebellar zones were targeted following previously established methods (Hewitt et al., 2015). Individual Purkinje cells were identified by the presence of CSs followed by a characteristic pause in SS activity (Fig. 10C) (Bloedel and Roberts, 1971;Thach, Jr., 1967). After conventional amplification and filtering (30 Hz-3 kHz band pass, 60 Hz notch), SSs were discriminated online using the Multiple Spike Detector System (Alpha Omega Engineering, Nazareth, Israel). Resulting spike trains were digitized and stored at 1 kHz. The raw electrophysiological data was also digitized and stored at 32 kHz. Using a combination of software and manual confirmation, CSs were discriminated and digitized offline (Hewitt et al., 2015). Using the fractional interval method, the SS trains were transformed to a continuous firing rate in 5 msec bins and the SS firing rates were not filtered in order to minimize autocorrelation artifacts. For display and analyses, the mean firing rate for each trial was subtracted from the instantaneous firing rate. The behavioral parameters were low pass filtered (4^{th} order Butterworth with a 5 Hz cut-off).

Analysis of complex spike modulation with behavior

The goal of this analysis was to determine significant CS modulation associated with the three kinematic measures as well as position error. Both data and original MATLAB code written for analysis can be made available on request. The analyses, evaluating the temporal relationship and spatial tuning of the Purkinje cell firing with the behavioral variables, were restricted to the track period and used a reverse-correlation approach (Schoppmann and Hoffmann, 1976;Borghuis et al., 2003). The reverse correlations were computed separately for each pair of parameters (e.g., VX and VY). First, each behavioral parameter was aligned to the times of all CSs across the recording session. Due to the low frequency of CS discharge, feedforward CS modulation was determined from behavior occurring during the 0 to 300 msec epoch after CS discharge and feedback CS modulation was determined from the behavior occurring during the 300 to 0 msec epoch prior to CS discharge (Fig. 10D). Each behavioral parameter was partitioned into 64 (8 x 8) equal bins ranging from -2 to 2 cm (0.5 cm x 0.5 cm bin) for XE and YE, -6 to 6 cm (1.5 cm x 1.5 cm bin s) for X and Y, -12 to 12 cm/s (3 cm/s x 3 cm/s bin) for VX and VY, and -32 to 32 cm/sec^2 (8 cm/sec^2 x 8 cm/sec^2 bin) for AX and AY. For each 300 msec epoch (before and after a CS), reverse correlation determines the number of data points in each bin during a given epoch normalized to the total number of data points in the same bin during entire recording session. For each parameter and epoch, we generated a two-dimensional probability map of the behavior in relation to CS discharge. Given that the reverse correlation probability is equal to the probability to observe a CS in each behavioral bin, we refer to the bin probability as CS probability.

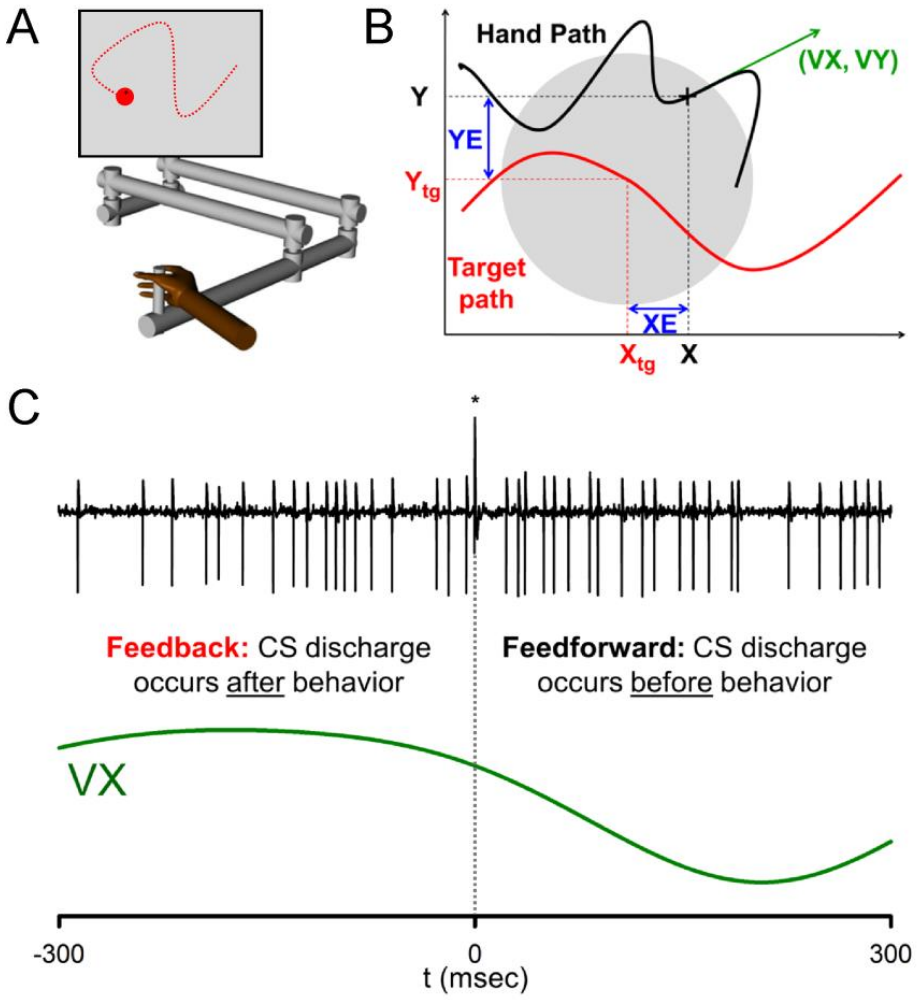

Figure 10: Behavioral paradigm and analysis of CS modulation. A) Rhesus macaques tracked a pseudo-randomly moving target (red circle) using a cursor controlled by a manipulandum (Hewitt et al., 2011;Popa et al., 2012). B) Kinematic parameters evaluated included position (X, Y), velocity (VX, VY) and acceleration (AX, AY, not shown). Position error (XE, YE) was defined as the difference between the cursor and the target center (modified from (Streng et al., 2017)). C) Purkinje cells were identified by the presence of complex spikes (asterisk (*)) followed by a pause in SS activity (top trace), and each parameter was aligned to CS occurrences (dashed vertical line) as shown for VX. CS modulation was quantified as the probability of behavior either 300 msec before (feedback) or 300 msec after (feedforward) CS firing.

The encoding strength and direction of either feedforward or feedback CS modulation with behavior were quantified using linear regression analysis. For each parameter, CS firing probability was modeled as a function of the "x" and "y" directions. For example, the following computations were performed for the feedforward CS firing probability associated with velocity (VX, VY):

$$CS_{prob}^{ffwd} = \beta_0 + \beta_{VX} * VX + \beta_{VY} * VY$$

(eqn. 1)

The regression resulted in the coefficient of determination (R^2) and the regression coefficients for each parameter (e.g., β_{VX}, β_{VY}). The preferred direction (θ) was then computed as the arctangent of the ratio of β_{VX} to β_{VY}:

$$Preferred\ direction\ (\theta) = \arctan\frac{\beta vy}{\beta vx}$$

(eqn. 2)

The magnitude of the preferred direction vector was computed as:

$$Vector\ magnitude = \sqrt{{\beta_{VX}}^2 + {\beta_{VY}}^2}$$

(eqn. 3)

The significance of the CS modulation with a parameter was determined by comparing the actual R^2 value and the magnitude of the preferred direction vector to bootstrapped noise distributions generated by randomly shuffling the bins in each map 10,000 times

(Best et al., 2016;Riehle et al., 2013). The bootstrapped noise distributions were generated by performing the linear regression analysis on each shuffled map. This analysis was performed separately for the feedforward and feedback CS epochs. CS modulation with a parameter was considered statistically significant if both the R^2 and vector magnitude exceeded the mean + 4SD of the shuffled distributions. This threshold ensured the identification of robust feedforward or feedback CS modulation with each behavioral parameter of interest.

Quantification of event-related complex spike modulation

To determine whether CS modulation with the parameters is continuous or a discrete, event-related representation (e.g., increasing CS probability with increasing position error versus evoked CS firing when the cursor leaves the target), we aligned CS firing to the timing of specific behavioral events. For positon error, we aligned the CS firing to the times during tracking when the cursor exited the target area. To account for the directional preference of CS firing and to capture the region in which CS firing increases, we restricted the analysis to the quadrant of the target within ± 45º of the preferred direction of the position error vector. For position error, the position at which the cursor exited the target edge corresponded to approximately the magnitude of the position error vector exceeding the mean + 1SD of the distribution of position error values. The experimental paradigm provides a definition of an error event, crossing out of the target, as this triggers the need for a timely corrective action. However, there are no similarly defined events for the kinematic parameters. Therefore, we used the equivalent statistical

threshold found for position error events (i.e., exiting out of the target) to define events related to the kinematic parameters (mean + 1 SD of the parameter). For these error and kinematic events, we calculated the cumulative probability of CS firing within a ± 500 msec window.

Analysis of simple spike modulation with behavior

We also assessed the SS modulation to determine the relationship between SS and CS encoding of behavior. SS modulation with behavior was analyzed using the same feedforward and feedback epochs and the same partitioning used for the analysis of CS firing. For feedforward SS modulation, we computed the average SS firing (mean-subtracted) in the 300 msec period prior to being in a given bin of the parameter workspace. For the feedback SS modulation, we computed the average SS firing (mean-substracted) in the 300 msec period after being in a given bin of the parameter workspace. For each parameter, linear regression analysis was performed on the SS firing maps as for the CS probability maps, obtaining both the R^2 and regression coefficients (βs). The latter were used to compute the preferred direction of SS modulation and the vector magnitude (see eqns. 2 and 3). The significance of the SS modulation was determined using the same bootstrapping method used for the CS firing maps. The interaction between SS and CS modulation was determined by comparing the preferred directions for each significant pair of CS and SS modulation for a given parameter and epoch (e.g., feedforward velocity CS versus feedforward velocity SS modulation).

Results

Random tracking and measurements of kinematics and performance error

Two rhesus macaques performed a visually guided, manual pseudo-random tracking task (Fig. 1A) (Hewitt et al., 2011;Popa et al., 2012). Using a robotic manipulandum, monkeys controlled a cursor to track a pseudo-randomly moving target on a screen. Three kinematic parameters, derived from the instantaneous hand position, describe the movements of the hand position (X, Y), velocity (VX, VY) and acceleration (AX, AY). Position errors (XE and YE) are defined as the difference between the cursor and the target center (Fig. 10B). To assess the statistics of the kinematic and error parameters relative to the workspaces, we determined the probability densities. Position, velocity, acceleration, and position error are concentrated in the center of the workspaces and are highly symmetrical and the position error plot shows that the animals strive to keep the cursor in the center of the target space (Fig. 11A-D), as observed previously during this task (Hewitt et al., 2011;Popa et al., 2012). While it is possible to compute other error measures, such as the discrepancy between cursor and target velocity (velocity error) and acceleration (acceleration error), we focus on position error for several reasons. Performance on pseudo-random tracking is dictated entirely by position error, as excursions outside the target edge lasting more than 500 msec result in trial failure. To show this, the magnitude of position error to position magnitude was compared to similar ratios for velocity and acceleration (Fig. 11E). There are no explicit constraints placed on either velocity or acceleration error. The animals tightly control the position error ratio during tracking, but not the corresponding velocity or acceleration error ratios (Fig. 11E).

This result is not unexpected as minimizing position error requires that velocity and acceleration deviate from target velocity and acceleration.

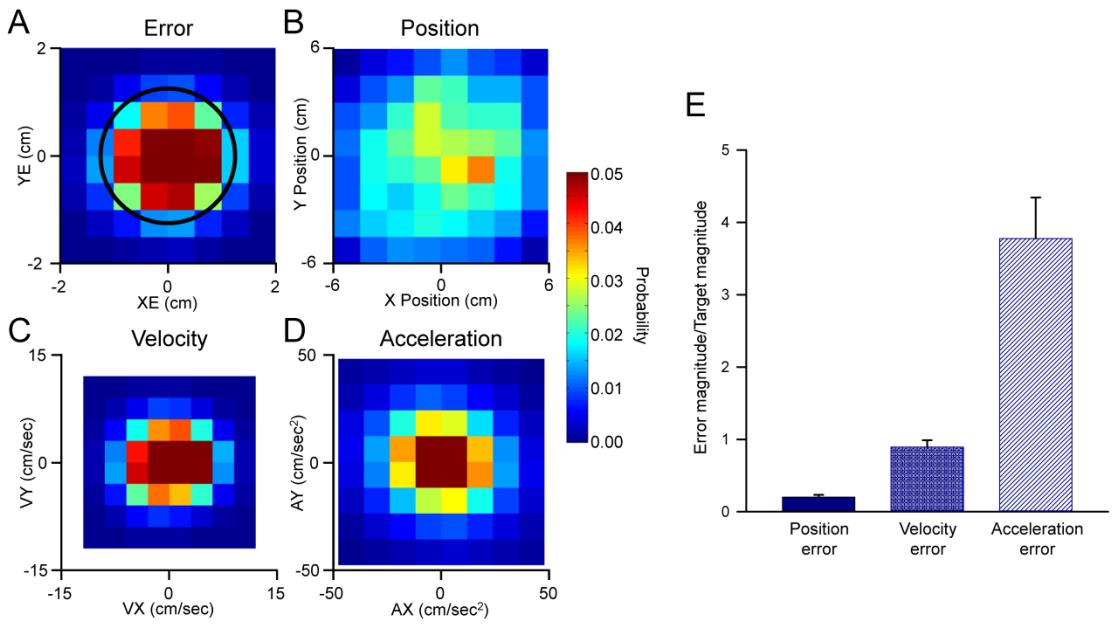

Figure 11: Behavioral parameters during pseudo-random tracking. Probability density plots of A) position error, B) position, C) velocity, and D) acceleration during pseudo-random tracking. The density plots were determined from all trials for all Purkinje cells recorded. Black circle in panel A indicates the target edge. E) Ratio of error to target kinematics for position, velocity, and acceleration error.

Complex spike modulation with kinematics and performance error

Forty-five Purkinje cells were recorded during pseudo-random tracking. This data set includes a re-analysis of 40 neurons used to describe the CS-coupled changes in SS sensitivity to kinematics and performance errors during random tracking (Streng et al., 2017) and an additional 5 Purkinje cells in which the CS firing was fully analyzed. The basic CS firing statistics are similar to previous reports, with an average of 0.87 ± 0.36

spikes/sec during the track periods (Fig. 12A), which overall involved 881 ± 752 CSs per session. On average, the animals completed 110 ± 71 trials in a recording session. We also analyzed the variability in CS firing rates across trials. There was no trend in firing rate across trials either for individual Purkinje cells (Fig. 12B) or across the population (Fig. 12C, $\rho = 0.16$, $p > 0.05$, Pearson correlation). As reported in the previous Chapter, there was little evidence for CS rhythmicity (see Figure 9 in Chapter 2).

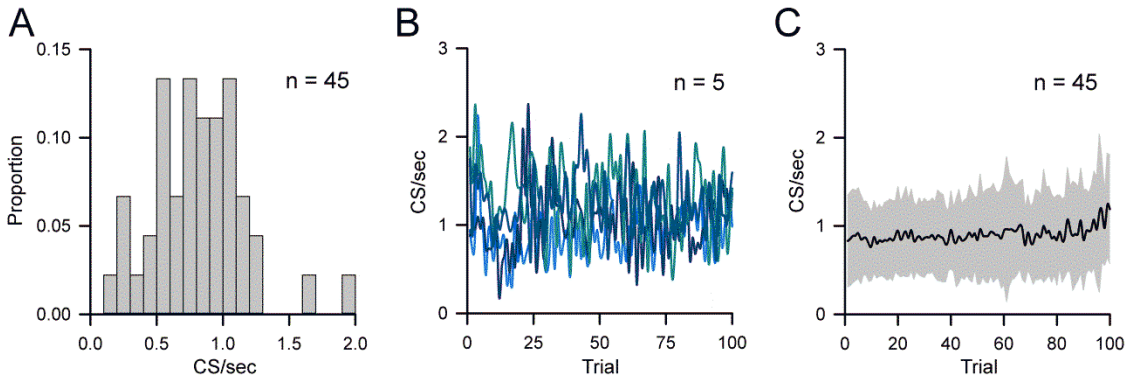

Figure 12: CS firing properties during pseudo-random tracking. A) Distribution of CS firing rates for all 45 Purkinje cells. B) Average CS firing rate over trials for 5 example Purkinje cells. C) Population averages of CS firing rates over 100 trials.

The goal of the analyses was to determine the spatial and temporal modulation of CSs during this pseudo-random tracking task. Using a reverse correlation approach, the modulation was characterized by the probability of being in a given bin of the parameter workspace either 300 msec before (feedback) or 300 msec after (feedforward) CS discharge. The binning of the behavior in these 300 msec intervals allows for determining changes in the CS firing probability that predict or respond as feedback to position, velocity, acceleration, and position error.

Figure 13 illustrates an example of a Purkinje cell in which CS firing modulates predictively with position error. The probability maps reveal spatial tuning in the 300 msec period prior to position error, as CS probability increases in the positive XE direction and decreases in the negative XE direction (Fig. 13A, feedforward). The probability maps were generated from the 371 CSs recorded during 59 successful trials for this example Purkinje cell. The spatial relationship between CS firing probability and position error was quantified by both the strength (R^2) and preferred direction (Fig. 13B) using linear regression analysis (see Materials and Methods). The significance of the CS modulation with behavior was assessed by comparing both the R^2 and vector magnitude to distributions obtained from 10,000 random shuffles of the CS probability maps. A significant relationship between CS modulation and behavior required that both the R^2 and vector magnitude exceeded the mean + 4SD of the shuffled probability maps. For the example shown in Fig. 13A, the R^2 and vector magnitude (CS prob/cm) fall far to the right of the distributions obtained from the shuffled probability maps (Fig. 13C and D, respectively), confirming the significance of the feedforward CS modulation. However, the CS firing probability is not significant for the 300 msec period following position error (Fig. 13A, feedback and E and F). For this Purkinje cell, only 4 additional CSs occur in both the feedforward and feedback epochs, demonstrating that the probability maps are not heavily influenced by the occurrence of these small number of intervening CSs. Finally, the spatial tuning is fundamentally different than the position error probability density maps (Fig. 13A), demonstrating that the increases in CS firing

probability cannot be explained by the number of occurrences of the behavior within the map.

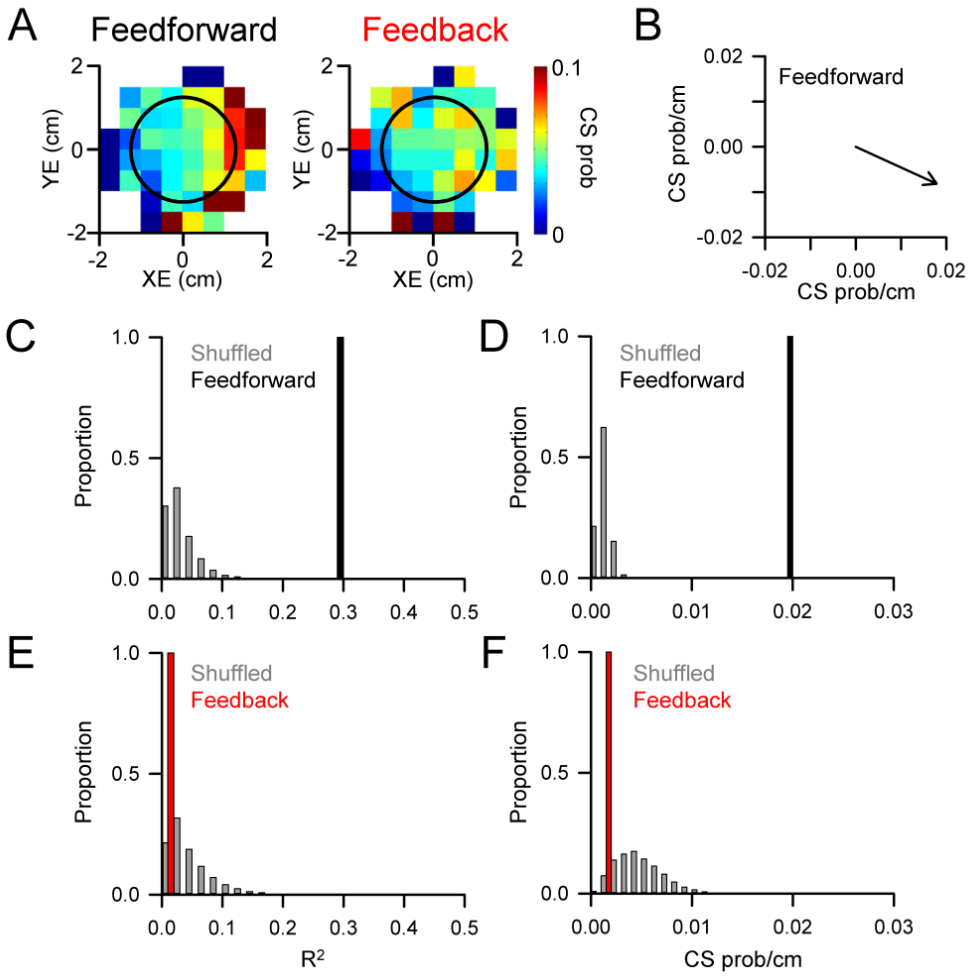

Figure 13: CS modulation with position error. A) Probability maps of feedforward and feedback CS modulation with position error determined using 371 CSs recorded during tracking in 59 trials. Black circle indicates target edge. B) Preferred direction of CS feedforward tuning with position error computed using the regression coefficients from the linear regression analysis (see Materials and Methods). C) Magnitude of the feedforward CS modulation with position error as quantified by the R^2 (black bar) compared to the distribution of R^2 values from shuffled probability maps (gray bars). D) Magnitude of the predictive CS preferred direction (black bar) compared to the distribution of vector magnitudes from shuffled probability maps (gray bars). E-F) Magnitude of feedback modulation as in C-D showing that neither the R^2 value nor magnitude of the preferred direction vector differs from the shuffled distributions.

Significant CS modulation with kinematics and position error occurs in 75% of Purkinje cells (n = 30/45), with robust spatial tuning for each of the four parameters evaluated. Examples of Purkinje cells with significant CS modulation with position, velocity, and acceleration are shown in Figure 14. For the first example (Fig. 14A-B), increased CS firing probability occurs with position in the left side of the position space during the feedback epoch (denoted by the red vector in Fig. 14B), however, the modulation during the feedforward epoch is not significant. For another Purkinje cell, strong feedforward CS modulation occurs for velocity with increased probability for negative VX and decreased probability for positive VX (Fig. 14C-D). No significant CS modulation with velocity is observed during the feedback period. The final example shows CS firing probability spatially tuned to and predicting acceleration, with increased CS firing in the lower left of the acceleration space (Fig. 14E-F). As for velocity, there is no significant feedback modulation with acceleration.

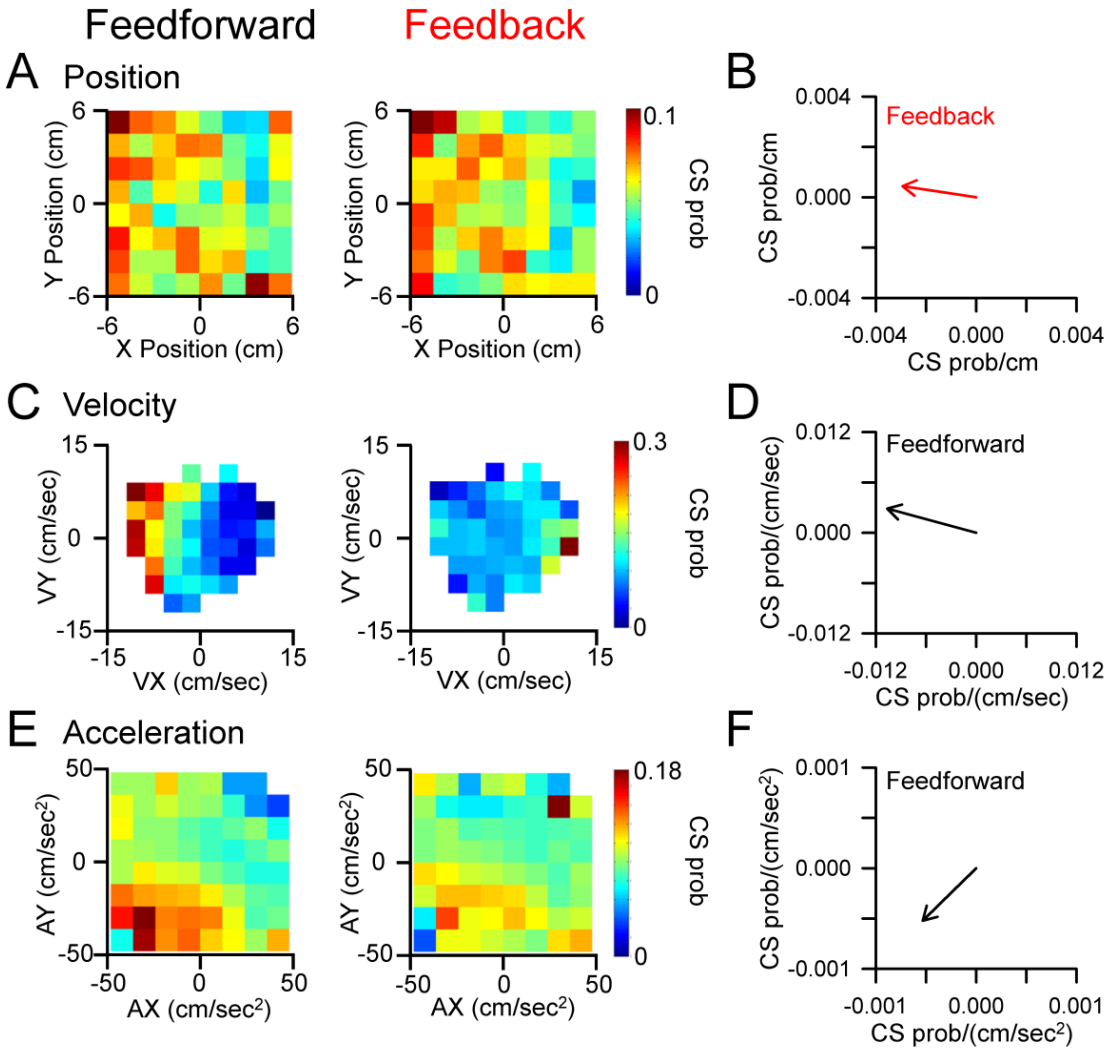

Figure 14: CS modulation with kinematics. A) CS probability maps illustrating an example Purkinje cell with significant feedback tuning with position. Feedforward modulation is not significant. The maps were computed using 1114 CSs during tracking from 110 trials. B) Preferred direction of CS feedback tuning with position. C -D) CS probability maps and preferred direction plot for another example Purkinje cell with significant feedforward tuning with velocity computed using 807 CSs recorded during tracking in 182 trials. Feedback tuning was not significant. E-F) CS probability maps and preferred direction plot for a third example Purkinje cell with significant feedforward tuning with acceleration computed using 3248 CSs recorded during tracking in 337 trials. Feedback modulation was not significant.

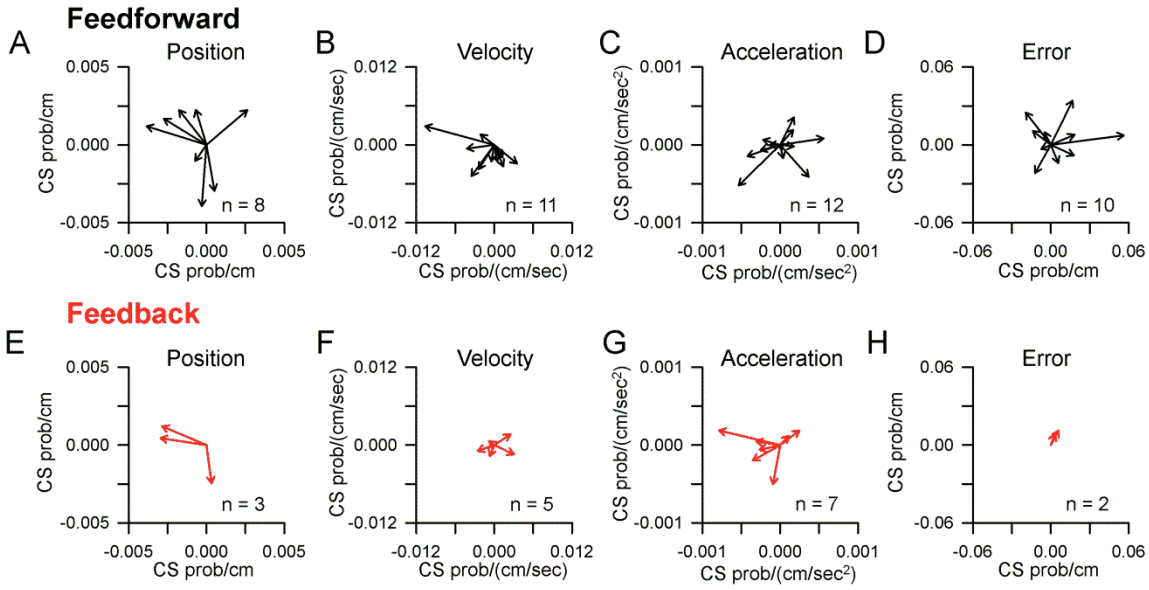

Figure 15: Population summary of CS spatial tuning with behavior. A-D) Preferred direction vectors for all Purkinje cells with significant feedforward CS modulation with A) position, B) velocity, C) acceleration and D) position error. E-H) Preferred direction vectors for all Purkinje cells with significant feedback CS modulation with the same kinematic and error parameters. N indicates the number of cells with significant modulation.

Across the population, CS modulation with behavior is strongly predictive for each parameter analyzed and considerably more frequent than feedback modulation (Fig. 15, top versus bottom row). The CSs are most commonly modulated in relation to velocity and acceleration. Purkinje cells have a significantly greater number of feedforward (n = 41) than feedback (n = 17) relationships between CS firing and behavior (χ^2 (3, n = 58) = 11.17, p = 0.011). Of particular interest given the climbing fiber error hypothesis, only 2 Purkinje cells have significant feedback CS modulation with position error and the magnitude of the modulation is small. In contrast, feedforward CS modulation with position error is found for 11 Purkinje cells. However, the strength of the relationship

between CS firing probability and behavior based on the R^2 values is similar for both predictive (Fig. 16, black bars) and feedback (Fig. 16, red bars) across all parameters ($t(56) = 0.5034$, $p = 0.6167$). Importantly, there was no relationship between the strength (R^2) of the relationship between CS firing probability and the overall CS firing rates (Fig. 16E, $\rho = 0.24$ $p > 0.05$, Pearson's correlation). Together, these results demonstrate that CS firing is highly modulated with both kinematics and position error during tracking, though feedforward CS encoding was considerably more prevalent than feedback encoding. The strength of the CS encoding is not related to the rate of CS discharge.

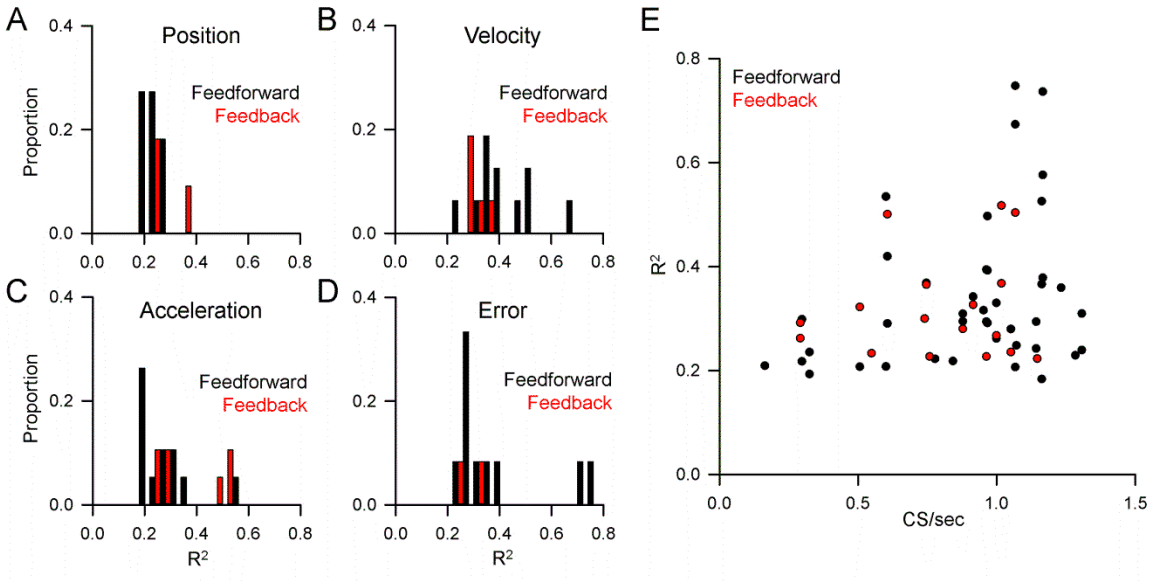

Figure 16: Population summary of the magnitude of CS encoding of behavior. Distribution of R^2 values for feedforward (black bars) and feedback (red bars) relationships between CS firing and A) position, B) velocity, C) acceleration, and D) position error. E) R^2 values for feedforward and feedback CS modulation as a function of mean CS firing rate.

Correlation among behavioral parameters is not reflected in complex spike modulation

CS modulation with multiple behavioral parameters was common, with an average of 1.93 ± 0.87 parameters per neuron. To ensure that CS modulation with multiple

parameters was not due to the interactions between parameters, we determined the degree to which the behavioral parameters were correlated over the 300 msec feedforward and feedback CS-aligned epochs (Fig. 17A). For most parameters, the correlations are minimal with a few exceptions. The highest correlations are for the individual position components (e.g., X_{Ffwd} and X_{Fbck}). However, correlations between the feedforward and feedback epochs for X and for Y position are expected due to the slowly changing nature of position over a 600 msec period. More modest levels of correlation include XE_{Fbck} with VX_{Ffwd} (R^2=0.29) and YE_{Fbck} with VY_{Ffwd} (R^2=0.30)(i.e. the brighter blue squares in Fig. 8A). To address this, we compared the correlation structure between a given pair of behavioral parameters (Fig. 17A) to the number Purkinje cells in which the CSs are significantly correlated with that pair of parameters (Fig. 17B). If the correlation structure in the behavior influences the CS responses, one would expect a similar correlation structure in the CS responses. This would be particularly true for any of the larger correlations observed among parameters (described above), for example for the correlations between X_{Ffwd} and X_{Fbck}, XE_{Fbck} with VX_{Ffwd} or X_{Ffwd} and X_{Fbck}. Consider position, which has the highest correlation between the feedforward and feedback epochs. Eight Purkinje cells exhibited CS feedforward modulation with position, however, none of these cells were also modulated with position feedback. The 3 Purkinje cells that had CS feedback modulation with position are different neurons and, conversely, did not have CS predictive modulation. Another key comparison is for both pairs of Err_{Fbck} and Vel_{Ffwd} parameters (i.e. XE_{Fbck} and $VX_{Ffwd,}$ YE_{Fbck} and VY_{Ffwd}) that also exhibit higher behavioral correlations (Fig. 17A). In contrast, only one Purkinje cell had CS modulation

with both Err_{Fbck} and Vel_{Ffwd}. The more common pairs of parameters with CS modulation, for example, Vel_{Fwd} and Err_{Fwd} that are dually encoded by 6 cells, have a negligible behavioral correlation ($R^2 < 0.005$). To relate the correlations between behavioral parameters to CS modulation, we plotted the correlation between each parameter pair (R^2 from Fig. 17A) against the total number of cells that had dual CS modulation with that parameter pair (from Fig. 17B). Across the population, the higher correlations between behavioral parameters are not reflected in the incidence of dual CS modulation with those parameters (Fig. 17C, $\rho = -0.08$, $p > 0.05$). Together, these results indicate that the interactions between behavioral parameters cannot explain the observed CS modulation, and that the analysis of behavior in the 300 msec feedforward and feedback epochs allows for a relatively independent characterization of the CS modulation, both predictive and feedback, with each of these parameters.

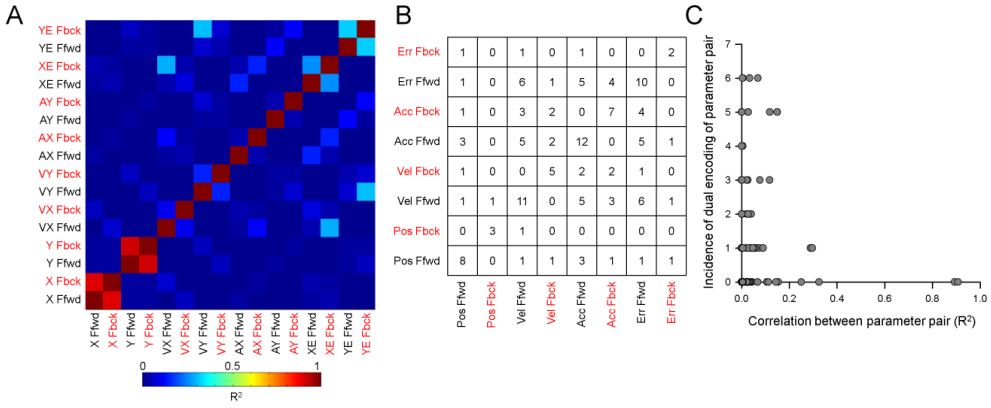

Figure 17: Correlations between parameters and CS modulation. A) Correlation matrix of the regression coefficient (R2) between each pair of behavioral parameters for both feedforward (Ffwd) and feedback (Fbck) epochs. The correlations between parameters were computed based on all trials for all Purkinje cells recorded. B) Frequency of CS modulation with multiple parameters. The numbers in each cell indicate the number of Purkinje cells that had significant modulation with parameters indicated in the row and column. C) Relationship between the frequency of CS modulation with behavior and the correlations between parameters.

Event-related complex spike modulation

To address whether climbing fibers are evoked in response to specific error events, we determined the CS modulation to the time at which the cursor crosses from inside to outside the target. Leaving the target is clearly an error event as only brief excursions outside the target center (<500 msec) are allowed. An error event requires rapid detection and correction to continue tracking and successfully complete a trial. To account for the spatial tuning of the climbing fiber input with position error (for example, see Fig. 18A), we evaluated only excursions occurring within ± 45º of the CS preferred direction determined using the linear regression analyses (Fig. 18B). The average error magnitude aligned to these excursions provides a measure of a position error event, in which the cursor exits the target at t = 0 msec and is followed by a corrective movement to bring the cursor back into the target (Fig. 18D). If responsive to position error events, the expectation is that CS firing would show a distinct increase (or decrease) after the cursor left the target (t = 0 msec in Fig. 18D). This increase should be evident in a plot of the cumulative probability of CS firing. For the example Purkinje cell, the CS firing is not modulated by these position error events, illustrated by the lack of a distinct change in the cumulative probability of occurrence at t = 0 msec. Instead, the cumulative CS firing probability linearly increases from the inside to the outside of the target (Fig. 18E).

A similar question is whether CSs are evoked by events related to hand position, velocity, or acceleration. While a position error event can be clearly defined as the moment the cursor exits the target, there are no such events for the kinematic parameters in our pseudo-random tracking paradigm. Therefore, we defined a kinematic event as when a specific kinematic parameter exceeded a threshold relative to the normal distribution of that parameter. The threshold for a kinematic event was based on the magnitude of a position error event in which the target edge corresponds to approximately the mean + 1SD of the total error magnitude workspace (Fig. 18C, red dashed line). Therefore, for each kinematic parameter an event was defined as the time at which the behavior exceeds the mean + 1SD of the parameter's workspace. An example of acceleration events is illustrated in Fig. 18F-J. For this Purkinje cell, the CS discharge is predictive and directionally tuned with acceleration, with a preferred direction toward the lower right area of the workspace (Fig. 18F-G). As for position error events, acceleration exceeding the mean + 1SD (Fig. 18H, red dashed line) and occurring within ± 45º of the preferred direction were selected as events. The average acceleration illustrates that the analysis identifies events as the acceleration rapidly increases after t = 0 msec, peaks and then returns to within mean + 1SD (Fig. 18I). As is the case for position error, the cumulative CS firing is not strongly related to acceleration events, as there is little change after an event at t = 0 msec (Fig. 18J).

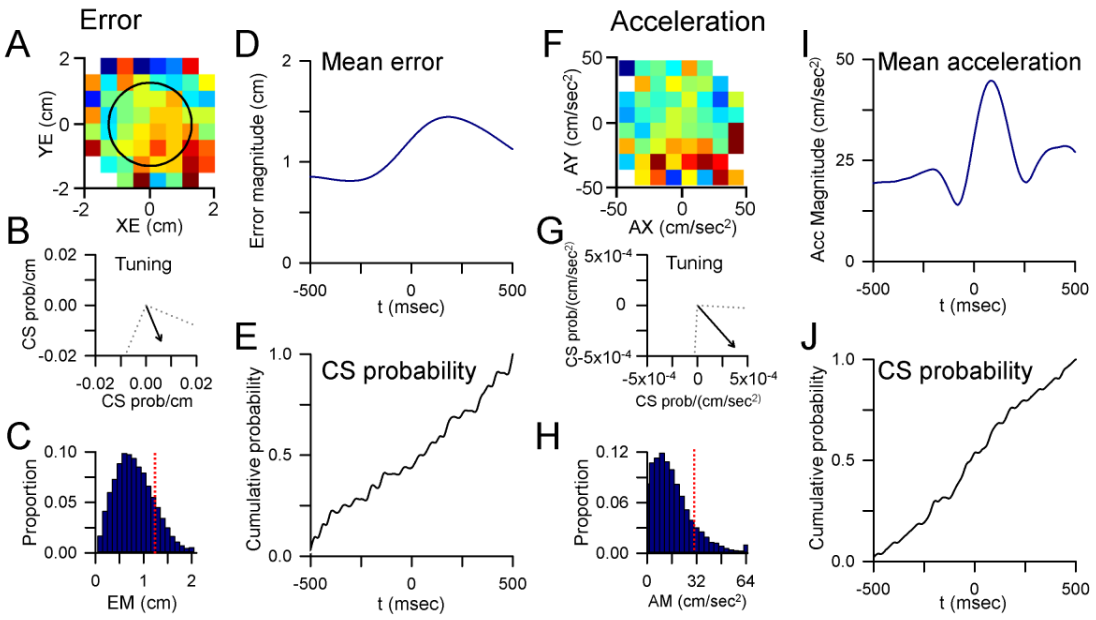

Figure 18: Event-related analysis of CS modulation. A) Example Purkinje cell with significant feedforward CS tuning with position error. B) Preferred direction of CS tuning with ± 45º window used for the analysis. C) Probability distribution of error magnitude (EM) during tracking. Red dashed line indicates the target edge. D) Average error magnitude aligned to the times, t = 0 msec, at which the cursor exited the target (error events) within ± 45º of the preferred direction vector shown in B. E) Cumulative probability of CS firing over a ± 500 msec window around the timing of error events. F) Example Purkinje cell with significant feedforward CS tuning with acceleration. G) Preferred direction of CS tuning. H) Probability distribution of acceleration magnitude (AM) during tracking. Red dashed line indicates the mean + 1 SD of the distribution, the threshold used for identifying acceleration events. I) Average acceleration magnitude aligned to the timing of acceleration events (t = 0 msec). J) Cumulative probability of CS firing over a ± 500 msec window around the timing of acceleration events.

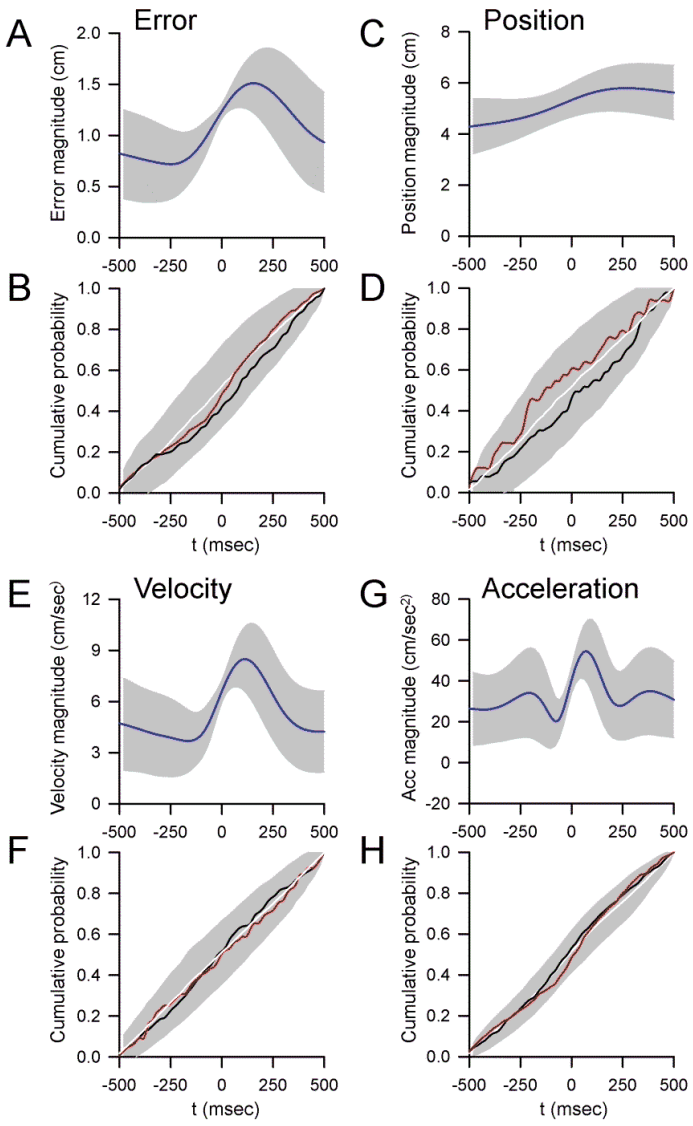

Figure 19: CSs are not evoked by behavioral events. A) Average error magnitude relative to the timing of error events for all Purkinje cells with significant CS tuning with position error (Shaded region indicates SD). B) Cumulative CS probability for all Purkinje cells with significant feedforward (black line) and feedback (red line) CS modulation with errors relative to trial shuffled error events (white line and shaded region = mean + 1 SD). C) Average position magnitude relative to timing of position events for all Purkinje cells with significant CS tuning with position. Conventions are as in A. D) Cumulative CS probability for Purkinje cells with significant CS tuning to position. Conventions are as in B. Average E) velocity and G) acceleration magnitudes and the corresponding cumulative CS probabilities for Purkinje cells with significant CS tuning with F) velocity and H) acceleration are also shown.

Across the population, similar results were obtained for each parameter. For Purkinje cells in which the climbing fiber input are significantly modulated with position errors (Fig. 19A-B), cumulative CS firing probability does not exhibit an inflection around the timing of position error events (Fig. 19B), regardless of whether the relationship between CS firing and position error was predictive (black trace) or feedback (red trace). Similar results are observed for position (Fig. 19C-D), velocity (Fig. 19E-F), and acceleration events (Fig. 19G-H). Together, these results show that during tracking, CSs are not related to behavioral 'events,' either for position error or kinematics. Instead, CS firing is linearly modulated across the workspace of each parameter.

Simple spike modulation with kinematics and position error

We recorded Purkinje cells in lobules IV-VI of the cerebellum, areas that have been shown to be strongly involved with arm movements based on electrophysiological recordings, functional imaging, and the results of lesions (Harvey et al., 1977;Thach, 1970;Fortier et al., 1989;Fu et al., 1997a;Coltz et al., 1999;Roitman et al., 2005;Pasalar et al., 2006;Marple-Horvat and Stein, 1987;Mano and Yamamoto, 1980;Hewitt et al., 2011;Schoch et al., 2006;Kitazawa et al., 1998;Diedrichsen et al., 2005). We thus next assessed the spatial tuning of SS discharge in the same feedforward and feedback epochs utilized for the CS firing. For each parameter, maps of the mean SS firing were determined for 300 msec before (feedforward) and 300 msec after (feedback) the behavior. The significance and preferred direction of SS firing maps were computed as

for the CS firing probability maps. The Purkinje cells recorded were very engaged in pseudo-random tracking, as 44 out of the 45 (98%) are significantly modulated by either kinematics or position error.

Figure 20A illustrates an example of a Purkinje cell with feedback SS modulation with position error. Feedforward SS modulation is not significant (not shown). The SS firing increases in the upper left quadrant of the position error workspace and has a preferred direction of 155º (Fig. 20B). Both the encoding and the magnitude of the SS modulation with position error are significant as assessed by noise distributions obtained from 10,000 shuffled maps (Fig. 20C and D, respectively). For each of the 44 Purkinje cells with significant modulation, we determined the absolute difference between the largest increase and decrease in SS firing for the best encoded parameter calculated using the SS modulation maps. This analysis provides a measure of the depth of modulation in the SS firing across the workspace for a given behavioral parameter. Across the population, the SS firing is highly modulated by kinematics and position errors during tracking, with an average range of 29 ± 13 spikes/sec. Therefore, these Purkinje cells are highly involved in this task.

Across the population, both feedforward and feedback SS modulation with kinematics and position errors is common, as observed previously (Hewitt et al., 2011;Popa et al., 2012). Purkinje cell SS discharge is strongly modulated by position (Fig. 20E, I), velocity (Fig. 20F, J), acceleration (Fig. 20G, K), and position error (Fig. 20H, L). In contrast to

the CS modulation, there is no bias towards either feedforward or feedback SS modulation with behavior (χ^2 (3, n = 167) = 1.61, p = 0.658). Together, these results demonstrate that SS firing contains rich representations of all kinematic and error parameters studied, with broad coverage of the individual workspaces.

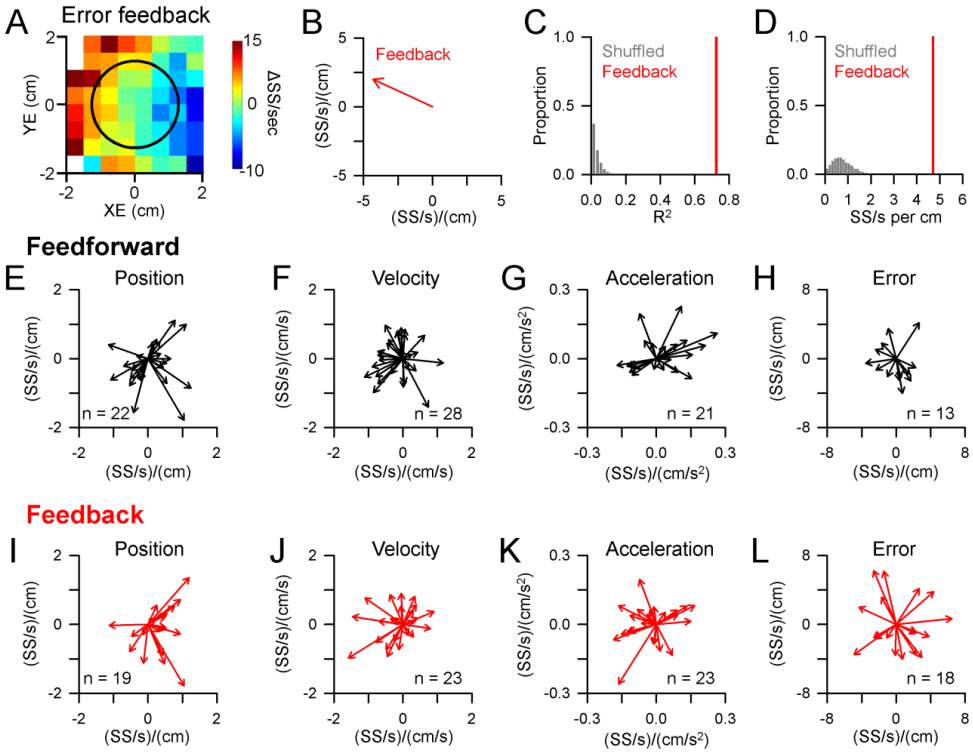

Figure 20: Linear SS modulation with behavior. A) Probability map of example Purkinje cell with feedback SS modulation with position error. Black circle indicates target edge. B) Preferred direction of SS feedback tuning with position error. Feedforward modulation was not significant. C) Magnitude of the feedback SS modulation with position error as quantified by the R^2 (red bar) compared to the distribution of R^2 values from shuffled probability maps (grey bars). D) Magnitude of the feedback SS preferred direction (red bar) compared to the distribution of vector magnitudes from shuffled probability maps (grey bars). E-H) The preferred direction and magnitude of significant feedforward SS firing modulation with E) position, F) velocity, G) acceleration and H) position error for the population. I-L) The preferred direction and magnitude of significant feedback SS firing modulation with the same kinematic and error parameters. N indicates the number of cells with significant modulation.

Directional tuning of complex spike and simple spike firing

A final question was the relationship between the directional tuning of the CSs and SSs, specifically the degree to which SS and CS modulation are reciprocal. All pairs of significant CS and SS modulation with a given behavioral parameter (e.g., velocity) for the same epoch (e.g., feedforward) were selected and the differences computed between the preferred directions (n = 38). Two examples of the spatial tuning of the SSs and CSs are illustrated in Figure 21. The first example Purkinje cell has both predictive CS and SS modulation with velocity, with approximately reciprocal spatial tuning, as evident both by the firing maps (Fig. 21A-B) and the 138º difference in their preferred directions (Fig. 21C).

Many Purkinje cells had CS and SS spatial tuning that was approximately reciprocal (Fig. 21G). However, many Purkinje cells did not follow this pattern as shown in the second example cell with significant feedforward CS and SS modulation with position error (Fig. 21D-E). While the feedforward CS modulation occurs predominantly in the upper right region of the error space, the SS modulation occurs in the lower right region of the space. The difference in the preferred directions is 48º (Fig. 21F). Across the population, the difference in the preferred directions between CS and SS modulation appears to be uniformly distributed, without a significant bias for a certain difference in preferred

direction (χ^2 (19, n = 38) = 16.74, p = 0.6077). Therefore, during pseudo-random tracking, there is not a fixed spatial relationship between the CS and SS modulation.

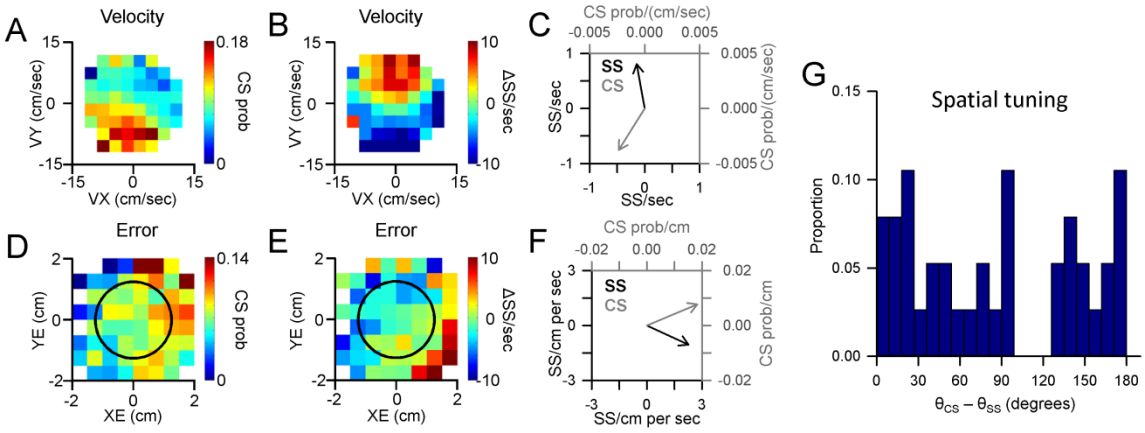

Figure 21: Interaction between CS and SS encoding. A-B) Example Purkinje cell with significant feedforward CS (A) and SS modulation with velocity (B). C) Preferred direction of CS tuning (grey vector) and SS tuning (black vector) (note the difference in scales on X and Y axes for SS and CS). D-E) A second example Purkinje cell with significant feedforward CS modulation with position error (D) and significant feedforward SS modulation with position error (E). F) Preferred direction of CS tuning (gray vector) and SS tuning (black vector). G) Population distribution of the angular differences between the preferred directions for all pairs of significant CS and SS modulation with a given behavioral parameter and the same epoch.

Discussion

This study describes several major observations about the information carried by climbing fiber input to the cerebellar cortex. First, CS discharge modulates not only with motor performance measures but also with movement kinematics. Intriguingly, acceleration was the parameter most commonly correlated with CSs. Second, CS discharge is predominantly predictive of upcoming kinematics and position error. Third, CS discharge is not related to discrete events, either for errors or kinematics. Instead CSs provide a linear representation of each parameter. Finally, CS and SS firing are

modulated by the same parameters, though the relationship between their spatial tuning is not always reciprocal. These results show that during online motor control, CS firing conveys considerable predictive information about multiple aspects of behavior rather than serving primarily as an error feedback signal.

The pseudo-random tracking task provides for a more thorough exploration of the kinematic and position error workspaces than many paradigms (Hewitt et al., 2011;Popa et al., 2012;Paninski et al., 2004). This task results in extensive combinations of kinematic parameters and performance errors and produces a robust data set to assess the signals that activate climbing fibers. The lack of correlation between many of the parameters (e.g., position and velocity) over the brief epochs reflects their orthogonality. Also, pseudo random tracking minimizes the correlations between the feedforward and feedback epochs for most of the parameters, with the exception of position. However, the feedforward-feedback correlations for X and Y are expected and reflect the slow changing nature of hand position. Overall, this task represents a considerable departure from those involving discrete movements, such as reaching or saccade tasks, which produce more stereotypic movement patterns. For example, during reaching there is a stereotypic bell-shaped velocity profile and strong coupling between position and velocity (Abend et al., 1982;Hewitt et al., 2011) or that during smooth pursuit, retinal slip error evokes a corrective eye movement, and thus a change in acceleration (Collewijn and Tamminga, 1984). The greater coverage of the workspaces and low correlations aid in

uncovering the multiple signals in the CS discharge and a fuller characterization of the properties of those signals.

The finding that CSs commonly encode acceleration is intriguing. To our knowledge, this is one of a few studies describing acceleration-dependent CS firing. During ocular following, while eye velocity was the strongest driver of CSs, the acceleration contribution to the CS modulation is greater for CSs than for the SSs (Kobayashi et al. 1998). During three-dimensional vestibular stimulation, CS discharge correlates with inertial acceleration (Yakusheva et al., 2010). The prevalence of acceleration encoding may clarify the commonly observed increase in climbing fiber activity at movement onset during reaching or single joint movements (Mano et al., 1986;Ojakangas and Ebner, 1994;Fu et al., 1997b;Hewitt et al., 2015), as movement onset involves large changes in acceleration. Furthermore, the observation of acceleration modulation, in combination with the other aspects of the movement encoded, emphasizes that CSs signal a wide spectrum of movement information.

For each parameter investigated, CS discharge provides a planar representation of the workspace, with a clear directional component characterized by a preferred direction vector. This planar encoding strengthens previous observations that the climbing fiber input provides graded information about the behavior (Fu et al., 1997b;Ebner et al., 2002;Kitazawa et al., 1998;Kobayashi et al., 1998). In contrast, the analyses failed to detect any evidence for a threshold or event-like signals at which CS firing was

preferentially evoked. Instead, a linear model provides a better fit of the data. Linear representations may optimize separation of patterns, are less susceptible to saturation and increase the dynamic range (Chen et al., 2016;Fujita, 1982;Park et al., 2012). Similar linear encoding characterizes SS firing in a variety of tasks (Hewitt et al., 2015;Popa et al., 2012;Hewitt et al., 2011;Medina and Lisberger, 2009;Dash et al., 2012;Shidara et al., 1993;Chen et al., 2016) and Purkinje cells are thought to linearly integrate parallel fiber and inhibitory interneuron inputs (Park et al., 2012;Walter and Khodakhah, 2006;Walter and Khodakhah, 2009). Therefore, the cerebellar cortex utilizes linear encoding of movement information in both the climbing fiber-Purkinje cell and the mossy fiber-granule cell-Purkinje cell circuits.

During pseudo-random tracking, the degree of reciprocal modulation between SS and CS firing was distributed uniformly among Purkinje cells (see Fig. 10). Reciprocal modulation of SSs and CSs is commonly observed during several behaviors, including the vestibulo-ocular and optokinetic reflexes (Graf et al., 1988;Kobayashi et al., 1998;Stone and Lisberger, 1990a;Kitama et al., 1999). Importantly, out of phase modulation is not due to the pause in SS activity that follows a CS (Yakusheva et al., 2010;Kobayashi et al., 1998). The climbing fiber projection itself plays a dominant role in the reciprocity as shown in the *Ptf1a::cre,Robo3*$^{lox/lox}$ mouse (Badura et al., 2013). In this mutant, climbing fiber input is rerouted and projects almost exclusively to the ipsilateral flocculus, yet the SS and CS discharge exhibit normal reciprocity. However, a spectrum of relationships between the directional tuning of SS and CS discharge have

been observed in reaching tasks (Ebner et al., 2002;Ojakangas and Ebner, 1994) and in-phase modulation has been reported for rotation in the dark and during three dimensional vestibular stimulation (Yakusheva et al., 2010;Winkelman et al., 2014). Therefore, while a reciprocal pattern of SS and CS firing occurs in many behaviors, this is not a completely "hard-wired" relationship, but instead appears to be task specific.

One of the more remarkable findings in this study is that for the majority of Purkinje cells, CS occurrence led the behavior. Furthermore, predictive CS signaling was observed across all parameters, extending our initial report of feedforward CS discharge during pseudo-random tracking (Streng et al., 2017). Many previous studies emphasized that CSs respond to sensory inputs or after the onset of movement. It was even argued that CS only respond to unexpected sensory feedback (Gibson et al., 2004). As noted in the Introduction, recent eye blink conditioning studies report CS increases prior to and predicting the conditioned response (Ohmae and Medina, 2015;Ten Brinke et al., 2015). In both of these studies, the predictive modulation was also accompanied by the CS response to the unconditioned stimulus. In contrast, during our demanding tracking task predictive CS modulation was greater than two times as common as the feedback responses (see Fig. 15).

The mechanism underlying the predictive encoding remains to be investigated and we can only speculate on the circuitry involved. The inferior olive receives a variety of excitatory and inhibitory inputs including from the spinal cord, nuclei at the

mesodiencephalic junction, cerebellar nuclei, and cerebral cortex (for reviews see (De Zeeuw et al., 1998;Oscarsson, 1980;Apps and Garwicz, 2005)), integrating both feedforward and feedback information. For the development of predictive CS signals during classical conditioning it was suggested that recurrent activity within the olivocerebellar network plays a major role (Ten Brinke et al., 2015). Another possibility is cerebral cortical involvement, specifically the motor cortices, in generating feedforward signals. Importantly, the responses of inferior olivary neurons to glutamatergic inputs from the motor cortex are bi-phasic in a manner that appears to penalize late inputs (Garden et al., 2017). This could create a bias toward early motor signals and thus a mechanism for the predictive CS modulation. Taken together, these observations suggest that, at least during pseudo-random tracking, CS discharge contains predictive motor signals about multiple aspects of the upcoming behavior instead of predominately providing sensory feedback.

Another intriguing observation is that the same behavioral parameters linearly modulate both CSs and SSs in the same reference frames. This suggests that these two activity modalities of Purkinje cells function in concert during movements as opposed to acting independently. Consistent with this hypothesis, it was demonstrated that when Purkinje cells are organized according to the CS directional tuning, the SS population response provides a better prediction of the speed and direction of saccades (Herzfeld et al., 2015). Moreover, we recently reported a mechanism that integrates online CS and SS activity, showing that CSs control the information encoded in the SS firing (Streng et al., 2017).

Both increases and decreases in the SS sensitivity to these same motor parameters are tightly timed to CS occurrence. For the Purkinje cells common to both studies, a number of encoding changes are also associated with significant CS modulation with behavior (9 cells, 12 parameters). Nearly all of those CS-coupled changes in SS encoding changes are associated with predictive CS modulation with behavior (10/12 parameters), consistent with the hypothesis that climbing fiber discharge alters the SS sensitivity in anticipation of a change in behavior. Furthermore, at the population level, these changes in encoding are consistent with optimizing behavior, with increases in SS encoding of the kinematic parameters followed by kinematic changes and increases in SS encoding of position error followed by decreases in position error. Therefore, we interpret the prevalence of feedforward CS modulation as a mechanism to inform the output of the cerebellar cortex of the need to update the information represented in the SS firing in anticipation of upcoming behavioral demands.

CHAPTER 4: SENSORY PREDICTION ERROR SIGNALS IN PURKINJE CELL SIMPLE SPIKE DISCHARGE

Introduction

Effective motor control requires continuous monitoring and correction for motor errors (Todorov and Jordan, 2002;Berniker and Kording, 2008;Shadmehr et al., 2010;Wolpert and Ghahramani, 2000). While early views postulated that error detection and correction was achieved primarily by closed-loop, sensory feedback-mediated control (Miall and Wolpert, 1996;Wolpert and Ghahramani, 2000;Shadmehr et al., 2010;Kawato, 1999), the delays imposed by sensory feedback loops render this type of control inadequate and even unstable (Miall and Wolpert, 1996;Wolpert and Ghahramani, 2000;Shadmehr et al., 2010;Kawato, 1999). Additionally, error correction occurs more rapidly than (Flanagan and Wing, 1997) and even in the absence of sensory feedback (Shadmehr et al., 2010;Xu-Wilson et al., 2009;Golla et al., 2008;Wagner and Smith, 2008), necessitating alternative mechanisms for error detection and correction.

One compelling hypothesis is that the central nervous system implements a forward internal model that predicts the sensory consequences of motor commands (Flanagan et al., 2003;Morton and Bastian, 2006;Robinson, 1975;Xu-Wilson et al., 2009;Maschke et al., 2004;Shadmehr et al., 2010;Imamizu et al., 2000;Diedrichsen et al., 2005). These predictions are then compared to the actual sensory consequences, resulting in a sensory prediction error (SPE) (Wolpert and Ghahramani, 2000;Shadmehr et al., 2010). It has

been proposed that SPEs are the critical error signals for both online control and motor learning (Shadmehr et al., 2010;Kawato and Wolpert, 1998;Miall and Wolpert, 1996;Wolpert and Ghahramani, 2000;Wong and Shelhamer, 2011;Mazzoni and Krakauer, 2006). Extensive behavioral, clinical, imaging, and physiological evidence suggests that the cerebellum serves as a forward internal model (Wolpert et al., 1998;Wolpert et al., 1995;Kawato, 1999;Shadmehr et al., 2010;Bell et al., 2008;Pasalar et al., 2006;Bastian, 2006). Additionally, the cerebellum has long been implicated in error processing (Oscarsson, 1980;Gilbert and Thach, 1977;Ito, 2000;Stone and Lisberger, 1986;Kawato and Gomi, 1992), and more recently in processing the SPEs essential for adaptation (Miall and Wolpert, 1996;Shadmehr et al., 2010;Diedrichsen et al., 2005;Tseng et al., 2007). The mechanisms by which SPEs are encoded, however, remain unknown. Of particular interest is the representation of SPEs in the discharge of cerebellar neurons.

A longstanding view is that errors are encoded exclusively by complex spike (CS) discharge of Purkinje cells (Gilbert and Thach, 1977;Kitazawa et al., 1998;Ito, 2000;Ito, 2013;Stone and Lisberger, 1986;Kawato and Gomi, 1992). Clearly, there has been compelling evidence for this hypothesis from studies of retinal slip (Graf et al., 1988;Kobayashi et al., 1998;Barmack and Shojaku, 1995;Stone and Lisberger, 1990b), arm movement perturbations (Gilbert and Thach, 1977;Kim et al., 1987;Kitazawa et al., 1998;Kitazawa et al., 1998;Lou and Bloedel, 1986;Andersson and Armstrong, 1987), and during learning (Yang and Lisberger, 2014). However, considerable evidence suggests

that CSs may not be the sole or simply an error signal in a variety of tasks (Horn et al., 1996;Catz et al., 2005;Dash et al., 2010;Prsa and Thier, 2011;Ebner et al., 2002;Fu et al., 1997b;Soetedjo et al., 2008a;Soetedjo and Fuchs, 2006). Furthermore, questions remain on whether the low frequency CS discharge (0.5-2.0 Hz) provides adequate bandwidth for continuous error monitoring(Ojakangas and Ebner, 1994;Kitazawa et al., 1998;Popa et al., 2012;Popa et al., 2014). Therefore, while CSs respond to errors in many tasks, the responsive properties are richer as we have shown during pseudo-random tracking (Chapter 3).

A complementary hypothesis is that the higher frequency simple spike (SS) discharge of Purkinje cells also encodes error signals. SS discharge modulates linearly with retinal slip velocity independent of eye movement kinematics (Kase et al., 1979). SS firing modulates with trial success or failure during reaching (Greger and Norris, 2005) and with direction or speed errors during circular tracking, including leading those errors (Roitman et al., 2009). Changes in SS firing following smooth pursuit adaptation appear sufficient to drive learning (Kahlon and Lisberger, 2000). Cerebellar-dependent VOR adaptation can be driven by instructive signals in the SS firing (Nguyen-Vu et al., 2013), even in the absence of climbing fiber input (Ke et al., 2009). During pseudo-random manual tracking, SS discharge encodes a dual representation of errors at both lead and lag timing. Furthermore, the SS firing can be used to decode both predictive and feedback errors with remarkable accuracy (Popa et al., 2012;Popa et al., 2017). The representations

have opposing effects on the SS firing, consistent with the predictive and feedback signals necessary to compute SPEs (Popa et al., 2012;Popa et al., 2014).

Therefore, SS discharge encodes the predictive and feedback information consistent with SPE (Popa et al., 2015). However, whether these SS signals have the properties needed to be labelled as predictive and feedback is unclear. To test this hypothesis, we investigated how disrupting sensory information pertinent to motor error prediction and feedback during the pseudo-random tracking task modulates SS activity. Visual feedback was reduced by hiding the cursor while it was inside the target or delayed by introducing a lag between manipulandum movement and cursor movement. In the feedback reduction paradigm, linear encoding of errors was reduced such that encoding was restricted to the target edge, where visual feedback was available. Conversely, the magnitude of predictive encoding of errors was not significantly affected. In the feedback delay paradigm, the timing of predictive encoding was negatively shifted equal to the duration of the delay, consistent with a forward internal model that has not adapted to the delay and makes predictions with respect to the manipulandum movement rather than the delayed cursor. Importantly, predictive and feedback encoding of arm kinematics was unaffected in both paradigms, suggesting a representation of arm movement irrespective of the visually-dependent performance errors. Our results suggest that dual encoding of errors and kinematics by SS discharge represents the predictive and feedback signals necessary for the generation of SPEs.

Materials and methods

All animal experimentation was approved by the Institutional Animal Care and Use Committee of the University of Minnesota and conducted in accordance with the guidelines of the National Institutes of Health.

Random tracking

This study utilized a variant of the pseudo-random tracking paradigm described previously (Hewitt et al., 2011;Popa et al., 2012;Paninski et al., 2004). Two rhesus monkeys were trained to use a robotic manipulandum (InMotion^2) that controls a cross-shaped cursor to track a circular shaped target (2.5-3.5cm in diameter) on a computer screen. The paradigm started with an initial hold inside a stationary target for a random period of time (500 – 3000 msec). The initial target position on the screen was also random. Next, the target moved along a trajectory selected randomly from 100 trajectories defined *a priori*. Pseudo-random target paths were generated from a sum of sine waves and ranged from 3-10s. Target speed was randomly varied so that the average speed was approximately 4 cm/s and conformed to the two-thirds power law (Viviani and Terzuolo, 1982;Lacquaniti et al., 1983). The trajectories were low-pass filtered and selected to avoid sharp turns and large changes in speed, and ended with a final hold period of 500-3000 msec. The paradigm required that the monkey maintain the cursor within the target, and allowed only brief excursions outside the target (<700 msec). Note that the hold times, length of trajectories and duration of permitted "excursions" were modified from the original studies in order to accommodate the increased difficulty of

tracking in the altered feedback conditions. Pseudo-random tracking has several advantages compared to other tasks including providing more comprehensive and uniform coverage of parameter workspaces and dissociating kinematic from error parameters (Paninski et al., 2004;Hewitt et al., 2011). Hand (X and Y, based on cursor position) and target (X_{tg}, Y_{tg}) position were sampled at 200 Hz. Cursor velocity (VX, VY) was derived by numerical differentiation of the hand position, and position error (XE, YE) was defined as the difference between cursor and target positions.

Visual feedback manipulations

This study applied two novel manipulations of visual feedback during pseudo-random tracking in order to test whether the SS modulation with performance errors and kinematics represents the predictive and feedback components of sensory prediction error. For a given recording session, a block of baseline trials were first collected. For the second block of trials, one of two manipulations of visual feedback were implemented during tracking. Visual feedback was delayed (delay condition) by introducing a lag between the movement of the manipulandum and resulting movement of the cursor on the computer screen by either 100 or 200 msec. Visual feedback was reduced (hidden cursor condition) by hiding the cursor from view while it is inside the moving target, allowing for a significant reduction in visual feedback without prohibitive difficulty of the task. Recording sessions typically consisted of blocks of 50 baseline trials followed by 50 visual feedback manipulation trials, though in many cases more trials were collected. Importantly, visual feedback manipulations were removed during the inter trial

intervals, during which the animal moved the cursor to a new target start position, in order to reduce any adaptation effects.

Surgical procedures, electrophysiological recordings and data collection

Head restraint hardware and a recording chamber targeting lobules IV-VI of the intermediate and lateral cerebellar zones were chronically implanted over the ipsilateral parietal cortex in each animal using aseptic techniques and full surgical anesthesia. The positions of the electrodes were confirmed by radiographic imaging techniques that combined a CT scan of the skull with an MRI of the cerebellum (Hewitt et al., 2011). After full recovery from chamber implantation surgery, extracellular recordings were obtained during normal daytime hours using Pt-Ir electrodes with parylene C insulation (0.8-1.5 MΩ impedance, Alpha Omega Engineering, Nazareth, Israel). Purkinje cells in lobules IV-VI of the intermediate and lateral cerebellar zones were identified by the presence of CSs followed by the characteristic pause in SS activity and recorded using previously established methods (Hewitt et al., 2015;Streng et al., 2017). After conventional amplification and filtering (30 Hz-3 kHz band pass, 60 Hz notch), SSs were discriminated online using the Multiple Spike Detector System (Alpha Omega Engineering, Nazareth, Israel). Resulting spike trains were digitized and stored at 1 kHz. The raw electrophysiological data was also digitized and stored at 32 kHz.

Analysis of simple spike modulation

SS firing relative to both error and kinematic parameters was analyzed using temporal linear regressions.(Popa et al., 2012;Hewitt et al., 2011) The goal of this initial analysis was to determine the predictive and/or feedback SS modulation with the behaviors of interest: position, velocity, and position error. Correlations between SS firing and each pair of error (XE and YE) and kinematic (X and Y or VX and VY) parameters is assessed at 20 msec time steps to determine the lead/lag (τ-value) between SS activity and behavioral parameters.(Hewitt et al., 2011;Ashe and Georgopoulos, 1994;Medina and Lisberger, 2009;Gomi et al., 1998;Popa et al., 2012) At each time step, SS variability associated with the rest of the parameters is removed by determining the firing residuals from a multi-linear model of SS firing that includes the kinematic and error parameters. The firing residuals are then regressed against the parameters of interest, generating the R^2 and regression coefficient (β) profiles as a function of τ. For example, the firing residuals needed to evaluate the SS modulation with position error are obtained by regressing actual firing (F) to this multi-linear model:

$$F(t) = ß_o(\tau) + ß_X(\tau)X(t + \tau) + ß_Y(\tau)Y(t + \tau) + ß_{VX}(\tau)VX(t + \tau) + ß_{VY}(\tau)VY(t + \tau) + \varepsilon(t + \tau) \quad \text{(eqn. 1)}$$

The resulting firing residuals (FR, equivalent to ε) are then regressed to the two position error terms, XE and YE:

$$FR(t) = ß_0(\tau) + ß_{XE}(\tau)\ XE(t + \tau) + ß_{YE}(\tau)\ YE(t + \tau)$$

(eqn. 2)

This regression results in, for each τ, an R^2 value indicating goodness of fit of the SS firing to both XE and YE, and two regression coefficients (ß), one for each error parameter. The overall SS sensitivity to position error is computed from the two regression coefficients:

$$\text{Sensitivity} = \sqrt{{\beta_{XE}}^2 + {\beta_{YE}}^2}$$

(eqn. 3)

The significance of the R^2 at each τ-value was assessed against a noise distribution of shuffled data. R^2 values were obtained from 100 repeats of the same regression analysis performed on firing and behavioral data uncoupled through random trial shuffling. The threshold for significance was defined as the mean ± 3SD of the shuffled distribution. For each parameter, significant correlations were defined if a local maximum of the R^2 profile at either predictive or feedback timings exceeded the trial shuffled noise level. Then, the timing (τ-value) of the peak lead and/or lag was determined. A similar analysis as outlined in eqn 1-3 was undertaken for velocity and position.

Analysis of visual feedback delay

For the visual feedback delay paradigm, our primary hypothesis was that introducing a lag between the movement of the manipulandum and the movement of the cursor would affect the timing of the SS encoding of position errors. Therefore, we determined the peak predictive and/or feedback timing (τ) of the SS modulation with each behavior of interest under both baseline and delay conditions using the regression analysis described

above. To ensure that we were accurately comparing the same SS signals between baseline and delay, peaks were selected for analysis if they were present in both baseline and delay conditions with the same sign regression coefficients (e.g. positive modulation with XE and YE in both baseline and delay). An additional question was whether the temporal specificity of SS modulation, defined as the width of the R^2 peak, was affected by the visual feedback delay. To address this, we quantified the slope of each peak in both baseline and delay conditions by computing the ratio between the peak magnitude and the half width of the peak.

Analysis of visual feedback reduction

During the hidden cursor condition, the effect of hiding the cursor while it is inside the target creates two conditions during tracking: one where there is no visual feedback available (cursor inside target boundary) and one where there is visual feedback available (cursor outside target boundary). Thus, to assess the effects of the hidden cursor paradigm, we performed two separate analyses: one to determine the SS encoding while the cursor was inside the target, where visual feedback was unavailable, and one while the cursor was outside the target, where visual feedback was available. For the first analysis, we performed similar temporal linear regression analyses (eqn. 1-3), but only using the time points during which the cursor was inside the target center (as well as the SS firing before and after those time points in 20 msec steps, as described above). The resulting R^2 and sensitivity profiles provided a quantification of the SS encoding of behavior inside the target for the both baseline and hidden cursor conditions. Encoding

decreases were considered significant if the peaks exceeded the statistical threshold for significance in the baseline but not hidden cursor conditions. Significant increases in error encoding (below threshold in baseline but above threshold in the hidden cursor condition) were uncommon, occurring in only 3 Purkinje cells.

Given that for the hidden cursor condition, visual feedback was only available outside the target boundary, we reasoned that the SS modulation may increase outside the target boundary. The goal of the second analysis for the hidden cursor condition was thus to determine whether there was increased SS modulation outside the target edge, where visual feedback was available. To accomplish this, we first computed the expected SS modulation with position error based on the linear model obtained under baseline conditions for each peak predictive and feedback τ. This resulted in a map of the error workspace, indicating the expected SS modulation for a given XE and YE error bin. We next compared these expected error maps to the observed maps obtained during the hidden cursor condition. The difference between the two maps indicated areas of the error workspace in which the SS modulation exceeded the modulation expected given the baseline conditions.

Analysis of kinematic modulation

We also assessed the effects of visual feedback manipulation on the SS encoding of kinematics. For the delay condition, we determined the timing of SS modulation with hand kinematics (position and velocity) in both baseline and delay conditions using the

same methods as those described for position error. For the visual feedback reduction, we determined the magnitude of predictive and feedback modulation with kinematics in both baseline and hidden cursor conditions. Importantly, we restricted the analysis to the behavior occurring only when the cursor was inside the target center as for position error.

Results

Visual feedback delay paradigm

Sixty-two Purkinje cells were recorded from two rhesus macaques during pseudo-random tracking under both normal (baseline) conditions and with visual feedback delay (delay condition). Of those 62, 43 were collected with a delay of 100 msec and 19 with a delay of 200 msec. As we have reported previously, the SS firing of Purkinje cells in lobules IV-VI of the intermediate and lateral cerebellar zones are highly modulated with both limb kinematics and performance errors (Hewitt et al., 2011;Popa et al., 2012;Streng et al., 2017). Purkinje cells can have both lead and lag spike representations of one or more behavioral parameters. Of this population, the SS firing of 7 Purkinje cells have at least one representation of position, 38 of velocity, and 30 of position error. In total, 50 cells had significant modulation with at least one parameter. The first set of analyses focuses on those cells with significant SS modulation with position error.

Both baseline and delay conditions result in similar coverage of the parameter workspaces (Fig. 22A-B), with no significant difference in the probability distributions for position ($F(1,127) = 0.67$, $p = 0.42$, ANOVA), velocity ($F(1,127) = 0.08$, $p = 0.77$,

ANOVA), and position error ($F(1,127) = 0.95$, $p = 0.33$, ANOVA) and the animals strive to keep the cursor near the target center (Fig. 22C). The similar coverage of all parameter workspaces suggests that the visual feedback delay does not induce a significant change in strategy during tracking. Importantly, the animals show no evidence for adaptation either across trials (baseline, $\rho = -0.12$ $p > 0.05$, Pearson's correlation, delay = 100, $\rho = 0.07$, $p > 0.05$) or recording days (baseline, $\rho = -0.27$ $p > 0.05$, Pearson's correlation, delay = 100, $\rho = -0.03$, $p > 0.05$) (Fig. 22D-E).

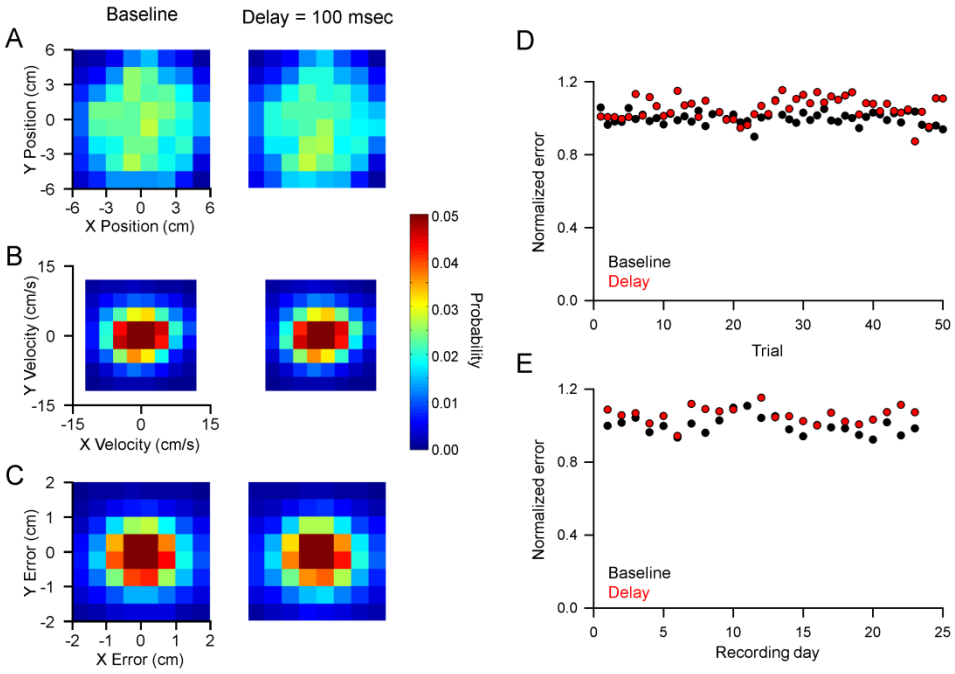

Figure 22. Behavior during pseudo-random tracking and effects of delayed cursor paradigm. Average probability densities for cursor position (A), velocity (B), and position error (C) across all recording sessions for both baseline (left column of A-C) and the 100 msec delay (right column of A-C) conditions. Average probability values are indicated by color bar. D) Average position error over trials for baseline (black circles) and 100 msec delay (red circles). Position error magnitudes were normalized to the average error magnitude in the baseline condition. E) Average position error over recording days for baseline (black circles) and 100 msec delay (red circles). Position error magnitudes were normalized to the average error magnitude in the baseline condition.

Visual feedback delay shifts feedforward encoding of position errors

The primary hypothesis tested by delaying the visual feedback concerned the lead SS encoding. A forward internal model that has not adapted to a delay in visual feedback will continue to make predictions with respect to non-delayed cursor movement, equivalent to the movement of the manipulandum (Fig. 23A). If the SS discharge functions as the output of a forward internal model, the expectation is that the predictive error signals will shift to longer feedforward leads (see Fig. 23B). The shift in the predictive timing is because the forward internal model continues to operate as if it were in the baseline condition in which there is no delay between the cursor and hand movement. As long as the forward internal model has not adapted, the model will make predictions about the upcoming sensory consequences at earlier leads by an amount equal to the imposed delay. The hypothesis also predicts that because the feedback error signals monitor the cursor movements, the timing of the SS feedback signals will not change.

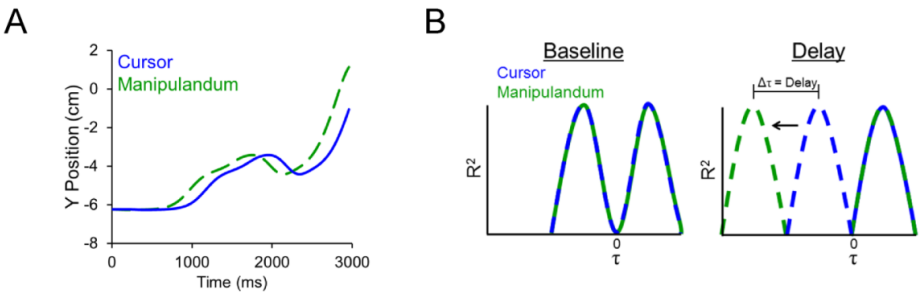

Figure 23. Visual feedback delay and expected results. A) Visual feedback delay was induced by introducing a lag between the movement of the manipulandum (green dashed line) and the cursor (blue solid line. B) The expected outcome of the visual feedback delay is a negative shift in the lead encoding to more feedforward times, indicating predictive encoding with the movement of the manipulandum and not the delayed cursor (indicated by shift in dashed green line). Conversely, the lagged encoding should be unaffected.

An example Purkinje cell that has both lead and lag modulation with position error is shown in (Fig. 24). Under baseline conditions, there is strong SS modulation in the lower half of the position error workspace that leads behavior by -400 to 0 msec. At more feedback times (200 to 600 msec), SS modulation is strongest on the right side of the error workspace. When visual feedback is delayed by 200 msec, the lead SS modulation shifts to more negative time points, and the strongest modulation occurs between -600 to -200 msec. Conversely, the timing of the strongest lag modulation is unaffected. The SS modulation with behavior at each time point is quantified using a temporal linear regression analysis (see Materials and Methods), resulting in R^2 (Fig. 24B) and sensitivity profiles (Fig. 24C) for both the baseline and delay conditions. Baseline SS encoding has lead and lag peaks at -100 and 440 msec, respectively. Under delay conditions, the timing of predictive encoding occurs earlier, with a peak at-280 msec. Conversely, the timing of feedback encoding, either for the R^2 or sensitivity profiles, is unaffected, with a peak at 420 msec.

Similar changes in the timing of lead encoding are observed across the population for both 100 and 200 msec delays (Fig. 24D), with the delay conditions resulting in a more significant shift for lead than lag encoding (Fig. 24E, $E(1,39) = 11.732$, $p = 0.002$, ANOVA). Importantly, this effect is significant across all cells with significant lead and/or lag encoding of position errors. The average shift in the lead encoding is approximately equal to the duration of the feedback delay, with an average shift of -118 ±

123 msec for 100 msec delay and -206 ± 105 msec for the 200 msec delay. As predicted by our hypothesis (Fig. 23), the lag SS modulation relative to position error is not affected by the delay, consistent with a visual feedback signal. In contrast, the feedforward SS modulation shifts earlier (more negative τ-value), consistent with a predictive signal that estimates the upcoming position errors given the movement of the manipulandum, not the delayed visual information. Also, the differential effects on the lead and lag encoding confirms the independence of these two aspects of the SS modulation. Together, these results suggest that the leading SS modulation encodes the prediction of performance errors, and that the timing shift observed in the visual feedback delay reflects the output of a forward internal model computing predictions made with respect to the movement of the manipulandum and not the delayed cursor.

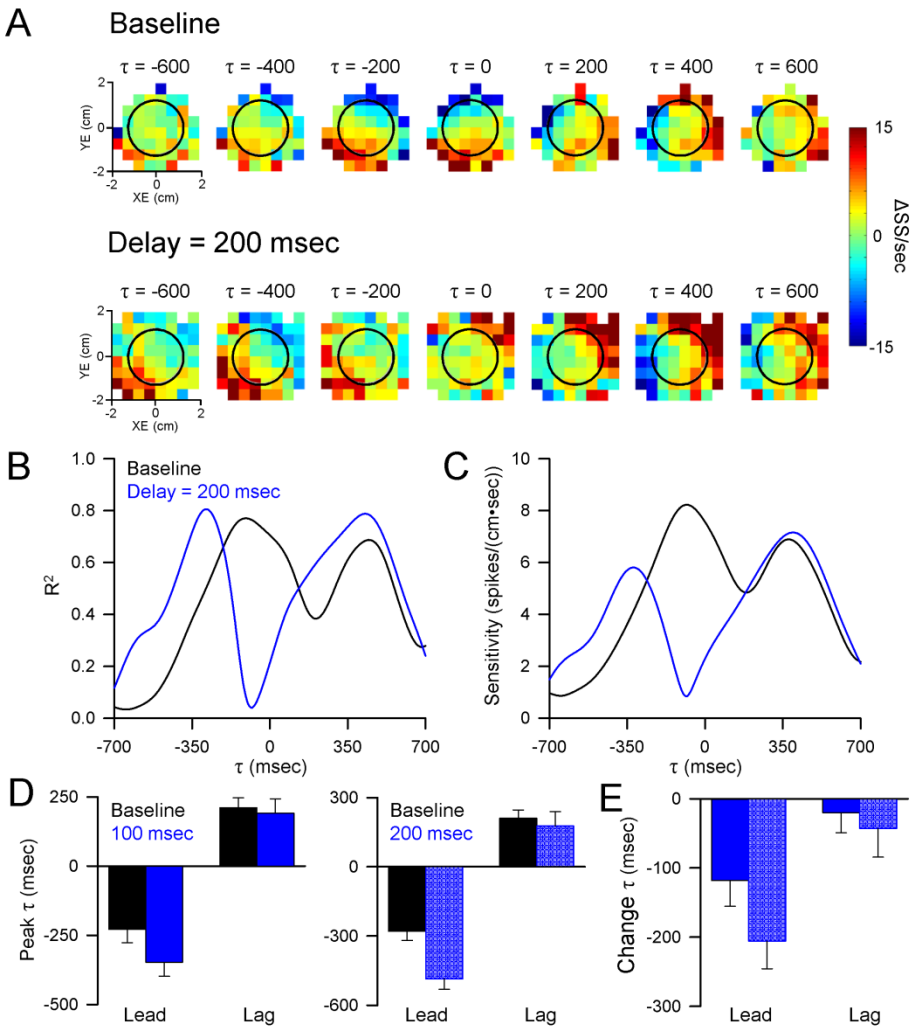

Figure 24. Visual feedback delay shifts predictive encoding of performance errors. A) Firing maps for an example Purkinje cell with lead and lag SS modulation with position error in both baseline (top row) and 200 msec delay (bottom row) conditions. Each map indicates SS modulation at a specific lead (negative time points) or lag (positive time points) τ. Black circle indicates target edge. R^2 (B) and sensitivity (C) temporal profiles computed using linear regression analyses (see Materials and Methods) quantifying the SS encoding of position error in both the baseline (black line) and 200 msec delay (blue line) conditions. As for the firing maps, negative τs indicate lead SS encoding. D) Average peak timing of lead and lag encoding for baseline and both 100 msec (left) and 200 msec (right) delays. Error bars denote SEM. E) Average change in the timing of peak lead and lag encoding in the 100 msec (solid blue) and 200 msec (checkered blue) conditions, illustrating a significant shift in the timing of lead SS encoding.

Feedback delay reduces temporal specificity of simple spike encoding

The delay in visual feedback is that it introduces a temporal mismatch between manipulandum movement and cursor movement. As such, we also assessed whether the temporal specificity of SS encoding was affected by the visual feedback delay. We reasoned that reduced temporal specificity of encoding would be reflected in the slope of the peak, such that decreased slopes would indicate decreases in the specificity. An example Purkinje cell is shown in Figure 25. Under baseline conditions, the R^2 and sensitivity profiles (Fig. 25A and B) for this cell reveal both lead and lag SS encoding of position error. As for the previous example, the 200 msec delay in visual feedback shifts the lead peak more negatively, while the lag peak is unaffected. However, both peaks show a decreased slope in the visual feedback delay condition. We computed the slope of each significant peak (change in R^2 over time) each in both baseline and delay conditions. Across the population, visual feedback delay results in a significant decrease in slope for both lead and lag peaks (Fig. 25C, $F(3,69) = 6.16$, $p < 0.001$, ANOVA). Together, these results suggest that the mismatch between manipulandum movement and cursor movement induced by the visual feedback delay condition alters both the timing and temporal specificity of SS encoding of position errors.

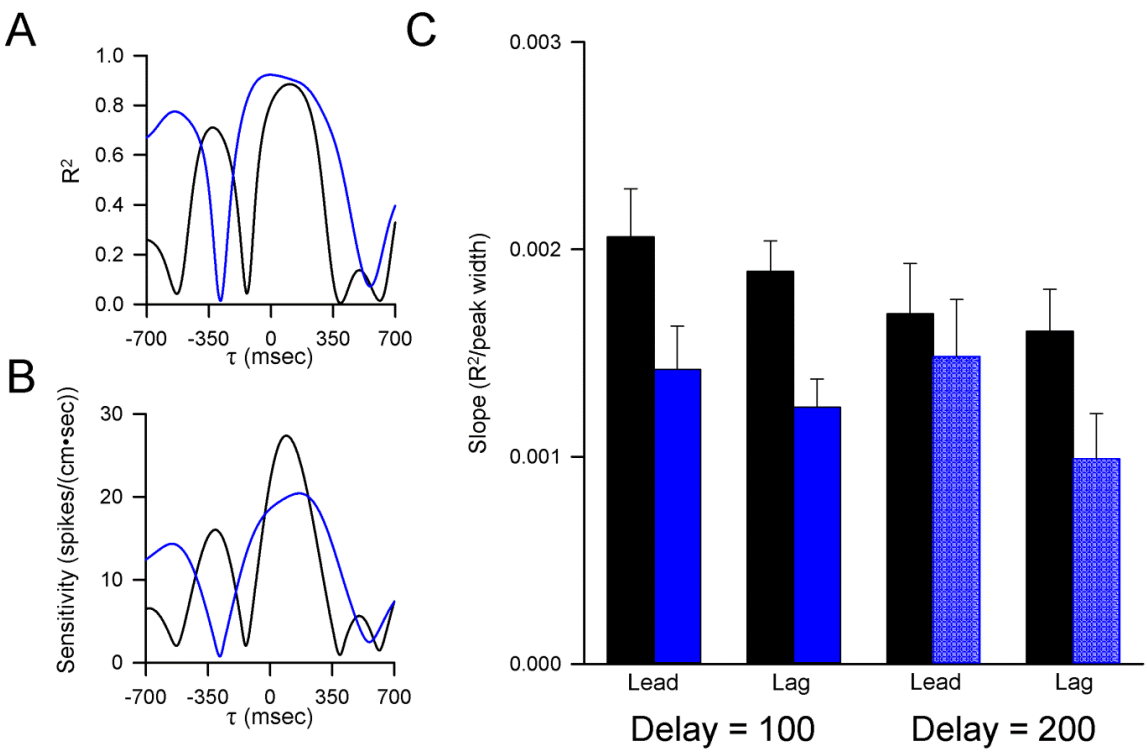

Figure 25. Visual feedback delay reduces temporal specificity of SS encoding. R^2 (A) and sensitivity (B) temporal profiles for an example Purkinje cell with both lead and lag encoding of position errors in baseline (black line) and 200 msec delay (blue line) conditions. C) Average peak slope for position error encoding for all Purkinje cells in the baseline (black bars), 100 msec delay (solid blue bars) and 200 msec delay (checkered blue bars) conditions, illustrating the significant decrease in peak slope in the visual feedback delay condition. Error bars denote SEM.

Visual feedback reduction paradigm

Thirty-six Purkinje cells were recorded during pseudo-random tracking under both normal (baseline) conditions and with visual feedback reduction (hidden cursor condition). As for those recorded in the feedback delay paradigm, the SS firing of Purkinje cells is correlated with many different combinations of behavioral parameters at different timings. Of the population, the SS activity of 16 Purkinje cells are correlated with position, 30 with velocity, and 25 with error (21 with lead encoding, 15 with lag

encoding. 10 cells had both lead and lag encoding). In total, 33 Purkinje cells had significant encoding of at least one parameter.

As for the delay paradigm, coverage of the parameter workspaces is similar in both baseline and hidden cursor conditions, with no significant change in the probability distributions for position (Fig. 26A, $F(1,127) = 1.74$, $p = 0.19$, ANOVA), velocity (Fig. 26B, $F(1,127) = 0.02$, $p = 0.90$, ANOVA), or position error (Fig. 26C, $F(1,127) = 0.002$, $p = 0.97$, ANOVA). The animals strive to keep the cursor near the target center (Fig. 26C), indicating that there is no change in strategy induced by the visual feedback reduction. Additionally, there is no evidence for improvement of performance across trials, with mean performance errors actually tending to increase over both trials (baseline, $\rho = 0.16$ $p > 0.05$, Pearson's correlation, hidden, $\rho = 0.29$, $p = 0.03$) and recording days (baseline, $\rho = 0.29$ $p = 0.11$, Pearson's correlation, hidden, $\rho = 0.62$, $p < 0.01$) in the hidden cursor, but not baseline condition (Fig. 26D-E).

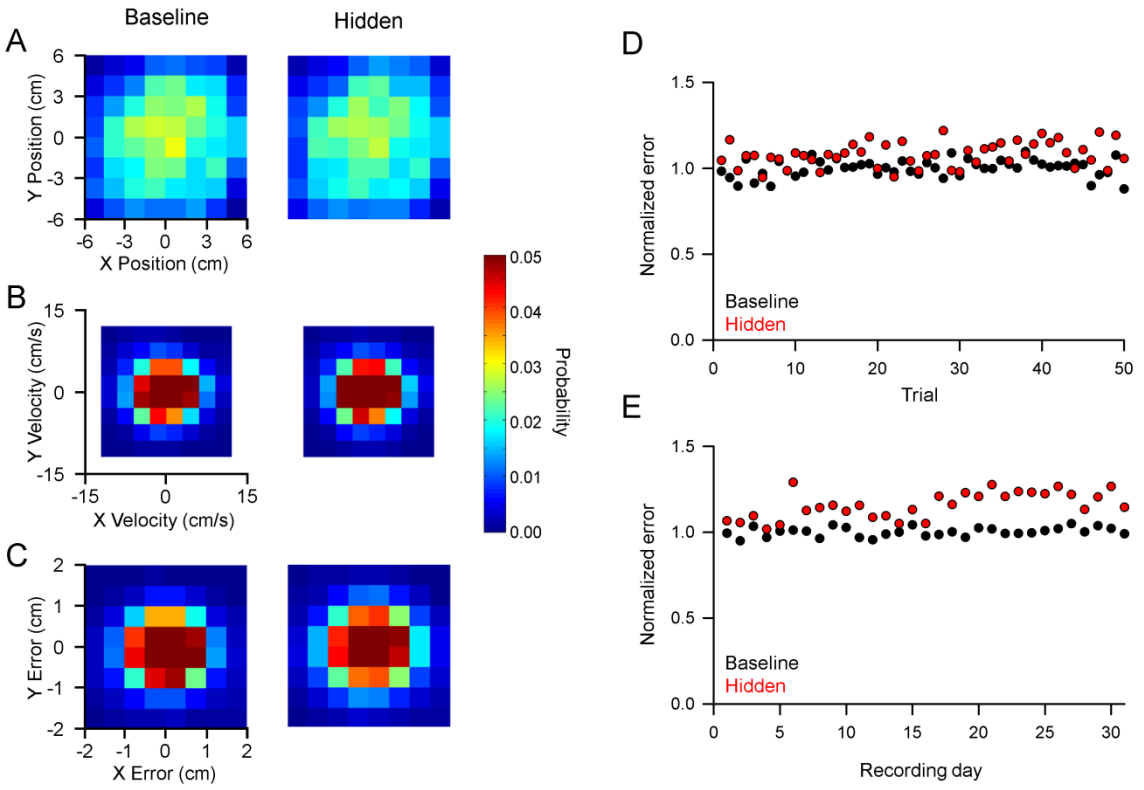

Figure 26. Behavior during pseudo-random tracking and effects of hidden cursor paradigm. Average probability densities for cursor position (A), velocity (B), and position error (C) across all recording sessions for both baseline (left column of A-C) and the hidden cursor (right column of A-C) conditions. Average probability values are indicated by color bar. D) Average position error over trials for baseline (black circles) and hidden cursor (red circles). Position error magnitudes were normalized to the average error magnitude in the baseline condition. E) Average position error over recording days for baseline (black circles) and hidden cursor (red circles). Position error magnitudes were normalized to the average error magnitude in the baseline condition.

Feedback encoding of performance errors is decreased by reduced visual feedback

The primary hypothesis tested by this feedback manipulation concerned the lagged SS encoding of position errors. Given that the cursor is hidden from view whenever it is inside the target edge (Fig. 27A), the expectation is that if the lagged SS modulation represents the feedback encoding of position errors, it should be reduced whenever the

cursor is inside the target. Conversely, if the lead encoding is a prediction of upcoming position errors, it should be relatively unaffected (Fig. 27B).

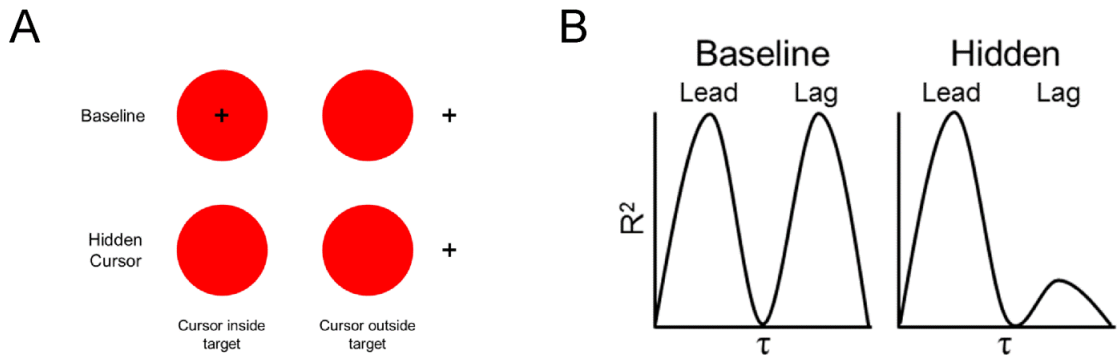

Figure 27. Hidden cursor paradigm and expected results. A) Visual feedback was reduced by hiding the cursor while it was inside the target. Whenever the cursor left the target boundary, the cursor became visible. B) The expectation is that reducing visual feedback should reduce the lagged encoding of position errors inside the target boundary. Conversely, the lead encoding should not be decreased.

An example Purkinje cell with both lead and lag SS modulation with position errors is shown in Figure 28. Under baseline conditions, there is strong modulation in the upper half of the error workspace that leads the behavior by -500 to -300 msec, and strong modulation in the lower half of the error workspace that lags the behavior by 100 to 300 msec (Fig. 28A). When the visual feedback is reduced in the hidden cursor position, the SS modulation leading the behavior is relatively maintained, with positive modulation in the upper half of the workspace both inside and outside the boundary of the target (indicated by black circle). The lagged SS modulation with position errors is markedly reduced, however, such that there is little to no modulation within the target boundary (Fig. 28A). The SS modulation was quantified using temporal linear regression analysis as for the visual feedback delay. However, we restricted our analysis to the behavior and

SS firing occurring inside the boundary of the target to quantify the effects of the feedback reduction, as we reasoned that the lagged SS encoding would be reduced within but not outside the target boundary. The R^2 (Fig. 28B) and sensitivity (Fig. 28C) profiles mirror the effects seen in the firing maps; significant lead and lag encoding of position errors is observed during baseline conditions, whereas visual feedback reduction greatly reduces the magnitude of lag, but not lead SS encoding (Fig. 28B-C). Therefore, the SS firing for this Purkinje cell during the hidden cursor paradigm strongly matched the predictions (Fig. 27).

Significant reductions in SS modulation were defined as encoding that exceeded the threshold for significance in the baseline but not hidden cursor condition. Across the population, significant reductions in lag encoding were observed in 11/15 of the Purkinje cells with significant lag encoding of position errors. In those cells with significant decreases, analysis of variance yielded a significant interaction between the feedback condition and the timing of encoding ($F(1,35) = 10.65$, $p = 0.0026$, ANOVA), with the hidden cursor condition significantly reducing the overall magnitude of the lagged encoding of position errors, but not the lead encoding (Fig. 28D). The 4 Purkinje cells with lagged encoding that did not decrease below threshold still showed an overall decrease in lagged encoding. Peak lag encoding for those 4 cells averaged at an R^2 of 0.79 ± 0.06 for baseline and 0.62 ± 0.12 for hidden cursor. Together, these results suggest that the lagged SS modulation represents feedback encoding of position errors. Conversely, the lead SS modulation is not altered with the reduction in visual feedback,

consistent with a predictive signal. Finally, as for the delay condition, the results confirm the independence of the feedforward and feedback modulation.

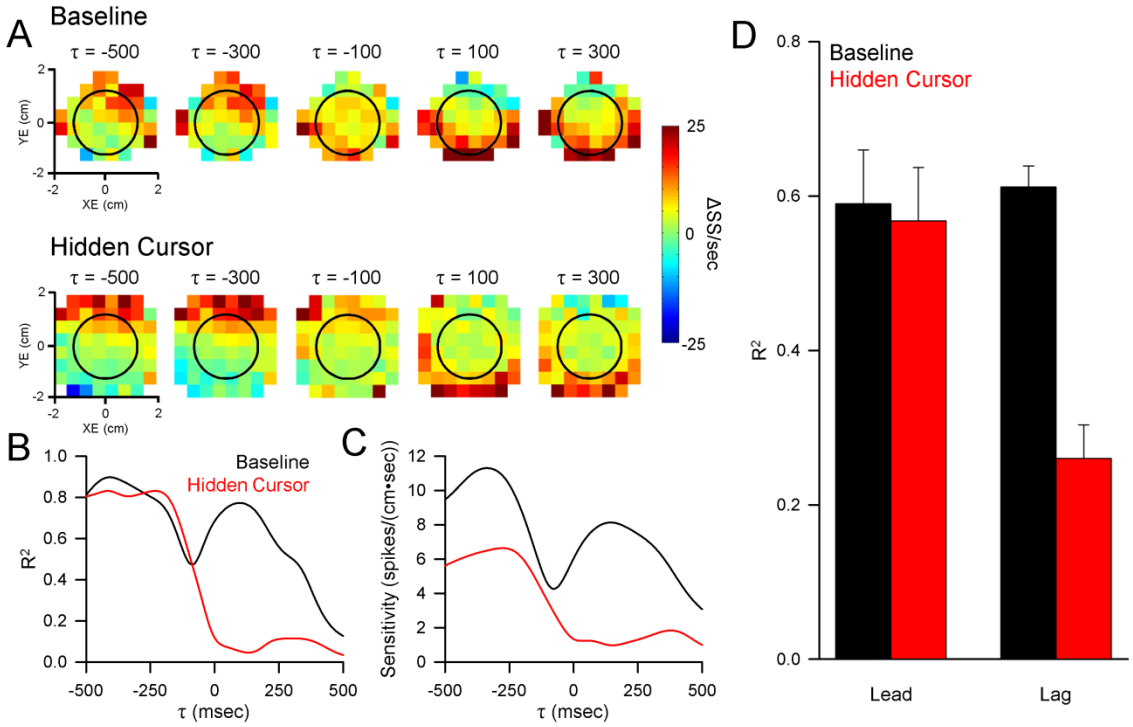

Figure 28. Hidden cursor reduces feedback encoding of performance errors. A) Firing maps for an example Purkinje cell with lead and lag encoding of position errors on both the baseline (top row) and hidden cursor (bottom row) conditions. Black circle indicates target edge. R^2 (B) and sensitivity (C) profiles for the Purkinje cell in (A), illustrating the decrease in lagged SS encoding of position errors. D) Average encoding strength (R^2) of both lead and lag encoding for the 11 Purkinje cells with significant decreases in SS encoding of position errors in the hidden cursor condition.

Simple spike modulation emphasizes information outside the target boundary during visual feedback reduction

One expectation for the visual feedback reduction paradigm is that, given that visual feedback is only available outside the target boundary, there may be an increase in the importance of cursor information outside the target. Intriguingly, while the SS

modulation inside the target is reduced by the hidden cursor condition, the SS modulation outside the target edge is not (see Fig. 28A). An additional hypothesis is that the increased relevance of position error information outside the target edge would be reflected as an increase in the SS modulation outside the target. To test this, we computed the expected lead and lag SS modulation with position errors from the behavior in the hidden cursor using the linear model derived from baseline firing at the peak τ (see Materials and Methods), and compared that expected modulation to the real SS firing observed during the hidden cursor paradigm. An example Purkinje cell with both lead and lag modulation with position errors is shown in Figure 29. The expected SS modulation maps are calculated using the linear model from baseline firing, and the observed maps are the actual SS modulation during the hidden cursor condition. The difference maps are the discrepancy between expected and observed SS modulation. For the lead encoding, there is an increase in SS firing outside the target edge, particularly on the right side of the workspace (Fig. 29A). For the lag encoding, the SS modulation outside the target edge shows an even greater increase, with the observed SS modulation exceeding expected for the majority of the bins outside the target (Fig. 29B).

We assessed for significant differences in expected versus observed SS modulation for each significant peak across the population (paired t-test) and found that the a large number of both predictive (10/21 Purkinje cells) and feedback (10/15 Purkinje cells) SS modulation was significantly greater than expected from baseline conditions. Across the population, we compared, for each bin of the error workspace outside the target

boundary, the expected versus observed SS lead and lag modulation. Analysis of variance of yields a significant interaction between the visual feedback condition and the timing of SS modulation ($F(1,2513) = 14.26$, $p = 0.0002$, ANOVA), with a significantly greater increase in observed modulation for lag encoding than for lead encoding. Together, these results suggest that the hidden cursor condition shifts the lagged SS modulation towards the target edge, where visual feedback is available.

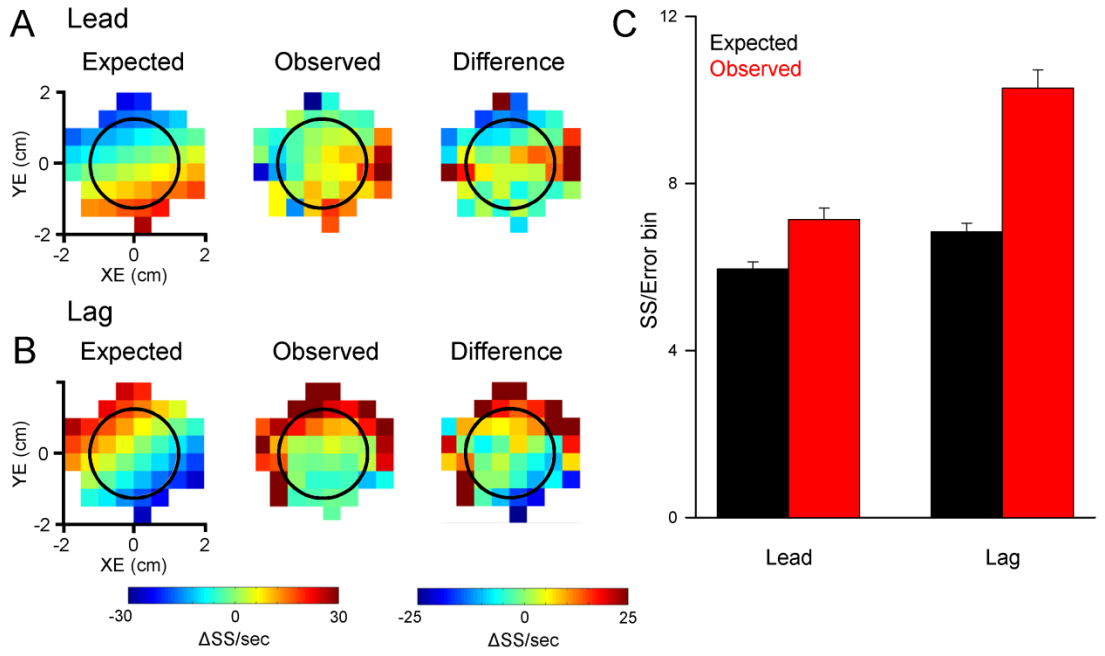

Figure 29. Hidden cursor paradigm increases SS modulation outside target edge. A-B) Firing maps for an example Purkinje cell with significant lead (A) and lag (B) encoding of position errors. Maps on the far left indicate the expected SS modulation at the peak τ in the hidden cursor using the linear model computed at the peak τ under baseline conditions (see Materials and Methods). The middle maps indicate the observed SS modulation at the peak τ in the hidden cursor condition. SS modulation is indicated by color bar on bottom left. The maps on the far right indicate the difference between observed and expected SS modulation, with increases (warmer colors) indicating observed modulation that is greater than expected. Change in modulation is indicated by color bar on bottom right. C) Average absolute magnitude of expected (black bars) versus observed (red bars) SS modulation across all error bins for all Purkinje cells with significant lead and/or lag encoding of position error (n = 25 Purkinje cells). Error bars indicate SEM.

Manipulations of visual feedback do not affect simple spike encoding of kinematics

While the SS firing during random tracking is highly correlated with position errors, multiple studies have shown that SS firing contains robust representations of kinematics, including hand positon and velocity (Hewitt et al., 2011;Popa et al., 2012;Streng et al., 2017;Popa et al., 2015). While the position errors are defined as the difference between cursor and target positions on the screen, measurements of kinematics reflect both the visual kinematics of the cursor as well as the kinematics of limb movement. As such, an additional question is whether the lead and lag SS modulation with kinematics primarily reflects the encoding of limb movements or the visual movements of the cursor. If the SS modulation with kinematics reflects limb movement information, then the timing of both lead and lag encoding of manipulandum movement should be unaffected in the visual feedback delay condition. Additionally, the magnitude of both lead and lag encoding of kinematics should be unaffected in the visual feedback reduction condition.

Two example Purkinje cells recorded during the feedback delay and feedback reduction conditions, respectively, are shown in Figure 30. The first example Purkinie cell has strong lead encoding of velocity in both baseline and delayed cursor conditions (Fig 30A-B). Importantly, the timing of both peak encoding strength (Fig. 30A) and sensitivity (Fig. 30B) are unaffected by a delay of 100 msec (note that the profiles reflect SS modulation with manipulandum velocity, not delayed cursor velocity). Similar results are observed across the population (n = 38 cells with significant encoding of manipulandum

position or velocity), with no significant change in the timing of lead or lag encoding of manipulandum kinematics (Fig. 30C, $p = 0.70$, ANOVA). The second example Purkinje cell also has strong lead and lag encoding of velocity in baseline and hidden cursor conditions. Note that, as for the error encoding, the SS modulation with manipulandum kinematics in both baseline and hidden cursor reflects the encoding inside the target boundary only. Unlike the encoding of position error inside the target boundary, the magnitude of the lagged encoding of velocity inside the target is unaffected by the feedback reduction paradigm (Fig. 30 D-E). Across the population (30 Purkinje cells with significant encoding of manipulandum position or velocity), there is no significant change in either lead or lag encoding of kinematics in the hidden cursor paradigm (Fig. 30F, $p = 0.22$, ANOVA). Together, these results suggest that SS modulation with kinematics during random tracking reflects the encoding of limb movements, not the visual movements of the cursor.

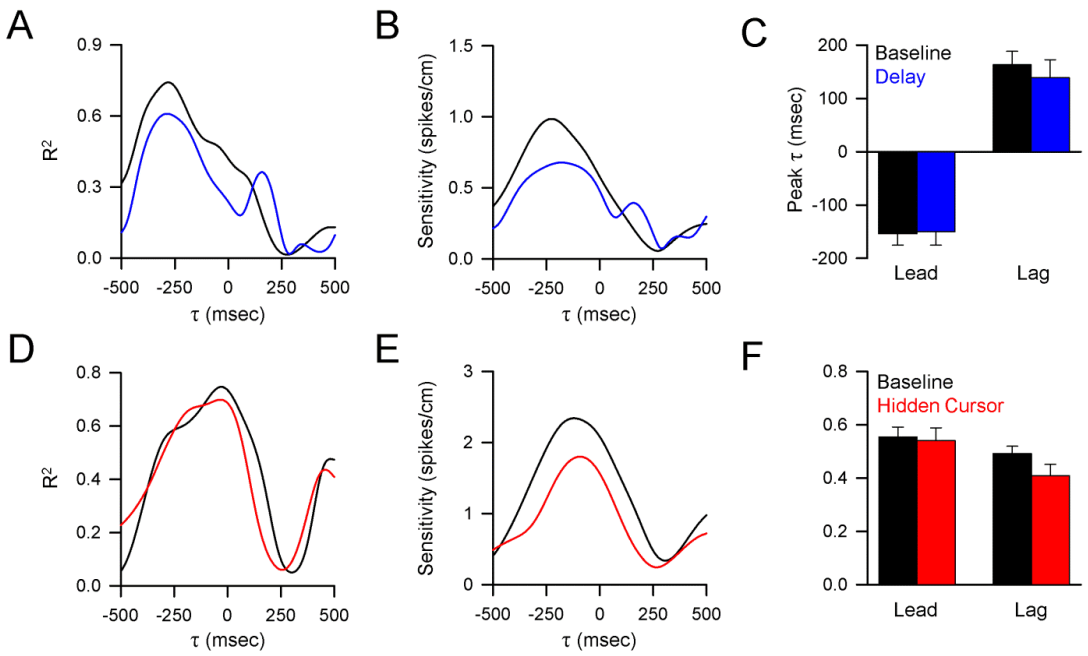

Figure 30. Kinematic encoding is unaffected by visual feedback manipulations. A) R^2 profile for an example Purkinje cell with significant encoding of manipulandum velocity in both baseline (black line) and 100 msec delay (blue line) conditions. B) Sensitivity profile for the example Purkinje cell in (A). C) Average peak timing of both lead and lag SS encoding of manipulandum kinematics in baseline and delay conditions. Error bars indicate SEM. D) R^2 profile for an example Purkinje cell with significant encoding of manipulandum velocity in both baseline (black line) and hidden cursor (red line) conditions. E) Sensitivity profile for the example Purkinje cell in (D). F) Average encoding strength (R^2) of lead and lag encoding for all Purkinje cells with significant encoding of kinematics.

Discussion

This study characterizes SS modulation with continuous measures of kinematics and performance errors during an on-line motor control task. Two novel manipulations of visual feedback applied during tracking reveal that the SS modulation encodes both predictive and feedback information about performance errors and kinematics consistent with the output of a forward internal model. Delaying visual feedback results in

predictive SS encoding about performance errors being shifted to earlier leads, consistent with a forward internal that has not adapter to the delay and continues to generate feedforward predictions with respect to the movement of the hand but not to the delayed movement of the cursor. The degree of the shift matches the duration of the delay used. Reducing visual feedback inside the boundary of the target shifts the SS feedback modulation primarily to outside the target boundary, where visual feedback is available, consistent with encoding of the visual feedback of performance errors. Conversely, SS modulation with hand kinematics was unaffected in both paradigms, consistent with the encoding of hand kinematics and not the visual cursor movement. The major findings of this study are that the SS firing during pseudo-random tracking is consistent with encoding the predictive and feedback components of sensory prediction error, the predictive and feedback signals are independent, and that the firing contains robust representations of both performance errors and kinematics.

Pseudo-random tracking and visual feedback manipulations

Pseudo-random tracking provides a considerable advantage for examining cerebellar signals relevant to online motor control, as it requires continuous monitoring and correction for errors. This is a substantial departure from other tasks involving reaching and saccades, which instead evoke discrete, highly stereotypic errors. The dynamic and highly challenging nature of pseudo-random tracking allows for a thorough evaluation of signals relevant to motor prediction and feedback in cerebellar neurons.

Both of the visual feedback manipulations implemented during pseudo-random tracking increase the difficulty of an already challenging task. However, the distributions of kinematics and performance errors show that the manipulations of visual feedback do not induce any major changes in the animals' strategy, as they still strive to maintain the cursor in the target center. The fact that the densities do not differ shows that the movement kinematics are comparable. Additionally, there is little evidence for any adaptation to the feedback manipulations, either over trials or recording sessions. This is likely due to the fact that the feedback manipulations are removed during the intertrial interval, as rapid switching between task conditions limits adaptation (Herzfeld et al., 2014;Gonzalez Castro et al., 2014). Thus, the changes in SS encoding observed during the delayed and hidden cursor paradigms are a product of the altered visual feedback and not any fundamental changes in the movement kinematics, strategy or adaptation effects.

Computing predictive and feedback

With approximately 200,000 parallel fiber-Purkinje cell synapses (Napper and Harvey, 1988) and less than 200 active synapses are required to generate a SS (Isope and Barbour, 2002), Purkinje cells appear to have the capacity to carry a large number of signals. Cerebellar granule cells, the origin of parallel fiber inputs to Purkinje cells, are modulated by a host of both sensory and motor parameters (Bengtsson and Jorntell, 2009;Huang et al., 2013;Chadderton et al., 2004;Ishikawa et al., 2015;Powell et al., 2015) This provides Purkinje cells with the necessary information to compute both predictions and feedback about movements. In support of this, cerebellar damage produces deficits in predictive

control of movement (Horak and Diener, 1994;Nowak et al., 2004;Martin et al., 1996;Smith and Shadmehr, 2005), and increased cerebellar activation is associated with predictable changes in target location during teaching (Diedrichsen et al., 2005). Increases in cerebellar activation occur with errors (Diedrichsen et al., 2005;Ide and Li, 2011;Imamizu et al., 2000) and omission of an expected sensory stimulus (Tesche and Karhu, 2000).

Changes in error sensitivity

One particularly striking findings is the increased SS modulation outside the target boundary in the hidden cursor condition. The degree to which the motor system responds to an error is highly dependent on the task and environment in which the errors are generated, leading to the concept of error sensitivity (Herzfeld et al., 2014;Huang and Shadmehr, 2009). Error sensitivity changes with error size (Robinson et al., 2003), task parameters (Wei and Kording, 2009), subjective value of error(Trent and Ahmed, 2013), and perturbation statistics (Herzfeld et al., 2014;Huang and Shadmehr, 2009;Gonzalez Castro et al., 2014). One possible mechanism that could underlie changes in error sensitivity is to alter how neurons respond to motor errors. In the visual feedback reduction condition, the SS sensitivity to performance errors is altered to emphasize the error information outside the target boundary, where visual feedback is available. This provides to our knowledge the first demonstration at the neuronal level for control of error sensitivity (Herzfeld et al., 2014;Huang and Shadmehr, 2009;Gonzalez Castro et al., 2014;Robinson et al., 2003) and a demonstration that cerebellar neurons adjust their

sensitivity to the available sensory feedback (Scott, 2004;Todorov and Jordan, 2002). This is consistent with optimal feedback control in that the motor system tunes the representations of sensory feedback to prevailing task demands (Diedrichsen et al., 2010;Scott, 2004;Todorov and Jordan, 2002).

Implications for forward internal models

If the predictive and feedback components of SPE are computed by Purkinje cells and encoded by their SS output, then an outstanding question is where the discrepancy between those signals, or the sensory prediction error itself, is computed. The deep cerebellar nuclei (DCN) are a likely candidate for the initial step in this integration due to the convergence of numerous Purkinje cells onto a DCN neuron.(Person and Raman, 2012;Chan-Palay, 1977;Palkovits et al., 1977) Responses of nuclear neurons are highly dependent on the synchronicity of Purkinje cell SS firing (Person and Raman, 2012;Bengtsson et al., 2011;Gauck and Jaeger, 2003;Gauck and Jaeger, 2000), and therefore, could integrate the predictive and feedback signals in a population of Purkinje cells to provide an estimate of their mismatch. In support of this, neurons of the rostral fastigial nucleus are selectively modulated by passive rather than active self-generated motion (Brooks and Cullen, 2013). During active self-generated motion, under ideal conditions the sensory consequences predictions would match the actual feedback, resulting in a negligible SPE. However, passive motion introduces unexpected sensory feedback, thus generating SPE. Similarly, dentate neurons appear to encode the omission

of a stimulus from a regularly presented sequence (Ohmae et al., 2013). The preference of DCN modulation for unexpected events could indicate a correlate of SPE encoding.

A crucial aspect of the forward internal model is the use SPEs to update motor commands and guide motor learning (Miall and Wolpert, 1996;Wolpert and Ghahramani, 2000;Wong and Shelhamer, 2011;Mazzoni and Krakauer, 2006;Taylor and Ivry, 2012;Gaveau et al., 2014). Thus, SPEs need to be transmitted to structures that specify the motor command. As the final output of the cerebellum (with the vestibular nuclei), DCN neurons can provide that information via excitatory projections to multiple brainstem nuclei and indirectly to numerous motor cortical areas via the thalamus (Thach, 1968;Goodkin and Thach, 2003;Flament and Hore, 1988;Meyer-Lohmann et al., 1977;van Kan et al., 1993;Strick, 1983;Chapman et al., 1986;Schmahmann and Pandya, 1997;Kelly and Strick, 2003;Gibson et al., 1985;Dum et al., 2002). An outstanding question is the mechanism by which the discrepancy between the predictive and feedback information in SS firing is used to update the forward model and subsequent predictions, an additional function of SPEs (Wolpert and Ghahramani, 2000;Shadmehr et al., 2010). One potential candidate for an update signal would be the climbing fiber input to the cerebellar cortex. As we have recently demonstrated, complex spike discharge is associated with robust and rapid changes in SS encoding (Streng et al., 2017). The DCN provide feedback to the inferior olive both directly via a population of GABAergic neurons and indirectly via the red nucleus (Lang et al., 1996;De Zeeuw et al., 1989;Teune et al., 2000;Bengtsson and Hesslow, 2006). Together, this allows for a loop in which

prediction and feedback is computed by the SS discharge, compared by the DCN, and the discrepancy between the two would alter subsequent predictions via CS-coupled changes in SS encoding.

CHAPTER 5: ADDITIONAL DISCUSSION AND NEXT STEPS

As reviewed in the Introduction, the cerebellum plays a crucial role in fine control of movements and error correction. In particular, extensive evidence suggests that the cerebellum serves as a forward internal model for motor control, predicting the sensory consequences of motor commands and comparing them to their actual consequences, generating sensory prediction errors which guide motor learning and adaptation (Wolpert et al., 1998;Wolpert et al., 1995;Kawato, 1999;Shadmehr et al., 2010;Bell et al., 2008;Pasalar et al., 2006). While the dominant hypothesis has been that CSs encode errors, this is not a universally accepted view, and emerging evidence suggests that CSs are not invariably activated by errors (Popa et al., 2014;Llinas, 2013). Additionally, the mechanisms by which the predictive and feedback components of a forward internal model are represented by cerebellar neurons have not been fully elucidated. The results in this thesis provides new insights into these questions and novel mechanisms by which the cerebellum contributes to effective motor control in a dynamic environment.

The role of climbing fiber input to the cerebellum

The results of Chapter 2 outline a highly novel hypothesis about the function of climbing fiber input to the cerebellar cortex. During pseudo-random tracking, climbing fiber discharge dynamically controls the information present in the SS firing, triggering robust and rapid changes in SS encoding of motor signals in 67% of Purkinje cells. The changes in encoding, tightly coupled to CS occurrences, consist of either increases or decreases in

the SS sensitivity to kinematics or position errors and are not due to differences in SS firing rates or variability. Nor are the changes in sensitivity due to CS rhythmicity. In addition, the CS-coupled changes in encoding are not evoked by changes in kinematics or position errors. Instead, CS discharge most often leads alterations in behavior. Increases in SS encoding of a kinematic parameter are associated with larger changes in that parameter than are decreases in SS encoding. Increases in SS encoding of position error are followed by and scale with decreases in error. The results suggest a novel function of CSs, in which climbing fiber input dynamically controls the state of Purkinje cell SS encoding in advance of changes in behavior.

Chapter 3 further expands on the observation that CS discharge tends to lead behavior by characterizing CS modulation with kinematics and performance errors. A reverse correlation approach was used to determine feedforward and feedback CS firing probability maps with position, velocity and acceleration, as well as position error. The direction and magnitude of the CS modulation were quantified using linear regression analysis. The major findings are that CSs significantly encode kinematics and position error. The modulation is not related to 'events,' either for position error or kinematics. Instead, CSs are spatially tuned and provide a linear representation of each parameter evaluated. The CS modulation is largely predictive. Similar analyses show the SS firing is modulated by the same parameters as the CSs. Therefore, CSs carry a broader array of signals than previously described and argue for climbing fiber input having a prominent role in online motor control.

Together, these findings are a major departure from the dominant views of cerebellar physiology, which for over 40 years asserted that complex spike firing serves primarily as the sole error signal in the cerebellar cortex (for reviews see (Boyden et al., 2004;Hansel et al., 2001;Gao et al., 2012;Ito, 2001;Marr, 1969;Albus, 1971;Jorntell and Hansel, 2006)). Instead, climbing fiber input to the cerebellum actively controls the information present in SS firing in advance of changes in behavior. While the observations of CS-coupled changes in encoding are similar to the 'gain change' and bi-stability hypotheses (Ebner et al., 1983;Loewenstein et al., 2005;Yartsev et al., 2009;McKay et al., 2007), the effects shown in Chapter 2 are manifest as a change in SS information rather than overall firing rates. Recent eye blink conditioning studies report similar predictive CS modulation, with CS increases prior to the conditioned response (Ohmae and Medina, 2015;Ten Brinke et al., 2015). However, the results of Chapter 3 indicate a much richer representation of behavior than previously reported, with CS modulation providing a planar, predictive representation of the workspace. One potential explanation for these major departures is the use of pseudo-random tracking, which provides for a more thorough exploration of the kinematic and position error workspaces than many previous paradigms (Hewitt et al., 2011;Popa et al., 2012;Paninski et al., 2004).

In conclusion, the results of Chapters 2 and 3 represent a new perspective on the role of climbing fiber input to the cerebellar cortex. Rather than serving as an error feedback signal, climbing fiber discharge is evoked in anticipation of a change in behavior, and its

action on the Purkinje cell is to appropriately tune the information present in the SS output in order to optimize control of behavior (Fig. 31).

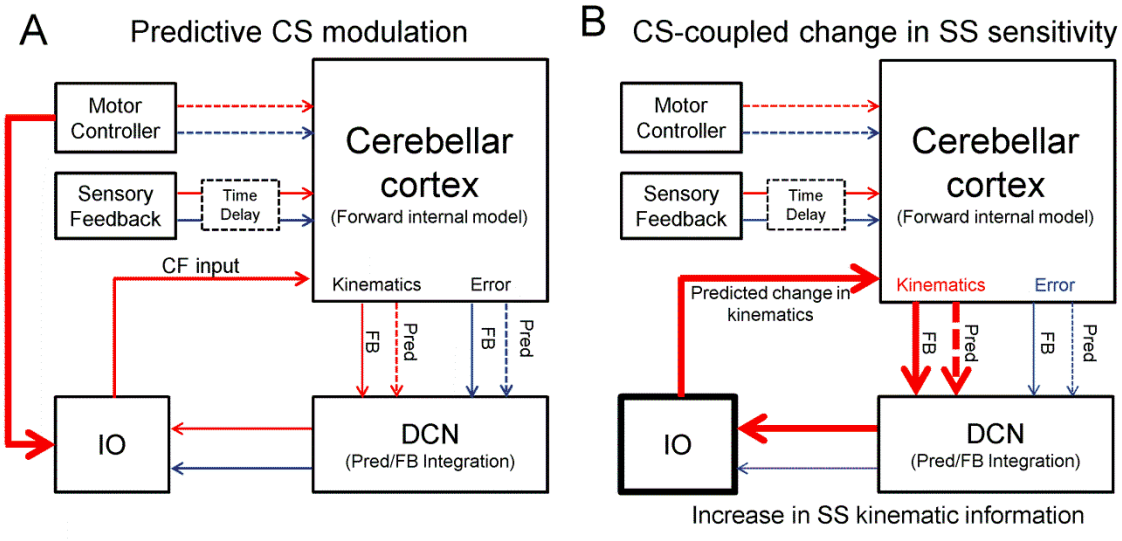

Figure 31: Hypothesized role of predictive CS modulation. A) Predictive (dashed lines) and feedback (solid lines) information about kinematics (red) and position errors (blue) is encoded by Purkinje cells of the cerebellar cortex and relayed to the deep cerebellar nuclei (DCN). B) Climbing fiber input to the cerebellar cortex, originating in the inferior olive (IO), modulates in advance of a change in behavior (in this schematic example, kinematics), and triggers an increase in SS encoding of kinematics.

Future experiments to determine the mechanisms of complex spike-coupled changes in encoding

The findings in Chapter 2 demonstrate that CS firing is associated with dramatic changes in SS encoding. However, a major outstanding question is the potential mechanism(s) by which these alterations in SS encoding occur. A number of candidates could explain the changes. First, the number of spikes in a given climbing fiber discharge will affect the CS burst pattern, influencing parallel fiber-Purkinje cell synaptic plasticity (Bazzigaluppi et al., 2012;Mathy et al., 2009). Previous work has shown that the duration of CS discharge can be associated with changes in motor learning (Yang and Lisberger, 2014;Rasmussen

et al., 2013). Thus, one potential future question is whether the number of wavelets in a CS affects the subsequent CS-coupled change in SS encoding. Rather than assessing encoding changes across the entire session as was done in Chapter 2, approaching this question would require examining either individual CSs or subsets of CSs with similar burst patterns. For example, using the methods of Yang et al(Yang and Lisberger, 2014), the duration of individual CSs could be defined and categorized, and the CS-coupled changes in SS encoding associated with different durations of CSs could be determined. If differences in the bursting patterns are responsible for the increases and decreases in SS encoding observed after CS discharge, then the expectation is that the number of wavelets in a CS should predict a change in SS modulation with behavior.

Additional mechanisms that could explain the CS-coupled changed in SS encoding are local inhibition by GABAergic interneurons and the timing of climbing fiber discharge relative to parallel fiber inputs. GABAergic inhibition generated by cerebellar interneurons locally modifies the conductance changes and Ca^{2+} fluxes evoked by climbing fiber input (Callaway et al., 1995;Kitamura and Hausser, 2011). Also, the timing of climbing fiber discharge may differentially modulate parallel fiber input and thereby determine the direction of synaptic potentiation (Piochon et al., 2012;Suvrathan et al., 2016). Addressing these possibilities would require probing the micro circuitry of the cerebellar cortex rather than the approach utilized here, in the nonhuman primate. Electrophysiological recordings from an individual Purkinje cell and surrounding interneurons would allow for the characterization of inhibitory activity relative to the

timing of climbing fiber discharge. If the CS-coupled changes are driven by relative activity of GABAergic interneurons, individual CSs should have differential effects on SS encoding depending on levels of inhibition from those interneurons. For example, increases in interneuron activity around the timing of CS discharge could predict a decrease in SS encoding, and vice versa.

While the changes in SS sensitivity are tightly coupled to the timing of CS discharge, this does not unequivocally prove that the CSs produce the changes in SS sensitivity. One experiment that could address this is by evoking synchronous CS firing via inferior olive stimulation. If the action of the climbing fiber discharge on the Purkinje cell truly causes the changes in SS encoding observed, the inferior olive stimulation should produce robust changes in SS sensitivity to behavior that are tightly coupled to the timing of stimulation. Another approach is to manipulate the required task in relation to CS discharge. For example, one could develop a paradigm requiring that the animal switch the information needed to perform the task. If our working hypothesis is correct, CSs should be evoked and change the SS encoding to the more salient parameter.

Future experiments to determine the role of predictive CS modulation

Chapter 3 further demonstrates that the role of climbing fiber activity in online motor control extends far beyond the classical error encoding hypothesis, with spatially rich predictive information about kinematics and performance errors present in CS firing. While this predictive modulation is often associated with CS-coupled changes in SS

encoding as illustrated in both Chapters 2 and 3, further characterization of its role in cerebellar function is essential. The inferior olive integrates both feedforward and feedback information from the spinal cord, nuclei at mesodiencephalic junction, cerebellar nuclei, and cerebral cortex (for reviews see (De Zeeuw et al., 1998;Oscarsson, 1980;Apps and Garwicz, 2005)), indicating that predictive climbing fiber discharge is feasible with various motor and non-motor information. However, the predictive CS modulation characterized in Chapter 3 was observed in highly skilled animals trained extensively on pseudo-random tracking. Thus, an interesting question is whether the predictive CS modulation with behavior is learned over time and/or correlated with performance. One potential experiment is to introduce a novel tracking experiment, with the same target trajectory presented repeatedly rather than chosen at random from 100 trajectories defined a priori as in Chapters 2-4. The expectation is that over the course of a session, the predictive CS modulation would increase to reflect the animals' learning the trajectory.

An intriguing observation from Chapter 2 is that the direction of CS-coupled encoding changes tends to be in the opposite direction to the state of SS encoding not associated with CS discharge, with CS-coupled increases in encoding associated with net decreases in the shuffled data, and vice versa. Taken with the observations of predictive CS modulation with behavior, this suggests that the CS-coupled change in SS encoding could be either in response to an encoding state that is suboptimal or anticipation of a change in behavior. However, future directions should aim to more fully unify the predictive CS

modulation and the changes in SS sensitivity. As mentioned above, one potential experiment would be to introduce a learning paradigm in which one aspect of the behavior (e.g., velocity) dominates more than others. For example, design pseudo-random trajectories in which the target kinematics contain large changes in target velocity with little variability in target position. The expectation is that over time, climbing fiber input would become highly tuned to changes in velocity, given that in this case, velocity represents the most salient aspect of behavior. Increases in CS modulation with velocity should also reallocate the bandwidth of SS firing, triggering increases in SS encoding of velocity and decreases in SS encoding of position. Finally, these changes in SS sensitivity should be associated with improved task performance.

Predictive and feedback information in Purkinje cell simple spike firing

The results of Chapter 4 suggest that the information needed to generate sensory prediction error is found in the SS discharge of Purkinje cells. These findings build upon previous observations of lead and lag SS encoding of kinematics and performance errors (Popa et al., 2012;Popa et al., 2015) through the implementation of novel manipulations of visual feedback.

In the feedback reduction paradigm, linear encoding of errors was reduced such that SS modulation was restricted to outside of the target, where visual feedback was available. Conversely, predictive encoding of errors was unaffected. In the feedback delay paradigm, the timing of predictive encoding was negatively shifted equal to the duration

of the delay, consistent with a forward internal model that has not adapted to the delay and makes predictions with respect to the manipulandum movement rather than the delayed cursor. Intriguingly, predictive and feedback encoding of arm kinematics was unaffected in both paradigms, suggesting a representation of arm movement irrespective of the visually-dependent performance errors.

Together, these results characterize robust and independent predictive and feedback information about a host of movement-related parameters in the SS firing. The dual encoding of errors and kinematics by SS discharge is consistent with the predictive and feedback signals necessary for the generation of sensory prediction error ((Popa et al., 2012;Popa et al., 2014;Popa et al., 2015;Wolpert and Ghahramani, 2000;Shadmehr et al., 2010)). The differential effects of these manipulations on error and kinematic encoding suggest the implementation of multiple forward internal models (Popa et al., 2015;Kawato and Wolpert, 1998). In this view, the cerebellum processes predictions and feedback about both the kinematics of arm movements and the more task-relevant performance errors to achieve optimal performance.

Future experiments assessing prediction and feedback in the cerebellum

The goal of the experiments in Chapter 4 was to determine whether the lead and lag SS modulation with behavior represented predictive and feedback information, respectively. The experimental design strived to reduce adaptation to the visual feedback manipulations, as any adaptation could have also influenced the SS encoding. This was

accomplished by removing the visual feedback manipulations during the inter trial interval, as rapid switching between task conditions attenuates adaptation (Herzfeld et al., 2014;Gonzalez Castro et al., 2014). Future experiments should assess effects of behavioral adaptation to similar visual feedback manipulations, and whether any adaptation is associated with changes in SS encoding. For example, Purkinje cells could be recorded during longer blocks of visual feedback manipulation trials, with the manipulations maintained for all movements (i.e., not removed during the inter trial interval). In these longer blocks, improvement in performance should be correlated with changes in SS encoding. For the visual feedback delay, adaptation to the delay should be reflected in the forward internal model integrating the delayed visual feedback into subsequent predictions. As such, the predictive encoding should shift back to the original τ-value as performance improves. For the visual feedback reduction, the expectation is that both the predictive and feedback encoding should be highly tuned to performance errors outside the target edge only.

An additional question is the role of CS firing during the visual feedback manipulations. One hypothesis is that, in the absence of adaptation as in Chapter 4, CS modulation with performance errors and kinematics will initially behave similarly to the SS firing. For example, the predictive modulation with performance errors should also be shifted earlier in the visual feedback delay, whereas kinematic modulation should be unaffected. In the visual feedback reduction paradigm, CS modulation with performance errors should also be shifted to outside the target boundary, where visual feedback is available.

An intriguing question is the role of CS-coupled encoding changes described in Chapter 2 in the visual feedback manipulations. As stated previously, the experiments implemented strived to minimize adaptation. However, one hypothesis would be that CS-coupled encoding changes should reflect changes in the reliability of information. For example, the delay in visual feedback produces temporally inaccurate, and thus unreliable predictions. One hypothesis would be that during the visual feedback delay paradigm, CS-coupled decreases in predictive SS modulation with position error would occur. Similarly, in the visual feedback reduction paradigm, the climbing fiber hypothesis outlined in Chapter 2 would predict that CS firing should reduce SS modulation with position error inside the target boundary, while increasing SS modulation outside the target boundary. It will be highly important to characterize CS modulation and its effects on SS encoding in future analyses.

If the predictive and feedback components of sensory prediction error are independently encoded by the SS firing of Purkinje cells as suggested by Chapter 4, then a major outstanding question is how and where those signals are compared in order to generate sensory prediction errors. The deep cerebellar nuclei (DCN) is a likely candidate for the initial step in this integration due to the convergence of numerous Purkinje cells onto a DCN neuron (Person and Raman, 2012;Chan-Palay, 1977;Palkovits et al., 1977) (Fig. 31A). There is evidence supporting DCN modulation with sensory prediction error, as increased activity of dentate neurons is associated with omission of a stimulus from a

regularly presented sequence (Ohmae et al., 2013), and rostral fastigial nucleus neurons are selectively activated by passive rather than self-generated motion (Brooks and Cullen, 2013). It would be highly interesting (and challenging) to record the activity of Purkinje cells and the nuclear neurons to which they project in the visual feedback manipulation experiments to determine whether increases in activity are associated with the mismatch between predictive and feedback signals in the SS firing.

Finally, as outlined in Chapter 4, the mechanism by which sensory prediction error is used to update the forward internal model has yet to be elucidated. A potential candidate for an update signal could be the CS-coupled changes in SS encoding described in Chapter 2. In this view, a mismatch in prediction and feedback signals computed by SS firing could be conveyed to the inferior olive via the DCN or in combination with other inputs (Lang et al., 1996;De Zeeuw et al., 1989;Teune et al., 2000;Bengtsson and Hesslow, 2006). This could then trigger climbing fiber discharge that updates subsequent information in the SS firing (Fig. 32B).

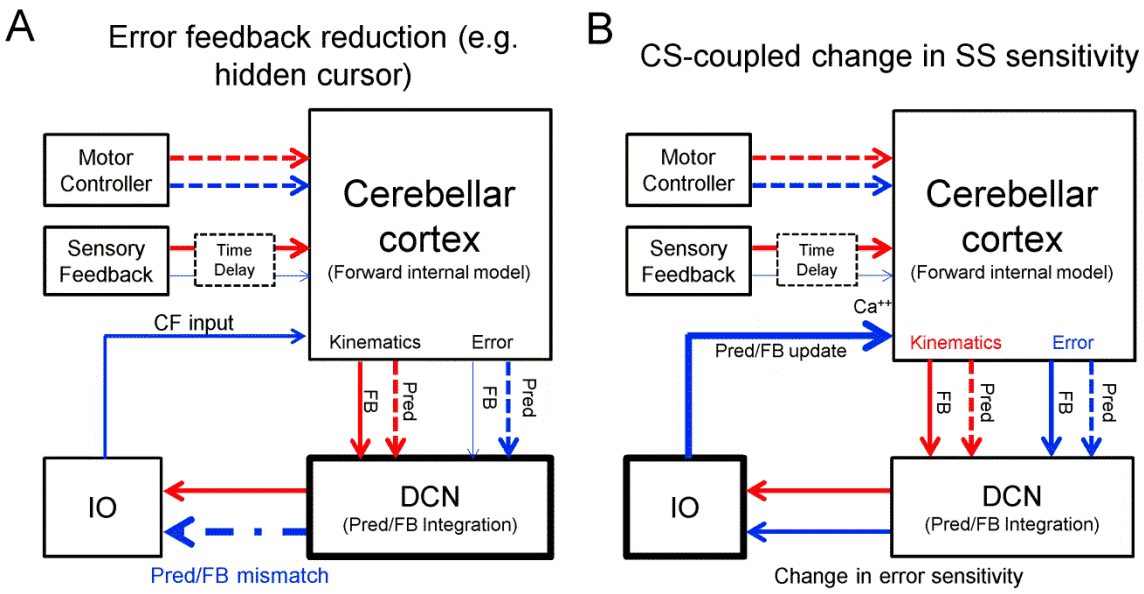

Figure 32: Hypothesized roles of simple and complex spike activity in the context of a forward internal model. A) Predictive (dashed lines) and feedback (solid lines) components of sensory prediction error are computed by Purkinje cells of the cerebellar cortex. The working hypothesis is that these signals are compared by the deep cerebellar nuclei (DCN). The mismatch between the two, for example, decreases in feedback encoding of position errors induced by the hidden cursor condition, would be relayed to the inferior olive (IO). This would result in an increase in climbing fiber activity (B), triggering a change in the SS sensitivity to position errors and thus updating the forward internal model.

Together, the results of this thesis outline a novel hypothesis about the encoding and control of sensory prediction error information on the cellular level. The predictive and feedback components of sensory prediction error are encoded by the SS discharge of Purkinje cells. Rather than serving as a pure error signal as postulated by classical views, CS discharge serves to tune the predictive and feedback information present in the SS firing. The CS-coupled changes in behavior can occur either in anticipation of a change in behavior, or in response to an encoding state that is suboptimal. The representation of motor information on the level of a single Purkinje cell is robust and accurate, but also

highly dynamic, changing to reflect differing conditions, either internally (as in Chapters 2 and 3) or externally (as in Chapter 4) generated.

REFERENCES

Abend W, Bizzi E, Morasso P (1982) Human arm trajectory formation. Brain 105:331-348.

Albus JS (1971) A theory of cerebellar function. Math Biosci 10:25-61.

Andersson G, Armstrong DM (1987) Complex spikes in Purkinje cells in the lateral vermis (b zone) of the cat cerebellum during locomotion. J Physiol 385:107-134.

Apps R, Garwicz M (2005) Anatomical and physiological foundations of cerebellar information processing. Nat Rev Neurosci 6:297-311.

Ashe J, Georgopoulos AP (1994) Movement parameters and neural activity in motor cortex and area 5. Cereb Cortex 4:590-600.

Badura A, Schonewille M, Voges K, Galliano E, Renier N, Gao Z, Witter L, Hoebeek FE, Chedotal A, De Zeeuw CI (2013) Climbing fiber input shapes reciprocity of Purkinje cell firing. Neuron 78:700-713.

Barmack NH, Shojaku H (1995) Vestibular and visual climbing fiber signals evoked in the uvula-nodulus of the rabbit cerebellum by natural stimulation. J Neurophysiol 74:2573-2589.

Barmack NH, Simpson JI (1980) Effects of microlesions of dorsal cap of inferior olive of rabbits on optokinetic and vestibuloocular reflexes. J Neurophysiol 43:182-206.

Bastian AJ (2006) Learning to predict the future: the cerebellum adapts feedforward movement control. Curr Opin Neurobiol 16:645-649.

Bazzigaluppi P, de G, Jr., van der Giessen RS, Khosrovani S, De Zeeuw CI, De Jeu MT (2012) Olivary subthreshold oscillations and burst activity revisited. Front Neural Circuits 6:91.

Bell CC, Han V, Sawtell NB (2008) Cerebellum-like structures and their implications for cerebellar function. Annu Rev Neurosci 31:1-24.

Bengtsson F, Ekerot CF, Jorntell H (2011) In vivo analysis of inhibitory synaptic inputs and rebounds in deep cerebellar nuclear neurons. PLoS ONE 6:e18822.

Bengtsson F, Hesslow G (2006) Cerebellar control of the inferior olive. Cerebellum 5:7-14.

Bengtsson F, Jorntell H (2009) Sensory transmission in cerebellar granule cells relies on similarly coded mossy fiber inputs. Proc Natl Acad Sci USA 106:2389-2394.

Berniker M, Kording K (2008) Estimating the sources of motor errors for adaptation and generalization. Nat Neurosci 11:1454-1461.

Best MD, Suminski AJ, Takahashi K, Brown KA, Hatsopoulos NG (2016) Spatio-Temporal Patterning in Primary Motor Cortex at Movement Onset. Cereb Cortex.

Bloedel JR, Roberts WJ (1971) Action of climbing fibers in cerebellar cortex of the cat. J Neurophysiol 34:17-31.

Borghuis BG, Perge JA, Vajda I, van Wezel RJ, van de Grind WA, Lankheet MJ (2003) The motion reverse correlation (MRC) method: a linear systems approach in the motion domain. J Neurosci Methods 123:153-166.

Boyden ES, Raymond JL (2003) Active reversal of motor memories reveals rules governing memory encoding. Neuron 39:1031-1042.

Boyden ES, Katoh A, Raymond JL (2004) Cerebellum-dependent learning: the role of multiple plasticity mechanisms. Annu Rev Neurosci 27:581-609.

Brenowitz SD, Regehr WG (2003) Calcium dependence of retrograde inhibition by endocannabinoids at synapses onto Purkinje cells. J Neurosci 23:6373-6384.

Brooks JX, Cullen KE (2013) The primate cerebellum selectively encodes unexpected self-motion. Curr Biol 23:947-955.

Callaway JC, Lasser-Ross N, Ross WN (1995) IPSPs strongly inhibit climbing fiber-activated [Ca^{2+}] increases in the dendrites of cerebellar Purkinje neurons. J Neurosci 15:2777-2787.

Cameron BD, Franks IM, Inglis JT, Chua R (2010) Reach adaptation to explicit vs. implicit target error. Exp Brain Res 203:367-380.

Catz N, Dicke PW, Thier P (2005) Cerebellar complex spike firing is suitable to induce as well as to stabilize motor learning. Curr Biol 15:2179-2189.

Cerminara NL, Apps R, Marple-Horvat DE (2009) An internal model of a moving visual target in the lateral cerebellum. J Physiol 587:429-442.

Cerminara NL, Rawson JA (2004) Evidence that climbing fibers control an intrinsic spike generator in cerebellar Purkinje cells. J Neurosci 24:4510-4517.

Chadderton P, Margrie TW, Hausser M (2004) Integration of quanta in cerebellar granule cells during sensory processing. Nature 428:856-860.

Chan-Palay V (1977) Cerebellar Dentate Nucleus. New YOrk: Springer.

Chapman CE, Spidalieri G, Lamarre Y (1986) Activity of dentate neurons during arm movements triggered by visual, auditory, and somesthetic stimuli in the monkey. J Neurophysiol 55:203-226.

Chen S, Augustine GJ, Chadderton P (2016) The cerebellum linearly encodes whisker position during voluntary movement. Elife 5.

Chen-Harris H, Joiner WM, Ethier V, Zee DS, Shadmehr R (2008) Adaptive control of saccades via internal feedback. J Neurosci 28:2804-2813.

Coesmans M, Weber JT, De Zeeuw CI, Hansel C (2004) Bidirectional parallel fiber plasticity in the cerebellum under climbing fiber control. Neuron 44:691-700.

Colin F, Manil J, Desclin JC (1980) The olivocerebellar system. I. Delayed and slow inhibitory effects: an overlooked salient feature of cerebellar climbing fibers. Brain Res 187:3-27.

Collewijn H, Tamminga EP (1984) Human smooth and saccadic eye movements during voluntary pursuit of different target motions on different backgrounds. J Physiol 351:217-250.

Coltz JD, Johnson MT, Ebner TJ (1999) Cerebellar Purkinje cell simple spike discharge encodes movement velocity in primates during visuomotor arm tracking. J Neurosci 19:1782-1803.

Dash S, Catz N, Dicke PW, Thier P (2010) Specific vermal complex spike responses build up during the course of smooth-pursuit adaptation, paralleling the decrease of performance error. Exp Brain Res 205:41-55.

Dash S, Catz N, Dicke PW, Thier P (2012) Encoding of smooth-pursuit eye movement initiation by a population of vermal Purkinje cells. Cereb Cortex 22:877-891.

Dash S, Dicke PW, Thier P (2013) A vermal Purkinje cell simple spike population response encodes the changes in eye movement kinematics due to smooth pursuit adaptation. Front Syst Neurosci 7:3.

Davie JT, Clark BA, Hausser M (2008) The origin of the complex spike in cerebellar Purkinje cells. J Neurosci 28:7599-7609.

De Zeeuw CI, Holstege JC, Ruigrok TJ, Voogd J (1989) Ultrastructural study of the GABAergic, cerebellar, and mesodiencephalic innervation of the cat medial accessory olive: anterograde tracing combined with immunocytochemistry. J Comp Neurol 284:12-35.

De Zeeuw CI, Simpson JI, Hoogenraad CC, Galjart N, Koekkoek SK, Ruigrok TJ (1998) Microcircuitry and function of the inferior olive. Trends Neurosci 21:391-400.

Diedrichsen J, Hashambhoy Y, Rane T, Shadmehr R (2005) Neural correlates of reach errors. J Neurosci 25:9919-9931.

Diedrichsen J, Shadmehr R, Ivry RB (2010) The coordination of movement: optimal feedback control and beyond. Trends Cogn Sci 14:31-39.

Dum RP, Li C, Strick PL (2002) Motor and nonmotor domains in the monkey dentate. Ann N Y Acad Sci 978:289-301.

Ebner TJ, Fu Q (1997) What features of visually guided arm movements are encoded in the simple spike discharge of cerebellar Purkinje cells? Prog Brain Res 114:431-447.

Ebner TJ, Hewitt A, Popa LS (2011) What features of movements are encoded in the discharge of cerebellar neurons during limb movements? Cerebellum 10:683-693.

Ebner TJ, Johnson MT, Roitman A, Fu Q (2002) What do complex spikes signal about limb movements? Ann NY Acad Sci 978:205-218.

Ebner TJ, Yu QX, Bloedel JR (1983) Increase in Purkinje cell gain associated with naturally activated climbing fiber input. J Neurophysiol 50:205-219.

Eccles JC, Ito M, Szentagothai J (1967) The Cerebellum as a Neuronal Machine. Berlin: Springer-Verlag.

Engbers JD, Fernandez FR, Turner RW (2013) Bistability in Purkinje neurons: ups and downs in cerebellar research. Neural Netw 47:18-31.

Fano U (1947) Ionization Yield of Radiations. II. The Fluctuations of the Number of Ions. Physical Review.

Flament D, Hore J (1988) Comparison of cerebellar intention tremor under isotonic and isometric conditions. Brain Res 439:179-186.

Flanagan JR, Vetter P, Johansson RS, Wolpert DM (2003) Prediction precedes control in motor learning. Curr Biol 13:146-150.

Flanagan JR, Wing AM (1997) The role of internal models in motion planning and control: evidence from grip force adjustments during movements of hand-held loads. J Neurosci 17:1519-1528.

Forrest MD (2014) Intracellular calcium dynamics permit a Purkinje neuron model to perform toggle and gain computations upon its inputs. Front Comput Neurosci 8:86.

Fortier PA, Kalaska JF, Smith AM (1989) Cerebellar neuronal activity related to whole-arm reaching movements in the monkey. J Neurophysiol 62:198-211.

Frens MA, Mathoera AL, van der SJ (2001) Floccular complex spike response to transparent retinal slip. Neuron 30:795-801.

Fu QG, Flament D, Coltz JD, Ebner TJ (1997a) Relationship of cerebellar Purkinje cell simple spike discharge to movement kinematics in the monkey. J Neurophysiol 78:478-491.

Fu QG, Mason CR, Flament D, Coltz JD, Ebner TJ (1997b) Movement kinematics encoded in complex spike discharge of primate cerebellar Purkinje cells. NeuroReport 8:523-529.

Fujita M (1982) Adaptive filter model of the cerebellum. Biol Cybern 45:195-206.

Gao Z, van Beugen BJ, De Zeeuw CI (2012) Distributed synergistic plasticity and cerebellar learning. Nat Rev Neurosci 13:619-635.

Garden DL, Rinaldi A, Nolan MF (2017) Active integration of glutamatergic input to the inferior olive generates bidirectional postsynaptic potentials. J Physiol 595:1239-1251.

Gauck V, Jaeger D (2000) The control of rate and timing of spikes in the deep cerebellar nuclei by inhibition. J Neurosci 20:3006-3016.

Gauck V, Jaeger D (2003) The contribution of NMDA and AMPA conductances to the control of spiking in neurons of the deep cerebellar nuclei. J Neurosci 23:8109-8118.

Gaveau V, Prablanc C, Laurent D, Rossetti Y, Priot AE (2014) Visuomotor adaptation needs a validation of prediction error by feedback error. Front Hum Neurosci 8:880.

Giaquinta G, Valle MS, Caserta C, Casabona A, Bosco G, Perciavalle V (2000) Sensory representation of passive movement kinematics by rat's spinocerebellar Purkinje cells. Neurosci Lett 285:41-44.

Gibson AR, Horn KM, Pong M (2004) Activation of climbing fibers. Cerebellum 3:212-221.

Gibson AR, Houk JC, Kohlerman NJ (1985) Relation between red nucleus discharge and movement parameters in trained macaque monkeys. J Physiol 358:551-570.

Gilbert PF, Thach WT (1977) Purkinje cell activity during motor learning. Brain Res 128:309-328.

Golla H, Tziridis K, Haarmeier T, Catz N, Barash S, Thier P (2008) Reduced saccadic resilience and impaired saccadic adaptation due to cerebellar disease. Eur J Neurosci 27:132-144.

Gomi H, Shidara M, Takemura A, Inoue Y, Kawano K, Kawato M (1998) Temporal firing patterns of Purkinje cells in the cerebellar ventral paraflocculus during ocular following responses in monkeys I. Simple spikes. J Neurophysiol 80:818-831.

Gonzalez Castro LN, Hadjiosif AM, Hemphill MA, Smith MA (2014) Environmental consistency determines the rate of motor adaptation. Curr Biol 24:1050-1061.

Goodkin HP, Thach WT (2003) Cerebellar control of constrained and unconstrained movements. I. Nuclear inactivation. J Neurophysiol 89:884-895.

Graf W, Simpson JI, Leonard CS (1988) Spatial organization of visual messages of the rabbit's cerebellar flocculus. II. Complex and simple spike responses of Purkinje cells. J Neurophysiol 60:2091-2121.

Greger B, Norris S (2005) Simple spike firing in the posterior lateral cerebellar cortex of Macaque Mulatta was correlated with success-failure during a visually guided reaching task. Exp Brain Res 167:660-665.

Guthrie BL, Porter JD, Sparks DL (1983) Corollary discharge provides accurate eye position information to the oculomotor system. Science 221:1193-1195.

Hansel C, Linden DJ, D'Angelo E (2001) Beyond parallel fiber LTD: the diversity of synaptic and non-synaptic plasticity in the cerebellum. Nat Neurosci 4:467-475.

Harvey RJ, Porter R, Rawson JA (1977) The natural discharges of Purkinje cells in paravermal regions of lobules V and VI of the monkey's cerebellum. J Physiol 271:515-536.

Held R, FREEDMAN SJ (1963) Plasticity in human sensorimotor control. Science 142:455-462.

Herzfeld DJ, Kojima Y, Soetedjo R, Shadmehr R (2015) Encoding of action by the Purkinje cells of the cerebellum. Nature 526:439-442.

Herzfeld DJ, Vaswani PA, Marko MK, Shadmehr R (2014) A memory of errors in sensorimotor learning. Science 345:1349-1353.

Hewitt A, Popa LS, Pasalar S, Hendrix CM, Ebner TJ (2011) Representation of limb kinematics in Purkinje cell simple spike discharge is conserved across multiple tasks. J Neurophysiol 106:2232-2247.

Hewitt AL, Popa LS, Ebner TJ (2015) Changes in Purkinje cell simple spike encoding of reach kinematics during adaptation to a mechanical perturbation. J Neurosci 35:1106-1124.

Horak FB, Diener HC (1994) Cerebellar control of postural scaling and central set in stance. J Neurophysiol 72:479-493.

Horn KM, Deep A, Gibson AR (2013) Progressive limb ataxia following inferior olive lesions. J Physiol 591:5475-5489.

Horn KM, van Kan PL, Gibson AR (1996) Reduction of rostral dorsal accessory olive responses during reaching. J Neurophysiol 76:4140-4151.

Huang CC, Sugino K, Shima Y, Guo C, Bai S, Mensh BD, Nelson SB, Hantman AW (2013) Convergence of pontine and proprioceptive streams onto multimodal cerebellar granule cells. Elife 2:e00400.

Huang VS, Shadmehr R (2009) Persistence of motor memories reflects statistics of the learning event. J Neurophysiol 102:931-940.

Ide JS, Li CS (2011) A cerebellar thalamic cortical circuit for error-related cognitive control. Neuroimage 54:455-464.

Imamizu H, Kuroda T, Yoshioka T, Kawato M (2004) Functional magnetic resonance imaging examination of two modular architectures for switching multiple internal models. J Neurosci 24:1173-1181.

Imamizu H, Miyauchi S, Tamada T, Sasaki Y, Takino R, Putz B, Yoshioka T, Kawato M (2000) Human cerebellar activity reflecting an acquired internal model of a new tool. Nature 403:192-195.

Ishikawa T, Shimuta M, Hausser M (2015) Multimodal sensory integration in single cerebellar granule cells in vivo. Elife 4.

Isope P, Barbour B (2002) Properties of unitary granule cell-->Purkinje cell synapses in adult rat cerebellar slices. J Neurosci 22:9668-9678.

Ito M (1984) The Cerebellum and Neural Control. New York: Raven Press.

Ito M (2000) Mechanisms of motor learning in the cerebellum. Brain Res 886:237-245.

Ito M (2001) Cerebellar long-term depression: characterization, signal transduction, and functional roles. Physiol Rev 81:1143-1195.

Ito M (2013) Error detection and representation in the olivo-cerebellar system. Front Neural Circuits 7:1-8.

Ito M, Kano M (1982) Long-lasting depression of parallel fiber-Purkinje cell transmission induced by conjunctive stimulation of parallel fibers and climbing fibers in the cerebellar cortex. Neurosci Lett 33:253-258.

Izawa J, Shadmehr R (2011) Learning from sensory and reward prediction errors during motor adaptation. PLoS Comput Biol 7:e1002012.

Jorntell H, Hansel C (2006) Synaptic memories upside down: bidirectional plasticity at cerebellar parallel fiber-Purkinje cell synapses. Neuron 52:227-238.

Kahlon M, Lisberger SG (2000) Changes in the responses of Purkinje cells in the floccular complex of monkeys after motor learning in smooth pursuit eye movements. J Neurophysiol 84:2945-2960.

Kase M, Noda H, Suzuki DA, Miller DC (1979) Target velocity signals of visual tracking in vermal Purkinje cells of the monkey. Science 205:717-720.

Kawato M (1996) Learning internal models of the motor apparatus. In: The Acquisition of Motor Behavior in Vertebrates (Bloedel JR, Ebner TJ, Wise SP, eds), pp 409-430. Cambridge: MIT Press.

Kawato M (1999) Internal models for motor control and trajectory planning. Curr Opin Neurobiol 9:718-727.

Kawato M, Gomi H (1992) A computational model of four regions of the cerebellum based on feedback-error learning. Biol Cybern 68:95-103.

Kawato M, Wolpert D (1998) Internal models for motor control. Novartis Found Symp 218:291-304.

Ke MC, Guo CC, Raymond JL (2009) Elimination of climbing fiber instructive signals during motor learning. Nat Neurosci 12:1171-1179.

Keating JG, Thach WT (1995) Nonclock behavior of inferior olive neurons: interspike interval of Purkinje cell complex spike discharge in the awake behaving monkey is random. J Neurophysiol 73:1329-1340.

Keller EL, Robinson DA (1971) Absence of a stretch reflex in extraocular muscles of the monkey. J Neurophysiol 34:908-919.

Kelly RM, Strick PL (2003) Cerebellar loops with motor cortex and prefrontal cortex of a nonhuman primate. J Neurosci 23:8432-8444.

Kim JH, Wang JJ, Ebner TJ (1987) Climbing fiber afferent modulation during treadmill locomotion in the cat. J Neurophysiol 57:787-802.

Kimpo RR, Rinaldi JM, Kim CK, Payne HL, Raymond JL (2014) Gating of neural error signals during motor learning. Elife 3:e02076.

Kitama T, Omata T, Mizukoshi A, Ueno T, Sato Y (1999) Motor dynamics encoding in cat cerebellar flocculus middle zone during optokinetic eye movements. J Neurophysiol 82:2235-2248.

Kitamura K, Hausser M (2011) Dendritic calcium signaling triggered by spontaneous and sensory-evoked climbing fiber input to cerebellar Purkinje cells in vivo. J Neurosci 31:10847-10858.

Kitazawa S, Kimura T, Yin PB (1998) Cerebellar complex spikes encode both destinations and errors in arm movements. Nature 392:494-497.

Kobayashi Y, Kawano K, Takemura A, Inoue Y, Kitama T, Gomi H, Kawato M (1998) Temporal firing patterns of Purkinje cells in the cerebellar ventral paraflocculus during ocular following responses in monkeys II. Complex spikes. J Neurophysiol 80:832-848.

Kolb FP, Rubia FJ, Bauswein E (1987) Cerebellar unit responses of the mossy fibre system to passive movements in the decerebrate cat. I. Responses to static parameters. Exp Brain Res 68:234-248.

Lacquaniti F, Terzuolo C, Viviani P (1983) The law relating the kinematic and figural aspects of drawing movements. Acta Psychol (Amst) 54:115-130.

Lang EJ, Sugihara I, Llinas R (1996) GABAergic modulation of complex spike activity by the cerebellar nucleoolivary pathway in rat. J Neurophysiol 76:255-275.

Lang EJ, Sugihara I, Welsh JP, Llinas R (1999) Patterns of spontaneous purkinje cell complex spike activity in the awake rat. J Neurosci 19:2728-2739.

Laurens J, Meng H, Angelaki DE (2013) Computation of linear acceleration through an internal model in the macaque cerebellum. Nat Neurosci 16:1701-1708.

Lisberger SG, Pavelko TA, Bronte-Stewart HM, Stone LS (1994) Neural basis for motor learning in the vestibuloocular reflex of primates. II. Changes in the responses of horizontal gaze velocity Purkinje cells in the cerebellar flocculus and ventral paraflocculus. J Neurophysiol 72:954-973.

Liu X, Robertson E, Miall RC (2003) Neuronal activity related to the visual representation of arm movements in the lateral cerebellar cortex. J Neurophysiol 89:1223-1237.

Llinas R, Sugimori M (1980) Electrophysiological properties of in vitro Purkinje cell dendrites in mammalian cerebellar slices. J Physiol 305:197-213.

Llinas R, Walton K, Hillman DE, Sotelo C (1975) Inferior olive: its role in motor learing. Science 190:1230-1231.

Llinas RR (2013) The olivo-cerebellar system: a key to understanding the functional significance of intrinsic oscillatory brain properties. Front Neural Circuits 7:96.

Loewenstein Y, Mahon S, Chadderton P, Kitamura K, Sompolinsky H, Yarom Y, Hausser M (2005) Bistability of cerebellar Purkinje cells modulated by sensory stimulation. Nat Neurosci 8:202-211.

Lou JS, Bloedel JR (1986) The responses of simultaneously recorded Purkinje cells to the perturbations of the step cycle in the walking ferret: a study using a new analytical method--the real-time postsynaptic response (RTPR). Brain Res 365:340-344.

Magescas F, Prablanc C (2006) Automatic drive of limb motor plasticity. J Cogn Neurosci 18:75-83.

Mano N, Kanazawa I, Yamamoto K (1986) Complex-spike activity of cerebellar Purkinje cells related to wrist tracking movement in monkey. J Neurophysiol 56:137-158.

Mano N, Yamamoto K (1980) Simple-spike activity of cerebellar Purkinje cells related to visually guided wrist tracking movement in the monkey. J Neurophysiol 43:713-728.

Marple-Horvat DE, Stein JF (1987) Cerebellar neuronal activity related to arm movements in trained rhesus monkeys. J Physiol 394:351-366.

Marr D (1969) A theory of cerebellar cortex. J Physiol 202:437-470.

Martin TA, Keating JG, Goodkin HP, Bastian AJ, Thach WT (1996) Throwing while looking through prisms. I. Focal olivocerebellar lesions impair adaptation. Brain 119:1183-1198.

Maschke M, Gomez CM, Ebner TJ, Konczak J (2004) Hereditary cerebellar ataxia progressively impairs force adaptation during goal-directed arm movements. J Neurophysiol 91:230-238.

Mathy A, Ho SS, Davie JT, Duguid IC, Clark BA, Hausser M (2009) Encoding of oscillations by axonal bursts in inferior olive neurons. Neuron 62:388-399.

Mazzoni P, Krakauer JW (2006) An implicit plan overrides an explicit strategy during visuomotor adaptation. J Neurosci 26:3642-3645.

McKay BE, Engbers JD, Mehaffey WH, Gordon GR, Molineux ML, Bains JS, Turner RW (2007) Climbing fiber discharge regulates cerebellar functions by controlling the intrinsic characteristics of purkinje cell output. J Neurophysiol 97:2590-2604.

Medina JF, Lisberger SG (2008) Links from complex spikes to local plasticity and motor learning in the cerebellum of awake-behaving monkeys. Nat Neurosci 11:1185-1192.

Medina JF, Lisberger SG (2009) Encoding and decoding of learned smooth pursuit eye movements in the floccular complex of the monkey cerebellum. J Neurophysiol 102:2039-2054.

Meyer-Lohmann J, Hore J, Brooks VB (1977) Cerebellar participation in generation of prompt arm movements. J Neurophysiol 40:1038-1050.

Miall RC, Christensen LO, Cain O, Stanley J (2007) Disruption of state estimation in the human lateral cerebellum. PLoS Biol 5:e316.

Miall RC, Wolpert DM (1996) Forward models for physiological motor control. Neural Netw 9:1265-1279.

Miles FA, Braitman DJ, Dow BM (1980a) Long-term adaptive changes in primate vestibuloocular reflex. IV. Electrophysiological observations in flocculus of adapted monkeys. J Neurophysiol 43:1477-1493.

Miles FA, Fuller JH, Braitman DJ, Dow BM (1980b) Long-term adaptive changes in primate vestibuloocular reflex. III. Electrophysiological observations in flocculus of normal monkeys. J Neurophysiol 43:1437-1476.

Miles FA, Lisberger SG (1981) The "error" signals subserving adaptive gain control in the primate vestibulo-ocular reflex. Ann N Y Acad Sci 374:513-525.

Miles OB, Cerminara NL, Marple-Horvat DE (2006) Purkinje cells in the lateral cerebellum of the cat encode visual events and target motion during visually guided reaching. J Physiol 571:619-637.

Montarolo PG, Palestini M, Strata P (1982) The inhibitory effect of the olivocerebellar input on the cerebellar Purkinje cells in the rat. J Physiol 332:187-202.

Morton SM, Bastian AJ (2006) Cerebellar contributions to locomotor adaptations during splitbelt treadmill walking. J Neurosci 26:9107-9116.

Najafi F, Giovannucci A, Wang SS, Medina JF (2014a) Coding of stimulus strength via analog calcium signals in Purkinje cell dendrites of awake mice. Elife 3:e03663.

Najafi F, Giovannucci A, Wang SS, Medina JF (2014b) Sensory-driven enhancement of calcium signals in individual Purkinje cell dendrites of awake mice. Cell Rep 6:792-798.

Napper RM, Harvey RJ (1988) Number of parallel fiber synapses on an individual Purkinje cell in the cerebellum of the rat. J Comp Neurol 274:168-177.

Nguyen-Vu TD, Kimpo RR, Rinaldi JM, Kohli A, Zeng H, Deisseroth K, Raymond JL (2013) Cerebellar Purkinje cell activity drives motor learning. Nat Neurosci 16:1734-1736.

Noda H, Suzuki DA (1979) The role of the flocculus of the monkey in saccadic eye movements. J Physiol 294:317-334.

Noto CT, Robinson FR (2001) Visual error is the stimulus for saccade gain adaptation. Brain Res Cogn Brain Res 12:301-305.

Nowak DA, Hermsdorfer J, Rost K, Timmann D, Topka H (2004) Predictive and reactive finger force control during catching in cerebellar degeneration. Cerebellum 3:227-235.

Ohmae S, Medina JF (2015) Climbing fibers encode a temporal-difference prediction error during cerebellar learning in mice. Nat Neurosci 18:1798-1803.

Ohmae S, Uematsu A, Tanaka M (2013) Temporally specific sensory signals for the detection of stimulus omission in the primate deep cerebellar nuclei. J Neurosci 33:15432-15441.

Ojakangas CL, Ebner TJ (1992) Purkinje cell complex and simple spike changes during a voluntary arm movement learning task in the monkey. J Neurophysiol 68:2222-2236.

Ojakangas CL, Ebner TJ (1994) Purkinje cell complex spike activity during voluntary motor learning: relationship to kinematics. J Neurophysiol 72:2617-2630.

Oscarsson O (1980) Functional organization of olivary projection to the cerebellar anterior lobe. In: The Inferior Olivary Nucleus: Anatomy and Physiology (Courville J, ed), pp 279-290. New York: Raven.

Palkovits M, Mezey E, Hamori J, Szentagothai J (1977) Quantitative histological analysis of the cerebellar nuclei in the cat. I. Numerical data on cells and on synapses. Exp Brain Res 28:189-209.

Paninski L, Fellows MR, Hatsopoulos NG, Donoghue JP (2004) Spatiotemporal tuning of motor cortical neurons for hand position and velocity. J Neurophysiol 91:515-532.

Park SM, Tara E, Khodakhah K (2012) Efficient generation of reciprocal signals by inhibition. J Neurophysiol 107:2453-2462.

Pasalar S, Roitman AV, Durfee WK, Ebner TJ (2006) Force field effects on cerebellar Purkinje cell discharge with implications for internal models. Nat Neurosci 9:1404-1411.

Person AL, Raman IM (2012) Purkinje neuron synchrony elicits time-locked spiking in the cerebellar nuclei. Nature 481:502-505.

Piochon C, Kruskal P, Maclean J, Hansel C (2012) Non-Hebbian spike-timing-dependent plasticity in cerebellar circuits. Front Neural Circuits 6:124.

Popa LS, Hewitt AL, Ebner TJ (2014) The cerebellum for jocks and nerds alike. Front Syst Neurosci 8:1-13.

Popa LS, Hewitt AL, Ebner TJ (2012) Predictive and feedback performance errors are signaled in the simple spike discharge of individual Purkinje cells. J Neurosci 32:15345-15358.

Popa LS, Streng ML, Ebner TJ (2017) Long-Term Predictive and Feedback Encoding of Motor Signals in the Simple Spike Discharge of Purkinje Cells. eNeuro 4.

Popa LS, Streng ML, Hewitt AL, Ebner TJ (2015) The errors of our ways: Understanding error representations in cerebellar-dependent motor learning. Cerebellum.

Powell K, Mathy A, Duguid I, Hausser M (2015) Synaptic representation of locomotion in single cerebellar granule cells. Elife 4.

Prsa M, Thier P (2011) The role of the cerebellum in saccadic adaptation as a window into neural mechanisms of motor learning. Eur J Neurosci 33:2114-2128.

Raman IM, Bean BP (1997) Resurgent sodium current and action potential formation in dissociated cerebellar Purkinje neurons. J Neurosci 17:4517-4526.

Rancz EA, Hausser M (2010) Dendritic spikes mediate negative synaptic gain control in cerebellar Purkinje cells. Proc Natl Acad Sci U S A 107:22284-22289.

Rasmussen A, Jirenhed DA, Zucca R, Johansson F, Svensson P, Hesslow G (2013) Number of spikes in climbing fibers determines the direction of cerebellar learning. J Neurosci 33:13436-13440.

Reimer J, Hatsopoulos NG (2009) The problem of parametric neural coding in the motor system. Adv Exp Med Biol 629:243-259.

Riehle A, Wirtssohn S, Grun S, Brochier T (2013) Mapping the spatio-temporal structure of motor cortical LFP and spiking activities during reach-to-grasp movements. Front Neural Circuits 7:48.

Robinson DA (1975) Oculomotor control signals. In: Basic Mechanisms of Ocular Motility and Their Clinical Implications (P Bachyrita, G Lennerstrand, eds), pp 337-374. Oxford, UK: Pergamon.

Robinson FR, Noto CT, Bevans SE (2003) Effect of visual error size on saccade adaptation in monkey. J Neurophysiol 90:1235-1244.

Roitman AV, Pasalar S, Ebner TJ (2009) Single trial coupling of Purkinje cell activity to speed and error signals during circular manual tracking. Exp Brain Res 192:241-251.

Roitman AV, Pasalar S, Johnson MT, Ebner TJ (2005) Position, direction of movement, and speed tuning of cerebellar Purkinje cells during circular manual tracking in monkey. J Neurosci 25:9244-9257.

Rubia FJ, Kolb FP (1978) Responses of cerebellar units to a passive movement in the decerebrate cat. Exp Brain Res 31:387-401.

Schlerf JE, Ivry RB, Diedrichsen J (2012) Encoding of sensory prediction errors in the human cerebellum. J Neurosci 32:4913-4922.

Schmahmann JD, Pandya DN (1997) The cerebrocerebellar system. Int Rev Neurobiol 41:31-60.

Schoch B, Dimitrov B, Gizewski ER, Timmann D (2006) Functional localization in the human cerebellum based on voxelwise statistical analysis: a study of 90 patients. NeuroImage 30:36-51.

Schonewille M, Gao Z, Boele HJ, Veloz MF, Amerika WE, Simek AA, De Jeu MT, Steinberg JP, Takamiya K, Hoebeek FE, Linden DJ, Huganir RL, De Zeeuw CI (2011) Reevaluating the role of LTD in cerebellar motor learning. Neuron 70:43-50.

Schonewille M, Khosrovani S, Winkelman BH, Hoebeek FE, De Jeu MT, Larsen IM, Van der BJ, Schmolesky MT, Frens MA, De Zeeuw CI (2006) Purkinje cells in awake behaving animals operate at the upstate membrane potential. Nat Neurosci 9:459-461.

Schoppmann A, Hoffmann KP (1976) Continuous mapping of direction selectivity in the cat's visual cortex. Neurosci Lett 2:177-181.

Scott SH (2004) Optimal feedback control and the neural basis of volitional motor control. Nature Reviews Neuroscience 5:532-546.

Shadmehr R, Krakauer JW (2008) A computational neuroanatomy for motor control. Exp Brain Res 185:359-381.

Shadmehr R, Smith MA, Krakauer JW (2010) Error correction, sensory prediction, and adaptation in motor control. Annu Rev Neurosci 33:89-108.

Shidara M, Kawano K, Gomi H, Kawato M (1993) Inverse-dynamics model eye movement control by Purkinje cells in the cerebellum. Nature 365:50-52.

Simpson JI, Wylie DR, DeZeeuw CI (1995) On climbing fiber signals and their consequence(s). Behav Brain Sci 19:385-398.

Smith MA, Shadmehr R (2005) Intact ability to learn internal models of arm dynamics in Huntington's disease but not cerebellar degeneration. J Neurophysiol 93:2809-2821.

Soetedjo R, Fuchs AF (2006) Complex spike activity of Purkinje cells in the oculomotor vermis during behavioral adaptation of monkey saccades. J Neurosci 26:7741-7755.

Soetedjo R, Kojima Y, Fuchs A (2008a) Complex spike activity signals the direction and size of dysmetric saccade errors. Prog Brain Res 171:153-159.

Soetedjo R, Kojima Y, Fuchs AF (2008b) Complex spike activity in the oculomotor vermis of the cerebellum: a vectorial error signal for saccade motor learning? J Neurophysiol 100:1949-1966.

Stone LS, Lisberger SG (1986) Detection of tracking errors by visual climbing fiber inputs to monkey cerebellar flocculus during pursuit eye movements. Neurosci Lett 72:163-168.

Stone LS, Lisberger SG (1990a) Visual responses of Purkinje cells in the cerebellar flocculus during smooth-pursuit eye movements in monkeys. I. Simple spikes. J Neurophysiol 63:1241-1261.

Stone LS, Lisberger SG (1990b) Visual responses of Purkinje cells in the cerebellar flocculus during smooth-pursuit eye movements in monkeys. II. Complex spikes. J Neurophysiol 63:1262-1275.

Streng ML, Popa LS, Ebner TJ (2017) Climbing fibers control Purkinje cell representations of behavior. J Neurosci 37:1997-2009.

Strick PL (1983) The influence of motor preparation on the response of cerebellar neurons to limb displacements. J Neurosci 3:2007-2020.

Suvrathan A, Payne HL, Raymond JL (2016) Timing Rules for Synaptic Plasticity Matched to Behavioral Function. Neuron 92:959-967.

Taylor JA, Ivry RB (2012) The role of strategies in motor learning. Ann N Y Acad Sci 1241:1-12.

Taylor JA, Klemfuss NM, Ivry RB (2010) An explicit strategy prevails when the cerebellum fails to compute movement errors. Cerebellum 9:580-586.

Ten Brinke MM, Boele HJ, Spanke JK, Potters JW, Kornysheva K, Wulff P, IJpelaar AC, Koekkoek SK, De Zeeuw CI (2015) Evolving Models of Pavlovian Conditioning: Cerebellar Cortical Dynamics in Awake Behaving Mice. Cell Rep 13:1977-1988.

Tesche CD, Karhu JJ (2000) Anticipatory cerebellar responses during somatosensory omission in man. Hum Brain Map 9:119-142.

Teune TM, Van der BJ, van der MJ, Voogd J, Ruigrok TJ (2000) Topography of cerebellar nuclear projections to the brain stem in the rat. Prog Brain Res 124:141-172.

Thach WT, Jr. (1967) Somatosensory receptive fields of single units in cat cerebellar cortex. J Neurophysiol 30:675-696.

Thach WT (1968) Discharge of Purkinje and cerebellar nuclear neurons during rapidly alternating arm movements in the monkey. J Neurophysiol 31:785-797.

Thach WT (1970) Discharge of cerebellar neurons related to two maintained postures and two prompt movements. II. Purkinje cell output and input. J Neurophysiol 33:537-547.

Todorov E, Jordan MI (2002) Optimal feedback control as a theory of motor coordination. Nature Neuroscience 5:1226-1235.

Trent MC, Ahmed AA (2013) Learning from the value of your mistakes: evidence for a risk-sensitive process in movement adaptation. Front Comput Neurosci 7:118.

Tseng YW, Diedrichsen J, Krakauer JW, Shadmehr R, Bastian AJ (2007) Sensory prediction errors drive cerebellum-dependent adaptation of reaching. J Neurophysiol 98:54-62.

Valle MS, Bosco G, Poppele R (2000) Information processing in the spinocerebellar system. NeuroReport 11:4075-4079.

van Kan PL, Houk JC, Gibson AR (1993) Output organization of intermediate cerebellum of the monkey. J Neurophysiol 69:57-73.

Viviani P, Terzuolo C (1982) Trajectory determines movement dynamics. Neuroscience 7:431-437.

Wagner MJ, Smith MA (2008) Shared internal models for feedforward and feedback control. J Neurosci 28:10663-10673.

Wallman J, Fuchs AF (1998) Saccadic gain modification: visual error drives motor adaptation. J Neurophysiol 80:2405-2416.

Walter JT, Khodakhah K (2006) The linear computational algorithm of cerebellar Purkinje cells. J Neurosci 26:12861-12872.

Walter JT, Khodakhah K (2009) The advantages of linear information processing for cerebellar computation. Proc Natl Acad Sci USA 106:4471-4476.

Wang JJ, Kim JH, Ebner TJ (1987) Climbing fiber afferent modulation during a visually guided, multi-joint arm movement in the monkey. Brain Res 410:323-329.

Wei K, Kording K (2009) Relevance of error: what drives motor adaptation? J Neurophysiol 101:655-664.

Welsh JP, Lang EJ, Suglhara I, Llinas R (1995) Dynamic organization of motor control within the olivocerebellar system. Nature 374:453-457.

White JJ, Sillitoe RV (2017) Genetic silencing of olivocerebellar synapses causes dystonia-like behaviour in mice. Nat Commun 8:14912.

Winkelman B, Frens M (2006) Motor coding in floccular climbing fibers. J Neurophysiol 95:2342-2351.

Winkelman BH, Belton T, Suh M, Coesmans M, Morpurgo MM, Simpson JI (2014) Nonvisual complex spike signals in the rabbit cerebellar flocculus. J Neurosci 34:3218-3230.

Wolpert DM, Ghahramani Z (2000) Computational principles of movement neuroscience. Nat Neurosci 3 Suppl:1212-1217.

Wolpert DM, Ghahramani Z, Jordan MI (1995) An internal model for sensorimotor integration. Science 269:1880-1882.

Wolpert DM, Miall RC, Kawato M (1998) Internal models in the cerebellum. Trends in Cognitive Sciences 2:338-347.

Wong AL, Shelhamer M (2011) Sensorimotor adaptation error signals are derived from realistic predictions of movement outcomes. J Neurophysiol 105:1130-1140.

Xu-Wilson M, Chen-Harris H, Zee DS, Shadmehr R (2009) Cerebellar contributions to adaptive control of saccades in humans. J Neurosci 29:12930-12939.

Yakhnitsa V, Barmack NH (2006) Antiphasic Purkinje cell responses in mouse uvula-nodulus are sensitive to static roll-tilt and topographically organized. Neuroscience 143:615-626.

Yakusheva T, Blazquez PM, Angelaki DE (2010) Relationship between complex and simple spike activity in macaque caudal vermis during three-dimensional vestibular stimulation. J Neurosci 30:8111-8126.

Yang Y, Lisberger SG (2014) Purkinje-cell plasticity and cerebellar motor learning are graded by complex-spike duration. Nature 510:529-532.

Yartsev MM, Givon-Mayo R, Maller M, Donchin O (2009) Pausing purkinje cells in the cerebellum of the awake cat. Front Syst Neurosci 3:2.

Zago M, Bosco G, Maffei V, Iosa M, Ivanenko YP, Lacquaniti F (2004) Internal models of target motion: expected dynamics overrides measured kinematics in timing manual interceptions. J Neurophysiol 91:1620-1634.